NAVAL POSTGRADUATE SCHOOL
MONTEREY, CALIFORNIA

THESIS

INTERACTION OF A SWIRLING JET
WITH A FREE SURFACE

by

Michael S. Feyedelem

March 1996

Thesis Advisor: T. Sarpkaya

Approved for public release; distribution is unlimited.

19960520 032

REPORT DOCUMENTATION PAGE			Form Approved OMB No. 0704-0188
Public reporting burden for this collection of information is estimated to average 1 hour per response, including the time for reviewing instruction, searching existing data sources, gathering and maintaining the data needed, and completing and reviewing the collection of information. Send comments regarding this burden estimate or any other aspect of this collection of information, including suggestions for reducing this burden, to Washington Headquarters Services, Directorate for Information Operations and Reports, 1215 Jefferson Davis Highway, Suite 1204, Arlington, VA 22202-4302, and to the Office of Management and Budget, Paperwork Reduction Project (0704-0188) Washington DC 20503.			
1. AGENCY USE ONLY (Leave blank)	2. REPORT DATE March 1996	3. REPORT TYPE AND DATES COVERED Master's and Engineer's Thesis	
4. TITLE AND SUBTITLE INTERACTION OF A SWIRLING JET WITH A FREE SURFACE			5. FUNDING NUMBERS
6. AUTHOR(S) FEYEDELEM, MICHAEL S.			
7. PERFORMING ORGANIZATION NAME(S) AND ADDRESS(ES) Naval Postgraduate School Monterey CA 93943-5000			8. PERFORMING ORGANIZATION REPORT NUMBER
9. SPONSORING/MONITORING AGENCY NAME(S) AND ADDRESS(ES)			10. SPONSORING/MONITORING AGENCY REPORT NUMBER
11. SUPPLEMENTARY NOTES The views expressed in this report are those of the authors and do not reflect the official policy or position of the Department of Defense or the U.S. Government.			
12a. DISTRIBUTION/AVAILABILITY STATEMENT Approved for public release; distribution is unlimited.			12b. DISTRIBUTION CODE

13. ABSTRACT (maximum 200 words)

The turbulent flow field of a swirling jet issuing from a nozzle, beneath and parallel to a free surface has been studied in as much detail as possible using a three-component laser Doppler velocimeter and flow visualization. The results have shown that the swirl leads to the faster spreading and quicker mixing of the jet. For strongly swirling jets ($S = 0.522$), the similarity is not reached within ten diameters downstream. The results have also shown that both the axial and tangential velocity components decrease outward from the jet axis, naturally leading to centrifugal instabilities. This, in turn, leads to the creation of large scale coherent structures at the periphery of the jet, particularly when it is in the vicinity of the free surface. The turbulent shear stresses exhibit anisotropic behavior, the largest always being in the plane passing through the jet axis. The change of TKE with S is not monotonic. It is maximum for $S = 0.265$, smallest for $S = 0.50$, and has an intermediate value for $S = 0.522$. This is due to the occurrence of vortex breakdown and the resulting intensification of the turbulence within the jet prior to its exit from the nozzle.

14. SUBJECT TERMS Swirling Jets, Ship Wakes, Free Surface			15. NUMBER OF PAGES 198
			16. PRICE CODE
17. SECURITY CLASSIFICATION OF REPORT Unclassified	18. SECURITY CLASSIFICATION OF THIS PAGE Unclassified	19. SECURITY CLASSIFICATION OF ABSTRACT Unclassified	20. LIMITATION OF ABSTRACT UL

INTERACTION OF A SWIRLING JET WITH A FREE SURFACE

Michael S. Feyedelem
Lieutenant, United States Navy
B.S., Purdue University ,1989

Submitted in partial fulfillment of the
requirements for the degree of

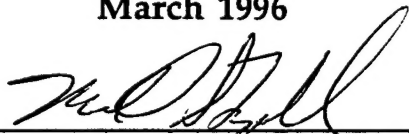## MASTER OF SCIENCE IN MECHANICAL ENGINEERING

AND

MECHANICAL ENGINEER
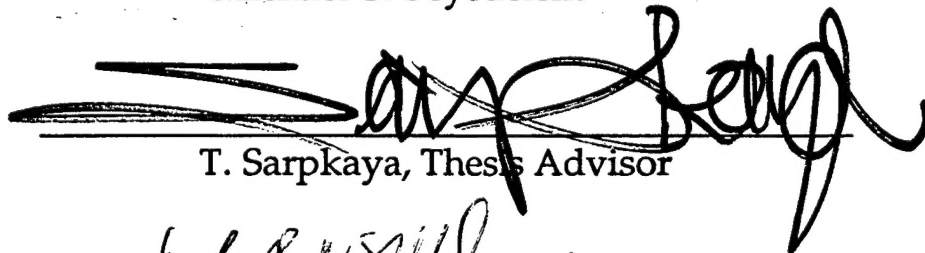
from the

NAVAL POSTGRADUATE SCHOOL

March 1996

Author: _____
Michael S. Feyedelem

Approved by: _____
T. Sarpkaya, Thesis Advisor

_____
Terry R. McNelley, Chairman,
Department of Mechanical Engineering

iii

ABSTRACT

The turbulent flow field of a swirling jet issuing from a nozzle, beneath and parallel to a free surface has been studied in as much detail as possible using a three-component laser Doppler velocimeter and flow visualization. The results have shown that the swirl leads to the faster spreading and quicker mixing of the jet. For strongly swirling jets (S = 0.522), the similarity is not reached within ten diameters downstream. The results have also shown that both the axial and tangential velocity components decrease outward from the jet axis, naturally leading to centrifugal instabilities. This, in turn, leads to the creation of large scale coherent structures at the periphery of the jet, particularly when it is in the vicinity of the free surface. The turbulent shear stresses exhibit anisotropic behavior, the largest always being in the plane passing through the jet axis. The change of TKE with S is not monotonic. It is maximum for S = 0.265, smallest for S = 0.50, and has an intermediate value for S = 0.522. This is due to the occurrence of vortex breakdown and the resulting intensification of the turbulence within the jet prior to its exit from the nozzle.

TABLE OF CONTENTS

LIST OF FIGURES

ix

xi

LIST OF SYMBOLS

a	= Distance to virtual origin normalized by diameter
d	= Diameter of nozzle
F	= Froude number, $U_O/\sqrt{gh}$, in this investigation
g	= Gravitational acceleration
G	= w_{mo}/u_{mo}
G_θ	= Axial flux of swirl momentum
G_x	= Axial flux of axial momentum
h	= Depth of nozzle axis from undisturbed free surface
p	= Pressure
p_∞	= Ambient pressure
r	= Radial distance
Re	= Reynolds number, $U_O d/\nu$, in this investigation
S	= Swirl number, Eq. (1)
TKE	= Turbulent kinetic energy
U	= A velocity
u	= Axial component of velocity
u'	= rms value of u', normalized by U_O
v	= Transverse component of velocity
v'	= rms value of v', normalized by U_O
u_{mo}	= Assumed plug velocity u at exit
U_m	= Maximum velocity u at a given x/d
U_O	= Mean velocity at nozzle exit
U_w	= Minimum phase velocity of capillary-gravity waves
$\overline{u'v'}$	= One of the Reynolds shear stresses
w	= Vertical component of velocity

w'	= rms value of w', normalized by U_O
We	= Weber number
w_{mo}	= Maximum swirl velocity at r = d/2
x	= Axial coordinate, origin at nozzle exit
y	= Lateral coordinate
z	= Vertical coordinate, origin on x axis
z^*	= z/(x+ad)
Γ	= Circulation of vortex
ν	= Kinematic viscosity
σ	= Surface tension
ρ	= Density of fluid

ACKNOWLEDGMENTS

The work contained within could not have been accomplished without the help of the following people:

The craftsmen from the Naval Engineering Machine Shop who were always available to assist in all of the system changes, modifications and repairs.

The curricular officer, CDR Bill Gray and the educational technician, Pam Davis, who provided endless support and always had an answer to my questions.

The Naval Engineering Faculty, who provided quality instruction and inspiration.

My loving parents, who made me what I am today.

Professor Sarpkaya, whose instruction and devotion extended far beyond the field of fluid dynamics. He has given me the education I never dreamed possible and my only regret in finishing this thesis is that my work with him has drawn to an end. I only hope that in my lifetime I can accomplish half of what this man has done for science and mankind itself.

Lastly, my wife, Melissa, whose love, support and understanding have given me the ability to conquer all the challenges that the world has to offer. This work is as much a credit to her as it is to me.

To all of these people, I thank you.

I. INTRODUCTION

The purpose of this investigation is to study in as much detail as possible the turbulent flow field of a round swirling jet issuing from a nozzle, beneath and parallel to a free surface, using a three-component laser Doppler velocimeter and flow visualization (laser-induced fluorescence and shadowgraph techniques). The project is driven partly by an innate curiosity to understand the physics of the phenomenon and partly by the need to understand the unsteady hydrodynamic phenomena in naval operations.

The current impetus for research on free surface phenomena began with the interaction of an ascending vortex pair with the free surface and became a mature subject during the past decade. The modulations of the flow field and the topological features of turbulence near the free surface resulting from an ascending vortex pair are not expected to be similar to those induced by a turbulent round jet, a streamwise vortex, a swirling jet, or an oscillating-grid, under similar circumstances (shallow or deep submergence). There is growing evidence from open channel (e.g., Komori et al 1982, Sarpkaya and Neubert 1994, Sarpkaya 1996) and oscillating-grid experiments (e.g., Brumley and Jirka 1987) that any turbulence field approaching the free surface may be restructured and quasi-two-dimensionalized by the free surface and forced to cascade some of its energy in the reverse direction through the occasional merging of the resulting surface-normal, like-sign, vortical structures or whirls. It is towards this objective that the vorticity flux, basic equations and boundary conditions, the role of surfactants, topology of interfacial interactions, characteristics of connections, disconnections, and

1

reconnections, and a number of canonical flows (single and paired vortices, jets, and vortex rings) have been recently reviewed by Sarpkaya (1996).

A brief discussion of two canonical flows (jets and streamwise vortices) will now be presented in order to lay the proper foundation for the investigation of swirling jets under similar circumstances. The common feature of round jets and streamwise vortices is that they have been studied extensively for both the shallow and fully submerged case (free turbulent jet and free turbulent streamwise vortex) . Thus, it is possible to distinguish the effects of the free surface on the evolution of these two flows by comparing and contrasting the free-surface cases with the fully-submerged or unbounded cases. The swirling jet case, however, has been studied only and extensively under either fully submerged case or in rigid-body confinements (e.g., a combustion chamber), i.e., there has not yet been any investigation of the interaction of a turbulent swirling jet with a free surface. Thus, it is hoped that investigations of fully-submerged and shallow jets, vortices, and swirling jets will complement each other and lead to a better understanding of the physics of the near-surface flows. It is only then that it will be possible to control their consequences.

If one were to attempt a numerical solution of these flows with the objective of evaluating a turbulent transport model, one has to deal with the uncertainties involved in imposing the proper free-surface boundary conditions on the turbulence model (Sarpkaya, 1996). Often a simple alternative, i.e., the 'rigid-lid' approximation, has been used. For example, Swean and Peltzer (1984) invoked this condition for the case of a flat plate moving near a free surface. The discrepancies between their numerical and

2

experimental results may be due to either the rigid-lid conditions being applied to a case with a real free-surface or the turbulence model or both. Obviously, the turbulence model can be verified under the simpler slip-free rigid-lid condition, independent of the complete free-surface boundary conditions, by carrying out experiments with an 'image body' such that an imaginary plane of symmetry exists between the two bodies or flows (e.g., two fully-submerged parallel jets in a vertical plane). The results may be used to refine the turbulence models for the specific case, but they do not shed any light on the effect of free surface deformations and non-linear boundary conditions on the evolution of the turbulent wake. As far as the understanding of the physics and the ultimate control of the free-surface/vorticity interaction are concerned, experiments will have to be carried out under free-surface conditions and the numerical simulations with non-linear free-surface conditions. It is only then that it will be possible to improve the understanding of the interaction of jets, vortices, and swirling jets with a free surface and the refinement of turbulence models and existing codes for more general flow fields, such as ship wakes.

A. JETS

The characteristics of a free turbulent jet, (in an unbounded environment, except for the geometrical limitations of the apparatus used), have been the subject of many investigations. Wygnanski and Fiedler (1969) have made extensive measurements and shown that the flux of downstream momentum is constant along the axis of the flow, i.e., the maximum mean velocity decays like x^{-1} and the width of the velocity profile increases like x,

3

where x is the distance measured along the jet axis. Kotsovinos (1976, 1978) and Schneider (1980, 1985) measured the behavior of the entrained fluid and have found that the momentum flux associated with the entrainment causes a continuous reduction in the momentum flux along the axis of the jet. To achieve a higher level of understanding of the internal structure of the flow, extensive turbulence measurements have been made, among others, by Browand and Laufer (1975); Yule (1978); Dimotakis, et al. (1983). These and similar measurements have shown that the initial laminar free shear layer gives rise to interacting and merging vortex-ring-like structures under the influence of instability waves. The potential core finally comes to an end when the vorticity associated with these structures reaches the axis of the jet and dictate the character of the remainder of the jet.

The interaction of a turbulent round jet with the free surface has been studied, among others, by Rajaratnam and Humphries (1984), when the free surface is located at the jet nozzle (h/d = 0.5 where d is the diameter of the nozzle and h, the distance from the undisturbed free surface to the nozzle axis), by Ramberg, et al. (1989), and more recently, by Madnia and Bernal (1994), over a six year period, using LDV, flow visualization, and circular jets at various depths below the free surface. Madnia and Bernal (1994) concluded that surface waves are generated by vortical structures in the jet. In addition, surface whirls come into existence due to vorticity normal to the free surface, an observation which was first reported by Sarpkaya and Henderson (1984, 1985) and Sarpkaya (1985, 1986). Madnia and Bernal (1994) also concluded on the basis of their scaling parameters, characterized by $U_o d / U_w h$ (U_o = velocity at the nozzle exit, in a vertical plane, U_w = the minimum phase velocity of

capillary-gravity waves) that the momentum loss in the interaction region due to surface contamination, wave generation, and the momentum flux associated with the surface currents are rather small.

B. STREAMWISE VORTEX PAIR

The motion of a free streamwise vortex has been studied over a long time both theoretically and experimentally, partly because of its fundamental importance and partly because of its far reaching technological applications. An extensive review of vortex dynamics, vortex stability, vortex breakdown, wing tip vortices, and vorticity interactions with a free surface are given in Green (1995).

The interaction of counter-rotating trailing vortices, generated at a relatively shallow depth by a lifting foil (moving in clean water at a negative angle of attack), was first reported by Sarpkaya and Henderson (1984, 1985), and Sarpkaya (1985, 1986). It has been shown that an ascending pair gives rise to characteristic surface disturbances (*scars and striations*, see Fig. 1). The striations are essentially three-dimensional free-surface disturbances (which appear as ridges) normal to the direction of motion of the lifting surface, and come into existence when the vortex couple is at a distance equal to about one initial vortex separation from the free surface. They are thought to be due to helical vorticity emanating from the primary vortex tubes. The scars are relatively narrow free-surface depressions, comprised of randomly distributed whirls in a whirlband. The dark circular regions in Fig. 1 are the local surface depressions or whirls and come into existence towards the end of the pure

5

striation phase, when the vortices are at a distance equal to about sixty percent of the initial vortex separation from the free surface.

Various mechanisms have been proposed to provide a feasible explanation of this dark band: (i) interaction of the wake of a vortex pair with the free surface (Sarpkaya and Henderson, 1984); (ii) suppression of surface waves near the ship track and an enhancement of the waves near the edges of the suppressed area by the vortices produced by the ship's hull; (iii) turbulence and surface mean flow resulting from ship motion, although it is not clear that turbulence alone is responsible for their appearance; (iv) a redistribution of surface impurities by large scale vortical motions or Reynolds ridges (see, e.g., Scott 1982); and (v) air subsequently entrained in the wake, bubble scavenging of surface and subsurface surfactant materials, the interaction of Kelvin waves, ambient waves, and momentum waves and the generation of vorticity-retaining inverse bubbles and drops by a Kelvin-Helmholtz instability. Each one of these models, and others not mentioned, tries to provide an explanation of the Synthetic-Aperture-Radar (SAR) images of ships' wakes.

C. SINGLE STREAMWISE VORTEX

The vortex pair/free-surface interaction subsequently led to the investigation of an even more fundamental problem: The interaction of a single streamwise vortex with a free surface. The reason for this is that the modulations of the flow field and the topological features of turbulence near the free surface are not expected to be similar either to those induced by a streamwise vortex in or near a rigid-wall boundary layer (Harvey and Perry,

6

1971; Shabaka et al 1985) or to those resulting from the mutual interaction of the free surface with a three-dimensional turbulence beneath the free surface. The emergence of fairly organized scale bands on either side of the vortex, rather than randomly distributed vortical structures, lead to further merging among like-sign and nearly-equi-strength vortices and enhance the longevity of the surface signatures.

The numerical experiments of Sarpkaya, Magee, and Merrill (1994), performed for various values of the Froude number ($F = \Gamma/h_o\sqrt{gh_o}$ = 3.75, 7.5, and 13.8), Reynolds number (Re = Γ/ν = 150, 300, and 550), and Weber number (We = $\sigma/\rho g h_o^2$ = 0.033, 0.165, and 0.33) where h_o is the depth of submergence of the vortex from the undisturbed surface, have shown that for a given Froude number, the surface tension of the magnitude determined by We = 0.33 flattens the surface to the extent that the surface is barely deformed. The role of the Froude number (here the decrease of the proximity of the vortex to the free surface) is more significant than the increase in surface tension. At high Froude numbers, the surface elevations and trajectories of vortex center are not sensitive to changes in Reynolds number. A two dimensional analysis such as this does not, however, provide any information about the stability of the vortex or the consequences of turbulence.

Sarpkaya (1992a, 1992b) observed that a single, deeply-submerged, trailing vortex (generated by a vertically submerged half rectangular foil) develops large-scale three-dimensional instabilities which play a vital role in the evolution and subsequent interaction of a laminar or turbulent vortex with a free surface. Experiments have shown that the vortex core and its

7

immediate surroundings are not comprised of smooth axisymmetric surfaces. Sheets of helical vorticity sprout out of the edges of the vortex core, transform into isolated turbulent patches and get thrown out from the edges of the core. In other words, the core of a turbulent vortex is not a benign, smooth, axisymmetric, solid body of rotation. The exchange of momentum between the outer regions and the core, augmented by the ambient turbulence, leads to the wandering of the vortex core. If the shed vortex sheets are in the vicinity of the free surface, they either become surface-normal vortices or stretch out parallel to the free surface and dissipate quickly.

Experimental, theoretical, and numerical analyses have shown that a streamwise vortex can become unstable to centrifugal and helical disturbances and to the consequences of having wake-like or jet-like velocity profiles. According to Rayleigh's criterion, a vortex is stable to axisymmetric disturbances if the square of the circulation does not decrease anywhere in the flow field. For example, the Lamb-Oseen vortex is stable whereas the Taylor vortex is subject to centrifugal instability. The much-studied Q-vortex[1] of Batchelor (1964) with a jet-like or wake-like velocity profile can become unstable even if its circulation increases (e.g., see Khorrami 1991).

Sreedhar and Ragab (1994) carried out large eddy simulations of longitudinal and stationary Taylor, Oseen, and Q-vortices with superimposed random perturbations to follow the evolution of mean-flow quantities and modal energies and to identify the large-scale structures that are created due to centrifugal instabilities. Taylor vortex, with $v = Ar \exp(-Br^2)$, is known to

---

[1] The so-called Q-vortex is an Oseen-vortex with an axial velocity defect or excess. Its tangential and axial velocities are given by: $U_\theta = (q/r)U_x$ and $U_x = 1 - \exp(-r^2)$.

be unstable to inviscid axisymmetric disturbances due to the nonmonotonic variation of circulation whereas the Oseen vortex is stable and the Q-vortex with a wake-like axial velocity distribution, as in ship wakes, has many growing modes according to the linear theory. Sreedhar & Ragab (1994) found that the Taylor vortex develops large-scale structures (counter-rotating vortex rings) around the core due to Rayleigh centrifugal instability (see Fig. 2). A linearly unstable Q-vortex (i.e., one with large enough velocity deficit) initially yields large-scale helical structures due to the amplification of the linear stability waves. Subsequently, these structures break down into small scale motions near the edge of the core. However, unlike the Taylor vortex, the Q-vortex eventually evolves into a state of stable mean flow. This is due to the reduction of the velocity deficit as the large structures begin to damp, i.e., the stability provided by the modified circulation distribution is strong enough to eradicate the consequences of the transient instability brought about by the initial profile.

D. SWIRLING JETS

Even though some insight has been gained into the understanding of the behavior of the free surface through experiments with jets, trailing vortices, and single streamwise vortices, it has not been possible to vary independently the ratio of the swirl velocity to the axial velocity under free-surface conditions in order to simulate the wake of a ship. As noted earlier, the case of a fully submerged jet has been studied extensively, but the case of a swirling jet near to and mutually-interacting with a free surface has not been previously investigated. Benchmark data are needed for comparison with

9

numerical predictions based on models for turbulent swirling flows and to guide the formulation of new models that will lead to the improved understanding and eventual prediction of vorticity/free-surface interaction for a variety of cases. It is because of this reason that a major investigation has been undertaken to measure the characteristics of the flow field of swirling jets (helical flows) in both the fully-submerged mode and the surface-proximity mode, at least for one Reynolds-number/Froude-number combination (to be defined later). The data obtained for the fully-submerged mode have been used partly for code validation, partly for comparison with similar data obtained by others, and partly to delineate the effect of the free surface on mean-flow and turbulence characteristics.

II. REVIEW OF FULLY-SUBMERGED SWIRLING JETS

A. INTRODUCTION AND DEFINITIONS

A swirling jet is a jet with axial as well as tangential or azimuthal velocity components at the exit of the nozzle of its origin. The characteristics of such a flow are highly complex for they depend partly on the pre-exit history of the flow within the nozzle and partly on the circumstances surrounding the jet after its exit from the nozzle. The matter is further complicated if the jet is near a liquid free surface. The mutual interaction of the swirling jet and the free surface leads to changes in all flow characteristics (mean velocities and turbulence quantities). The results have shown that the swirl has large effects on jet growth, shape, stability, and entrainment and decay. Before delving into finer details of the resulting flow characteristics, it is necessary to characterize the flow as precisely as possible so that the data of various investigators may be compared and contrasted.

To be sure, there are no precise means to characterize the degree of swirl imparted to the flow because of the strong influence of the nozzle conditions. In fact, there is a real need for the development of additional non-dimensional parameters to fully characterize the near-field behavior of turbulent helical flows. Nevertheless, several proposals have been made and used over the years. The one most widely used is the *swirl number* S, defined by Chigier and Chervinsky (1967) as,

$$S = G_\theta / [G_x (d/2)] \tag{1}$$

where $(d/2)$ is the equivalent nozzle radius; G_θ represents the axial flux of swirl momentum, given by

11

$$G_\theta = \int_0^\infty (\rho uw + \rho u'w')r^2 dr \qquad (2)$$

and G_x represents the axial flux of axial momentum, given by

$$G_x = \int_0^\infty (\rho u^2 + \rho u'^2 + (p - p_\infty))r\,dr \qquad (3)$$

Integration of the second equation of motion yields

$$\int_0^\infty (p - p_\infty)r\,dr = -\frac{\rho}{2}\int_0^\infty (w^2 + w'^2 + v'^2)r\,dr \qquad (4)$$

which, when combined with Eq. (3), yields

$$G_x = \rho\int_0^\infty [u^2 + u'^2 - \frac{1}{2}(w^2 + w'^2 + v'^2)]r\,dr \qquad (5)$$

Chigier and Chervinsky (1967) introduced a number of simplifications into the definition of S by ignoring, for example, the turbulent stress terms, and/or omitting the pressure term, or assuming the jet, at the exit, to be a solid body rotation plug flow (i.e., the axial velocity u is a constant flat profile ($u = u_{mo}$) and the swirl velocity w increases from 0.0 at $r = 0$ to a maximum value of w_{mo} at $r = d/2$. The use of the foregoing simplifications leads to

$$G_x = \frac{\pi}{2}\rho u_{mo}^2 (d/2)^2\left[(1 - (G/2)^2\right] \qquad (6)$$

and to

$$S = \frac{G/2}{1 - (G/2)^2} \qquad (7)$$

where $G = w_{mo}/u_{mo}$. The comparison of the S values evaluated through the use of the exact values of G_x and G_θ with those obtained from Eq. (7) shows that for G greater than about 0.4 (i.e., S larger than about 0.2), the approximate characterization of the flow deviates considerably from the actual values. The primary reason for this is that the plug-flow assumption becomes less and less representative of higher swirl flows at the nozzle exit and that most of the flow exits near the periphery of the nozzle. In addition, the axial velocity begins to exhibit wake-like behavior. Chigier and Chervinsky (1967) found that by changing $[1- (G/2)^2]$ in Eq. (6) to $(1- G/2)$ one obtains a semi-empirical approximation [Eq. (8)]

$$S = \frac{G/2}{1-(G/2)} \tag{8}$$

which provides a closer fit to the experimental results.

Other approximate definitions of S are:

(1) Relating S to the swirl vane angle through an approximate relationship (Sarpkaya, 1971; Gupta et al., 1984). Such a definition deteriorates as the vane angle increases.

(2) Using the ratio of the maximum swirl velocity to the maximum axial velocity in the exit plane.

In spite of the fact that G_θ and G_x are invariants of the jet, the characterization or simplification of S in any of the forms cited above is still unsatisfactory and one cannot expect identical results from various nozzles even if S is kept identical. This is partly because S is an integrated quantity and partly because the evaluation of the integrals requires the measurement of pressure and turbulence quantities in Eqs. (2) and (5). As noted by Farokhi

et al (1989), "it is possible to generate swirling jets with different initial tangential velocity profiles ranging from solid-body rotation to near free-vortex flow with constant S." Moreover, since the static pressure field is coupled to the tangential velocity distribution through the momentum equations and dominates the swirling jet evolution in the near field, vastly different mean jet behavior (e.g., mean centerline velocity decay) should be observable in swirling jets with constant S. The discussion is, of course, related to the ultimate purpose of the definition of S: to enable one to compare data originating from various sources through the use of a representative Reynolds number and swirl number. This is only approximately possible at the present time since dimensionless parameters based on integrated quantities do not lead to universal invariants. In the present investigation, the swirl number was calculated as exactly as possible, for the nozzle tested, through the use of Eqs. (1, 2, and 5).

B. PREVIOUS INVESTIGATIONS

Only a handful of contributions were made to swirling flows prior to 1950. Shepherd and Lapple (1939) discussed the flow patterns and pressure drop in cyclone dust collectors and Taylor (1948) discussed the mechanics of swirl atomizers. Both works proved to be technologically important and were followed up in subsequent years by others. Perhaps the most significant contribution of the 1936–1950 period was that of Burgers (1940) on, what is now known as, the Burgers Vortex model. Burgers (1940), and subsequently Rott (1958), considered steady swirling motions where the dependence of the tangential velocity is restricted to the radial direction (r) and that of the axial

14

velocity to the axial direction (z). This resulted in an explicit expression for the tangential velocity which differs from the potential velocity distribution only for r smaller than a core radius r_c. It is a well-known fact that Burgers' vortex can neither be created nor destroyed in an unbounded domain since it requires infinite kinetic energy and would acquire infinite angular momentum. Nevertheless, Burgers' contribution became an inspiration to many other vortex-model makers. Binnie & Hookings (1948), Binnie (1949), Binnie & Davidson (1949), and Taylor (1948) realized that the potential flow theory may be used for the outer region of an ideal vortex if the core region of the vortex can be naturally extracted from the flow field. Swirling liquid flows with air cores at their axes are most suited for such idealization. Even though Binnie (1949) continued to pursue the potential flow analysis, particularly for large systems, with fair agreement, Taylor (1948) concluded that the effects of the wall boundary layer in his small swirl atomizer rendered the potential theory inapplicable.

Considerable research has been carried out since the early sixties on swirling flows (see, e.g., Rose, 1962; Chigier and Chervinsky, 1967; Pratte and Keffer, 1972; Gupta, Lilley, and Syred, 1984; Hallett and Toews, 1987; Farokhi, Taghavi, and Rice, 1989; Kihm, Chigier, and Sun, 1990; Panda and McLaughlin, 1994). These may be classified broadly as: (1) fully-submerged (free) swirling jets discharging into identical stationary or moving medium (air into air or liquid into liquid); (2) confined swirling flows in variable area ducts (e.g., combustion aerodynamics); (3) swirling flow in turbomachinery annuli; (4) vortex control and management in external/internal

aerodynamics; and (5) leading-edge vortex breakdown over a high-angle-of-attack delta wing.

The present investigation deals partly with swirling turbulent liquid jets discharging into a large medium of water to establish a reference data base and partly with identical jets beneath and parallel to a free surface, the ultimate purpose being the understanding of the consequences of the mutual interaction of the jet and the free surface. It is because of this reason that the brief review of the state of the art will deal with swirling turbulent free jets. There are no previous studies of the swirling-jet/free-surface interaction.

Rose (1962) used a swirling jet of air issuing from rotating pipe into a reservoir of motionless air. He measured mean velocities and one component of the turbulence intensity through the use of a hot-wire anemometer. His measurements were confined to a region extending from the pipe discharge out to a distance of 15 pipe diameters. He found that, contrasted with the nonswirling jet, the jet with swirl spreads at a larger angle, entrains reservoir fluid more rapidly, and thus displays a more rapid reduction of mean-velocity and growth of turbulence intensity.

Chigier and Chervinsky (1967) produced the most quoted reference in swirling flows. They have used an 'axial plus tangential-entry' swirl generator. Experiments were carried out with a series of axisymmetric free turbulent jets with degrees of swirl covering the weak, moderate, and strong ranges, including the case of the onset of reversed flow in the central region of the jet. In order to find the virtual origin of the jet, i.e., the upstream distance 'a' to the jet origin from the nozzle exit, for use in similarity tests, they have plotted $1/U_m$ versus x to the value of $U_m = 0$, where U_m is the

maximum velocity at a given x/d, and x is the downstream distance from the nozzle exit. This gave a value of x = –2.3d or $|x/d| = a = 2.3$. They have found that after a distance of 10 diameters, the influence of the swirl becomes negligible, and similarity of the profiles is obtained farther downstream. For strongly swirling jets, the maximum was displaced from the jet axis and similarity was not established until about 10 diameters downstream.

Pratte and Keffer (1972), like Rose (1962), used a rotating pipe. The Reynolds number was 2300, based on the mean axial velocity and pipe diameter. The effective origin of the jet was found to be at x = –3d, i.e., 'a'= $|x/d| = 3$, by extrapolating back to a point source on the axis of symmetry. Even though Pratte and Keffer (1972) carried out tests only for S = 0.3, they claimed that 'a' was independent of S. Be that as it may, their 'a' value is identical to that obtained in the present investigation. Their measurements have also shown that the flow achieved a self-similarity for the mean velocities rather quickly while the normal turbulent intensities reached a self-similar state after a longer period of jet development. The entrainment rate and angle of spread for the swirling jet were found to be nearly twice that of the nonswirling free jet.

Gupta, et al. (1984) summarized the state-of-the art for both combusting and non-combusting swirling flows in a monograph. Hallett and Toews (1987) dealt primarily with the effects of the inlet conditions and expansion ratio on the onset of flow reversal in a swirling flow subjected to sudden expansion. Their objective was the understanding of the central recirculation zone produced by a strongly swirling flow towards the stabilization of flames and intensifying mixing in swirl burners and combustors. For design

17

purposes, a knowledge of the minimum swirl needed to produce recirculation is required, as swirl levels much above the minimum result in higher pressure losses without proportional improvement in mixing or stability.

Farokhi, et al. (1989) used the common practice of combining axial and tangential streams to produce swirl. Their apparatus was unique in the sense that it had numerous elbow nozzles mounted on three concentric circular rings. This allowed them to control the initial tangential velocity distribution. Unlike most other investigators, they have used a convergent nozzle (bellmouth), the consequences of which will be discussed later. Suffice it to note that the modifications to their swirl system enabled Farokhi, et al. (1989) to produce distinctly different swirl velocity profiles. They have shown that the time-averaged jet characteristics in the near field are significantly influenced by the initial tangential velocity distribution. They too have noted, as did others before them, that the swirl number S is insufficient to describe the character of swirling flows. At S = 0.48, vortex breakdown, a phenomenon associated with relatively high swirl, occurred. The fact that the swirling jet has been brought to the point of breakdown at a swirl number of S = 0.48, significantly lower than the critical value (often assumed to be S_{cr} = 0.6), was regarded by Farokhi, et al. (1989) as the most remarkable result of their investigation. Their finding is essentially confirmed by the present investigation, which yielded $S_{cr} \approx 0.5$.

Kihm, et al. (1990) used three different flat-vane swirlers. Even though their design is not shown in sufficient detail, it is stated that the swirler exit is located 10 mm behind (upstream from) the nozzle exit. Air flow emerges

from the swirler as a series of jets between the individual vanes of the swirler. These individual jets merge in the annular passage between the swirler exit and nozzle exit. Kihm, et al. (1990) have ascertained, through the measurement of the radial and circumferential velocity traverses made at the nozzle exit, that the flow is axisymmetric without a trace of the individual jets that emerge between the vanes. The measurements were made at $x/d =$ 0.1, 1, 2, 4, and 8. The measured quantities were the mean velocities, their rms values, the Reynolds stresses, and the turbulent kinetic energy.

III. EXPERIMENTAL EQUIPMENT

The experiments were conducted in a low turbulence water tunnel with an open test section of about 50 cm wide, 50 cm deep (maximum), and about 600 cm long. The ambient fluid is of course kept at rest during the experiments. During off-test periods, a small pump continuously filtered the tunnel water through a micro filtration system to remove rust and other suspended fine particles, down to about 10 μm, from the water (the filtration system was turned off during the experiments).

A thorough examination of the previous investigations have shown that swirl may be generated either using a tangential entry (axial plus tangential entry swirl generators), or through the use of guided vanes (swirl-vane pack or swirler), or by direct rotation of the pipe. Not all of these methods allow one to vary swirl while maintaining the Reynolds number constant. This and other considerations led to the use of an 'axial-plus-tangential entry' swirl generator, similar to that devised by Chigier and Chervinsky (Fig. 3) in 1967. The final design is shown in Fig. 4. The most important differences between the Chigier–Chervinsky design and the one used herein are: (i) Figure 4 has four tangential inputs (coming from a common reservoir further upstream), and (ii) the nozzle in Fig. 4 has a smooth constriction whereas that of Chigier–Chervinsky is a straight tube. Several other investigators (e.g., Farokhi, et al., 1989; and Panda and McLaughlin, 1994) have also used converging nozzles. Batchelor (1967) has shown that the axial velocity distribution becomes nonuniform when a jet having an initial uniform axial velocity and solid body rotation passes through an area of constriction. This is because the vortex lines, which are

initially parallel to the axis, turn into spirals during the passage through the constricted area. Thereby, an additional azimuthal component of vorticity is produced. This yields a negative value of dU/dr, so that a contraction of the stream tube produces a maximum of axial velocity at the axis. Thus, the exit flow acquires a higher axial velocity at the nozzle exit (jet-like behavior). This phenomenon is of special importance in connection with the occurrence of vortex breakdown in swirling flows and will not be discussed here further.

The mean velocities and turbulence intensities were measured with a Laser-Doppler Anemometer. Bragg-cell frequency shifting by 0.5 MHz was used to detect the flow reversals. The probe volume (approximately 50 μm in diameter and about 150 μm in length) was positioned at the required location by use of a remotely driven x-y-z traversing unit. The scattering particles used were titanium dioxide of rutile crystalline form and were approximately 12 μm in size. The data are reported without any velocity-bias-correction.

The measurements for the free swirling jet were made at x/d = 0.14 (very near the nozzle exit), 1, 2, 3, 4, 5, 7, and 10. For the near free surface case, the nozzle axis was placed at h = 3.5d from the undisturbed free surface, i.e., at h/d = 3.5. and the measurements were made at x/d = 0.14, 0.5, 2, 4, 6, 8, 10, 12, and 16. At each section, all velocity and turbulence quantities were measured along the vertical z axis (y = 0) and along the lateral y axis (z = 0). In addition, a number of measurements were made very near the free surface, along the lines parallel to the y axis at x/d = 10.

Every precaution has been taken and a conscientious effort has been made to obtain archival quality data for use in the validation of numerical simulations. Subsequently, the data have been post-processed with no

corrections what-so-ever and are presented here in graphical forms. The degree of accuracy of the data is discussed in connection with the presentation and discussion of results. Nevertheless, it suffices to note that the velocities are found to be correct within $\pm 2\%$ and the turbulence quantities within $\pm 5\%$. Finally, many measurements have been repeated at different times, with gratifying comparisons with those obtained previously, in order to explore the possibility of systematic errors.

IV. DISCUSSION OF RESULTS

A. GENERAL COMMENTS

The discussion and presentation of the results will be in the order of increasing swirl numbers. In the present investigation, S had values of 0.265, 0.50 and 0.522.

The measurements along a given axis normally yield nine quantities, six of which describe the mean velocities u, v, w and the rms values u', v', w', and the remaining three represent the Reynolds shear stresses u'v', u'w', and v'w'. It is understood that quantities such as u' and u'v' denote in reality $\sqrt{\overline{u'^2}}$ and $\overline{u'v'}$. The shorter notations are used for all components of turbulence throughout the text and figures for sake of simplicity.

It is customary to discuss the results in terms of dimensionless parameters in order to understand the physics of the phenomenon. It is with this objective in mind that the results presented herein are normalized by suitable parameters. This will be discussed in some detail for there are a large number of ways of normalizing the data under consideration. For example, the mean velocities may be normalized by Uo (the cross sectional mean velocity at the nozzle exit) or by Um (the maximum velocity in a given distribution) along a given line, at a prescribed section, or by a representative velocity at the 50% level and the position at which it occurs. After a careful consideration of all the possibilities, both Uo and Um were used to bring out the special features of the velocity profiles, as needed. The higher order quantities such as u'w', were normalized by U_o^2.

The distances from the jet axis in various directions were normalized by a special length which required the use of the diameter d of the nozzle and the virtual origin of the jet from the jet exit back into the nozzle. In other words, the distances are not measured from the nozzle exit, but rather from the virtual origin. Thus, a distance in the x direction (axis of the swirling jet) is normalized by x+ad, with 'a' = 3. The y axis is obviously normal to the x-z plane and situated in the horizontal plane normal to the x and z axes. A few words are necessary regarding the actual jet axis and x axis. It is a well known phenomenon that the wakes of single screw ships and submarines drift to the right or left depending on the direction of rotation of the propeller because of the swirl induced momentum. The magnitude of the drift depends on the axial momentum of the flow. In the present investigation, U_0 was 2.79 m/s (corresponding to a Reynolds number of $Re = U_0 d/\nu = 18,000$ and a Froude number of $F = U_0/\sqrt{gh} = 6$) and that the said drift was negligible within a distance of 30 diameters or so, and certainly much smaller than the deflection of the jet axis towards the free surface because of its mutual interaction with its image. Furthermore, for sake of consistency, all the velocity and turbulence plots were made relative to the x-axis (the ideal center of the jet) rather than the local center of the jet.

Prior to the discussion to follow, it is to be emphasized that, considerable number of measurements were made to delineate the characteristics of the flow and the range of the parameters in which interesting phenomena have occurred. Otherwise, a massive undertaking of the measurement of all velocity and turbulence quantities on a fine grid at each section, at various swirl numbers, and for various nozzle depths from

the free surface would have produced no less than 10,000 plots. Even for archival purposes, this is an impossible undertaking. Thus, the identification of the most important governing parameters and the measurement of velocities and turbulence quantities in the judiciously selected range of these parameters could bring out the physics of the flow, without the overwhelming number of data points and plots. This particular thought has been foremost in mind from the start to the completion of the investigation.

In search of fundamental parameters and interesting phenomena, Fig. 5 is offered where u/U_o is plotted as a function of $x/(x+ad)$ in terms of five S values. It shows the gradual decrease of the axial velocity along the x axis for relatively small S values. The other swirl ratios show first the natural decrease of the axial velocity due to centrifugal expansion of the jet, as in the case of S = 0.265; the rapid decrease to nearly zero and the subsequent increase to about $0.3U_o$ of the axial velocity, as in the case of S = 0.50 and S = 0.51; and finally, the reversal of the axial velocity in or at the exit of the nozzle and the occurrence of the phenomenon known as the vortex breakdown, as in the case of S = 0.522. It is now clear why the three S values used herein were chosen. The first, S = 0.265 (a mild swirl) shows the significant differences between a swirling jet and a simple free jet; the second (a critical swirl), shows a region of near stagnation and divides the states of no-flow reversal and flow reversal; and finally, the third shows the effect of strong swirl on the reversal of the flow and the occurrence of vortex breakdown.

B. THE CASE OF SWIRLING JET WITH S = 0.265

The discussion to follow will concentrate on several important aspects of the data and the evolution of the jet itself.

The purpose of the first few sets of data is the establishment of the quality of the data rather than the discussion of the physics of the phenomena. Figures 6 and 7 show u/U_m and v/U_m as a function of $z/(x+ad)$, hereafter denoted by z^*. One data set is for the fully submerged free swirling turbulent jet and the other for the same jet whose axis is at a distance of $h = 3.5d$ from the undisturbed, clean, free surface. These data were obtained months apart at a downstream distance of $x/d=0.14$ where the free surface effects were absent. It is obvious that there is excellent agreement between the two sets of data for both u/Um and v/Um and attests to the quality of the data and the care that went into its acquisition. Figures 8 and 9 show u'/Uo and v'/Uo, again as a function of z^*, for both the shallow and deep modes. Hereafter, the "shallow mode" refers to $h=3.5d$ and the "deep mode" refers to the case of the fully submerged jet. Aside from the fact that the agreement of the data for the two modes and two rms values are as good as can be expected, the data also show the ability of the measurement system and techniques to capture intense turbulence in the very thin shear layers between the jet and the ambient environment. At $x/d = 0.14$, $z^*=\pm0.16$, the rms values of u' and v' acquire very large values, as shown in Figs. 8 and 9, and the agreement between the shallow and the deep mode rms values are excellent.

The Reynolds stresses shown in Figs. 10-12 show equally well the agreement between the deep and shallow modes at a higher level of sensitivity and also point out the Reynolds stresses at the shear layers as

28

noted previously. The reversal of the sign of the Reynolds stresses at $z^*=$ –0.16 relative to that at $z^*=0.16$ is due to the effect of swirl.

Figures 13-26 are plotted in the same spirit as that of Figs. 6-12, i.e., to demonstrate the quality of the data obtained at different times at other x/d values, namely at $x/d = 2$ (Figs. 13-19) and $x/d=4$ (Figs. 20-26). A careful perusal of the data shows that the axial component of velocity differs no more than 2%, the swirl component (v/Um) differs from one mode to another about 3-4% at the peak values of swirl. The turbulence quantities u'/Uo and and v'/Uo (Figs. 22-23), differ between the deep and shallow modes by about 4% or less. However, the same turbulence elements differ by a larger amount between the two states in Figs. 15 and 16. Of the three Reynolds stresses (Figs. 24-26), $u'w'$ shows the least scatter relative to the other two stresses. In fact, the order of the scatter is $u'w'$, $v'w'$ and $u'v'$, the last exhibiting the largest scatter. There are a number of reasons for this. The first is the fact that $u'w'$, as in all turbulent flows, is the largest of all three (see Fig. 26). This stress is in the vertical plane passing through the axis of the jet and represents the stresses in that plane. It should be noted that here, w' is the rms value of the velocity fluctuations along the z axis. The usual textbook discussion of turbulence, particularly in connection with wall boundary layers, will refer to this stress as $u'v'$ since the z axis is often denoted as the y axis normal to the boundary. Suffice it to note that this stress is the largest of them all and the others are often ignored in turbulent boundary layer approximations of the equations of motion.

The second reason for the larger scatter in $v'w'$ and $u'v'$ is that the stress denoted by $v'w'$ is in the plane normal to the jet axis and its magnitude

is significant only where the swirl velocity is larger. However, if one observes that (see Figs. 20 and 21) the maximum value of the normalized swirl velocity is only about 15% of the maximum of the normalized axial velocity, one appreciates the fact that v'w' is at least 15% smaller than u'w'. Consequently, the differences in the smaller quantities appear to exhibit larger scatter, though the scatter is certainly within the range of acceptable experimental expectations. As far as u'v' is concerned, unlike v'w' and u'w', it is not in a single plane, but in planes normal to the z axis all the way from, say $z^* = -0.6$ to $z^* = 0.8$. Coupled with the fact that v' is already an order of magnitude smaller than w', and that the two fluctuations are in two different planes, enhances the degree of scatter relative to the other two.

The next case to be taken up is that for section x/d=10, still for S = 0.265. Here the objective of the discussion is not so much the quality of the data, for it has already been established, but rather the effect of the free surface on the characteristics of flow, interpreted in terms of deep mode measurements.

Figure 27 shows that even though the magnitude of the normalized axial velocity does not differ between the two modes, a careful examination of the data for the shallow and deep modes shows that the velocity profile for the shallow mode is shifted upwards. This will become more evident as one examines similar profiles at larger distances. At this stage of the discussion, one must emphasize certain facts and note certain expectations for a clearer understanding of the discussion to come. First, it appears that for x/d smaller than about 10, it is nearly impossible to distinguish the presence of a free surface in all velocity and turbulence quantities; second, one expects that the larger the swirl, the larger the deviation between the deep and shallow modes

30

at x/d=10 will be; third, the larger the swirl the sooner is the start of influence of the free surface; lastly, and more importantly, the effect of the free surface is not a simple phenomenon which could be expressed in terms of a few simple parameters. It is because of these reasons and expectations that the effect of the free surface will be examined in a different light. The cases where the interaction is small regardless of the value of the swirl number, the interaction will be called "weak" or "zero interaction." The cases where the bulk flow characteristics (such as u, v, w) are not yet measurably affected by the turbulence quantities will be called the "transitional interaction", and finally, the cases where all flow characteristics differ from the free swirling jet will be called "strong interaction."

Returning to the discussion of Figs. 27-28, it has been noted that the bulk flow characteristics differ relatively little between the deep and shallow modes. However, the turbulence quantities like u', v', and w' exhibit characteristics which demonstrate more clearly the presence of the free surface. Figures 29-31 show that the symmetry of the turbulence quantities relative to the jet axis is visibly lacking and that the maximums are shifted towards the free surface as is the case of bulk characteristics. In particular, w' (the turbulence component normal to the free surface) is enhanced relative to the deep mode because of the fluctuations of the free surface. These fluctuations are sufficiently strong and deposit enough kinetic energy in a thin layer where the jet and its image interact non-linearly. Even though the overwhelming non-linearity of the interaction between small-scale turbulent quantities and the macro-scale fluctuations cannot yet be analyzed with the existing turbulence models with non-linearized free surface conditions, the

31

turbulent kinetic energies (TKE), to be discussed later, indirectly demonstrate the nature of the interaction.

Figures 32-33 show u'v' and v'w' components of the Reynolds stresses which are, as expected, small relative to u'w'. Figure 34 shows the quality as well as the behavior of the largest Reynolds stress, i.e., u'w'. The shallow mode data is shifted only slightly upwards relative to the deep mode case and that shift is clearly visible in spite of the scatter of the data and is certainly above the threshold limit for experimental errors.

The next case to be discussed for the same value of S = 0.265, is the flow at x/d = 16. Here only the data for the shallow mode case will be presented partly for sake of clarity and partly for the fact that the comparison of the upper and lower halves of the jet clearly demonstrate the effect of the free surface. It will become evident that this section does in fact fall in the regime of strong interaction. The asymmetry about the jet axis of the upper and lower halves of u, v, and w are obvious in Figs. 35-36. It is also clear that whereas u/Um at $z^* = -0.17$ is about 0.18, the same velocity component at $z^* = 0.17$ is 0.41. In other words, the near surface axial velocity is at least twice as large as the velocity that would have been at the same location had the jet been in an unbounded medium. It shows that the shear free surface moves at a faster rate, just as demonstrated, but also affects all of the bulk flow characteristics as seen in both Figs. 35 and 36. As anticipated in the case of strong interaction, not only the bulk flow but also turbulence quantities show significant changes. For example, in Figs. 37 and 38, the two turbulence quantities u' and v' clearly show the effect of the free surface and v' begins to demonstrate the fact that the kinetic energy near the free surface is

redistributed, the larger share going to v'. Figures 29-31 show that u', v', and w' are nearly identical, within reason, and that when the free surface and the jet interaction is weak, turbulence is essentially isotropic. However, if one compares Figs. 37, 38 and 39, one finds that the axial component of turbulence (u') has almost doubled relative to the other two components (v' and w'). In other words, in the strong interaction region, turbulence has become anisotropic. The far reaching consequences of this finding is not just the demonstration of the influence of the free surface as a transformer of the state of isotropy to anisotropy, but rather in the fact that one should not expect to predict through computational fluid dynamics the flow field through the use of simple isotropic turbulence models or simple eddy viscosity models and the fact that any validation calculations must be based on anisotropic turbulence models.

Figures 40-42 show the Reynolds stresses, and the two components u'v' and v'w' are of comparable magnitude, and rather small relative to u'w'. Figure 42 shows, not only in its magnitude but also in its consistency, with very little scatter, that u'w' near the free surface ($z^* = 0.16$) is about 40% smaller than that at $z^* = -0.16$, emphasizing once again the fact that a swirling jet in the vicinity of a free surface becomes increasingly anisotropic. As noted earlier, it is the recognition of this fact that the proper numerical simulations based on anisotropic turbulence models will eventually lead to the prediction of quantities that either have not been measured or could not yet be measured. This is expected to lead to the development of passive or active non-conventional means of controlling the scars carved on the ocean's surface by the ships. It is also true that the understanding and validated

33

predictions of the behavior of the free-surface turbulence in the manner experimented here, to provide archival data for simulations, will eventually lead to the understanding and prevention of the consequences of unsteady ship motions where the visibility is likely to be enhanced.

In the foregoing, the variations of the velocity and turbulence quantities with respect to z^* were discussed in detail. Even though such plots are significant in demonstrating the consistency of the data and the effect or lack thereof of the free surface effects, they do not yield any information about the evolution of their shape and magnitude along the jet axis. It is because of this reason that the variations of u, v, u', v' and u'w' are shown in Figs. 43-47 at various axial stations. Figure 43 shows that the axial velocity at the nozzle exit is as expected on the basis of Batchelor's (1967) analysis, i.e., the contraction of the nozzle increases the maximum velocity at the axis and the profile becomes less top-hat like. It is also seen that at an axial distance of as small as two diameters and beyond, the axial velocity becomes almost perfectly similar. The minor exception of the case of $x/d = 10$ near $z^* = \pm 0.2$ seems to suggest that the profile has finally acquired a Gaussian shape as observed by others such as Chigier and Chervinsky (1967). The swirl component of the velocity shown in Fig. 44 exhibits exactly the same behavior, as far as $x/d = 10$ is concerned. Figure 45a shows, in a somewhat crowded figure, the normalized rms values of the axial velocity fluctuations, again in terms of z^*. Even though one can sort out the evolution of this component of the turbulence intensity, Fig. 45b is plotted as a duplicate of Fig. 45a, but with connecting lines to facilitate the understanding of this evolution. Clearly, at $x/d = 0$, u' is smallest in the entire cross-section with

34

the exception of the two peaks at the shear layers. At a distance of only 2 diameters downstream, u' jumps to its highest values and begins to spread toward the jet axis. It is also interesting to note that, the maximum of the u' at x/d = 2 is larger than the maximum of u' at x/d = 0.14. This shows that the shear layers are still evolving and widening. As the downstream distance increases, u' steadily decreases and becomes more Gaussian as evidenced by the case for x/d = 10. Figures 46a and 46b show the evolution of the swirl component with similar results, with two exceptions. The maximum of v' at x/d = 2 is smaller than the maximum of v' in the shear layer at x/d = 0.14. The reason for this is the rapid spreading of the shear layer and thus the decrease of v' along the jet axis. The second exception is that at x/d = 10, v' drops to values even lower than that which is encountered at x/d = 0.14. This is because of the enlargement of the vortex core. Finally, Fig. 47 shows the largest Reynolds stress (u'w') at four axial distances. As expected, it increases rapidly within a distance of 2d and then gradually decreases to initial values at x/d = 0.14.

Figures 48-50 show for the shallow mode case, the representative turbulence quantities at various axial distances. As before, one of the plots shows the data with no connecting lines and the next one shows it with connecting lines, to facilitate the examination of the data (as in Figs. 48a and 48b). There is practically no difference in the conclusions reached between the deep and shallow modes shown in Figs. 45b and 48b with the rather coincidental difference that u' at x/d = 16 becomes identical to u' at x/d = 0.14 within the central region of the jet. As before, the shear layers grow and the profiles become more uniform, however, the speed with which u' becomes

uniform is evident from a comparison of the u' values at x/d = 4 in Figs. 45b and 48b. The effect of the free surface seems to increase the rms value of the swirl component relative to the deep mode (Figs 46b and 49b). This is in conformity with all of the previous measurements (see e.g., Komori et al., 1982) that the larger portion of the turbulence energy is taken up by the lateral fluctuations of turbulence. Finally, the normalized values of u'w' are presented in two nearly identical plots. Figure 50a shows u'w' at six axial stations whereas Fig. 50b shows it only at three representative x/d values for a better understanding of the decay of the most important Reynolds stress. Figures 50a and 50b show that u'w' acquires its largest value near x/d = 2, not at the nozzle exit, and then decays rapidly within an additional four diameter distance as seen in Fig. 50b. By the time one reaches the section at x/d = 16, the magnitude of u'w' decreases by an order of magnitude.

The two most important components of velocity fluctuations (u', v') were examined in a region very close to the free surface. For this purpose, y-traverses were made at z* = 0.230 and at z* = 0.254. Figures 51 and 52 show that the u' component decreases slightly near the free surface and the v' component remains not only unchanged but also of nearly the same magnitude as u', at the lower horizontal level. In other words, while the two components at lower depths exhibit an isotropic behavior, near the free surface the turbulence becomes anisotropic. This issue was taken up before in connection with the discussion of the variation of the rms values along the z-axis. The earlier findings stand confirmed by the measurements in the near surface horizontal planes.

C. THE CASE OF SWIRLING JET WITH S = 0.5

The discussion of the results for this swirl ratio will be confined to the planes in the axial distances of 10d and 16d. Figures 53-55 show the axial, swirl and radial components of the velocity both in the deep and shallow modes for the distance of x = 10d. Clearly, the data for the two modes are quite comparable including the scatter for the cases of swirl and radial velocity and it is not possible to discern any effect of the free surface at that axial distance. It must also be noted that the u component is about an order of magnitude larger than the other two components and this provides a partial explanation for the scatter relative to that in the axial component.

The normalized rms values of u', v' and w', are shown in Figs. 56-58. Two facts stand out: The first is that the deep and shallow modes are almost indistinguishable; the second is that the data show remarkably little scatter in spite of the fact that it represents random turbulence components. In all three cases, the fluctuations decrease near the free surface and the u' and v' components remain essentially of equal magnitude whereas the w' component is about 10% smaller. This is simply an indication of the onset of anisotropy throughout the flow field. Finally, the three Reynolds stresses are shown in Figs. 59-61. As expected, u'v' and v'w' are very small and almost negligible relative to the u'w' component. In other words, the largest Reynolds stress is in planes passing through the jet axis.

Figures 62-64 show the axial, swirl and radial velocities as a function of z* in a composite manner that enables one to compare them with each other. Figure 62, more emphatically than others, shows the effect of the free surface on the global characteristics of the swirling jet. The u component increases

for the free surface case which may be explained simply as the freedom of the free surface to move unimpeded by additional stresses as in the case of the deep mode. The normalized rms values of the fluctuations of the velocity components are shown in Figs. 65-67. A brief perusal of these figures also shows that the u' component becomes significantly larger than the other two. In other words, the turbulence becomes increasingly anisotropic with increasing axial distance. Finally, Figs. 68-70 show the Reynolds stresses. The first two, i.e., u'v' and v'w' are negligible. However, u'w' (the Reynolds stress in the plane passing through the jet axis) is considerably larger and shows more emphatically the effect of the free surface. The stress in planes normal to any radial line and parallel to the x-axis (u'v'), are one to two orders of magnitude smaller then the u'w'. The comparison of the turbulence components (u'v', v'w', u'w') at sections 10d and 16d, clearly shows that as the anisotropy increases with distance, the stress in planes passing through the jet axis (e.g., x-z plane) increase at the expense of the stresses both in planes normal to the jet axis and in planes orthogonal to the x-z plane. It is understood that the entire coordinate axis may be rotated about the x-axis so that the z-axis, in reality, represents any radial direction. Thus, one can say that the stresses increase in any plane formed by the axial and radial lines and decrease in all planes normal to the radial and axial directions.

D. THE CASE OF SWIRLING JET WITH S = 0.522

As in the previous case, the discussion of the results for this swirl ratio will be confined to the planes in the axial distances of 10d and 16d. Figures 71-

73 show the axial, swirl and radial components of the velocity both in the deep and shallow modes for the distance of x = 10d. Clearly, the data for the two modes are quite comparable except very near the free surface. Once again, the u component is about an order of magnitude larger than the other two components and this provides a partial explanation for the scatter relative to that in the axial component.

The normalized rms values of u', v' and w', are shown in Figs. 74-76. It is seen that the data for the deep and shallow modes are almost indistinguishable. The data show remarkably little scatter in spite of the fact that it represents random turbulence components. In all three cases, the fluctuations decrease near the free surface and the u', v', and w' components remain essentially equal, i.e., the turbulence is still quite isotropic. It is recalled that for the case of S = 0.5, the turbulence becomes anisotropic at x = 10d. Also, one cannot help but note that the two sets of data (deep and shallow modes) taken months apart compare exceedingly well where there is isotropy. Finally, the three Reynolds stresses are shown in Figs. 77-79. As expected, u'v' and v'w' are very small and almost negligible relative to the u'w' component. In other words, the largest Reynolds stress is in planes passing through the jet axis.

Figures 80-83 show the axial, swirl and radial velocities as a function of z*. Figures 80 and 81 show, more emphatically than others, the effect of the free surface on the global characteristics of the swirling jet. The u component increases for the free surface case which may be explained simply as the freedom of the free surface to move unimpeded by additional stresses which would otherwise prevail in unbounded regions (the deep mode), simulated

here by a simple inversion of the lower half of the jet (see Figs. 80 and 81). The normalized rms values of the fluctuations of the velocity components are shown in Figs. 84-86. A brief perusal of these figures also shows that the u' and v' components are nearly identical and the w' component becomes smaller. In other words, the turbulence becomes increasingly anisotropic with increasing axial distance. The effect of the free surface on all three rms values are clearly seen. Finally, Figs. 87-89 show the Reynolds stresses. The first two, i.e., u'v' and v'w' are negligibly small, however, u'w' (the Reynolds stress in the plane passing through the jet axis) is considerably larger and shows more emphatically the effect of the free surface. The numerical simulation of this data will indeed be a challenge in computational fluid dynamics.

E. TURBULENT KINETIC ENERGY (TKE)

Figures 90 through 95 show the turbulent kinetic energy TKE = $[0.5(u'^2 + v'^2 + w'^2)]$ for three values of S (0.265, 0.50, 0.522) and two values of x/d as a function of z^*. Figure 90 shows that TKE does not differ measurably for the shallow and deep modes. The significant points about this figure are that the data are remarkably consistent and that TKE decreases near the z^* values corresponding to the free surface. Figure 91 shows TKE for S = 0.265 at x/d = 16. Clearly, TKE is about one half of that for x/d = 10, however, there is no indication of free-surface effects.

Figures 92 and 93, corresponding to Figs. 90 and 91, show TKE for S = 0.50. At x/d = 10 (Fig. 92), there is no measurable free surface effect. At x/d = 16 (Fig. 93), the free-surface proximity is clearly discernible, though the

differences are rather small. Furthermore, TKE becomes more uniform along z* in both cases. If there are any dramatic effects of the free surface that are not seen here, they are certainly confined to a very thin layer within two or three millimeters of the free surface.

Figures 94 and 95, corresponding to Figs. 92 and 93, show TKE for S = 0.522. At x/d = 10 (Fig. 94), the free-surface effect is discernible in that near the free surface TKE is larger relative to the deep mode. This is explained in terms of the deposition of the pressure energy in the layer adjacent to the free surface. In the deep mode, the energy is radiated to larger distances. At x/d = 16 (Fig. 95), the free-surface proximity is clearly discernible. The near-free-surface values of TKE are somewhat larger than those for the deep mode.

The effect of the change in S is brought about more emphatically in Figs. 96 (for x/d = 10) and 97 (for x/d = 16). Comparing only these two figures, it is evident that TKE is maximum for S = 0.265 and that it decreases for both x/d = 10 and x/d = 16 with increasing S. However, the decrease has two surprises. First, in either case, TKE is smallest for S = 0.50, not for S = 0.522, as one might have otherwise expected. Second, TKE for x/d = 10 becomes nearly identical for all values of S, both near the free surface and far from the free surface (z* < -0.2). For x/d = 16, however, TKE values become nearly identical only for z* smaller than about -0.15. Near the free surface, TKE values for S = 0.265 and S = 0.522 become indistinguishable, but for S = 0.5, TKE remains considerably smaller than the other two for all z* values larger than about -0.15. The reasons for these facts are not yet clear. The fact that the TKE values merge near the free surface for x/d = 10 may be explained by the fact that the free surface effects are relatively small or negligible at this particular

41

x/d for all values of S encountered in this investigation. One may also conjecture that the merging of the TKE values in the vicinity of the free surface for S = 0.265 and S = 0.50 may be due to the increasing anisotropy of the turbulence with x/d, as noted numerous times earlier. However, TKE for S = 0.522 acquiring values intermediate to those for S = 0.265 and S = 0.50 may be explained only in terms of the creation, initial development, and the subsequent evolution of the swirling jet. It has been noted in connection with the discussion of Fig. 5 that (i) for S = 0.265, the axial velocity decreases gradually due to the centrifugal expansion of the jet; (ii) for S = 0.50 and S = 0.51, the axial velocity decreases rapidly to nearly zero and then increases to about $0.3U_o$; and finally, (iii) for S = 0.522 and larger, the axial velocity reverses in or at the exit of the nozzle, signaling the occurrence of the vortex breakdown (see Figure 98).

It is a well-known fact that (see, e.g., Sarpkaya, 1971, 1995) vortices may experience breakdown (an impressive structural change) depending on the nature and nurture of their creation and evolution. The understanding of the consequences of the breakdown depends in part on the understanding of its topology and in part on a detailed map of its velocity, turbulence, and stress field, validated by experiments or numerical calculations. Since its discovery, many theoretical and experimental studies have been conducted. The difficulties experienced in describing the nature, identifying the occurrence, and predicting the characteristics of the breakdown in tubes, over delta wings, and in covered or topless cylindrical containers have been well documented. In the present case, the swirling flow is discharging into a relatively large medium, not into a pipe. It is because of this reason that the

swirl ratios needed are significantly different from those encountered in swirling pipe flows. For small values of S, the adverse pressure gradients set up by the decaying swirl velocity are insufficient to cause flow reversal and the swirling jet becomes an example of a thin shear layer distorted by the imposition of an extra rate of strain. When the swirl ratios exceed about 0.51 (for the conditions of the present experiments), the adverse pressure gradients are sufficiently large to cause flow reversal and vortex breakdown. This, in fact, is the case for S = 0.522. The behavior of TKE in Figs. 96 and 97 is attributed to the occurrence of vortex breakdown, the accompanying flow reversal, and, most importantly, to the turbulence produced from the bursting of the vortex, particularly when it occurs inside the nozzle (the case of S = 0.522). The intensification of the turbulence within the jet prior to its exit from the nozzle can and does alter the velocity and turbulence distributions strongly enough to cause the surprising changes noted in TKE. It must also be noted that the shear layer growing along the outer periphery of the jet interacts with the vortex breakdown or bursting and loses its coherence, leading to random turbulence. The fact that the occurrence of vortex breakdown manifests itself more emphatically in the variation of TKE is not too surprising since TKE is the most important characteristic of turbulence at a given point in a turbulent flow relative to any other flow characteristic, particularly in a swirling turbulent flow.

F. FLOW VISUALIZATION

The shadowgraph and the laser-induced fluorescence techniques have been used extensively to visualize the surface manifestations and side views

of the swirling jet for various values S and h/d, with and without surface contamination. Although many photographs and video tapes have been made over a wide range of nozzle depths and swirl numbers for both the free and partially-submerged swirling jet, here only the most representative photographs are shown for sake of brevity. Figure 99 shows the surface structures resulting from the impulsive start of the swirling flow (Re = 18,000, F = 6, h/d = 3.5) and two prominent heterostrophic vortices just downstream of the nozzle. Figure 100 shows the surface signatures at an arbitrary instant in time for the same flow conditions. Figure 101 shows a free swirling turbulent jet in deep-submergence mode. The same jet is shown in the vicinity of the surface in Fig. 102. It is clear that the effect of the free surface is to enhance the expansion of the jet and the development of small-scale coherent structures resulting from the centrifugal instability (see the lower part of the jet in Fig. 102). Finally, Figs. 103 and 104 show the flow patterns resulting from a swirling jet decelerating in the vicinity of a free surface. The symmetry of the structures is due to the capture of both the real and reflected images on film.

G. ASSESSMENT OF NUMERICAL SIMULATIONS

Attempts have been made to predict numerically the behavior of swirling jets discharging into an infinite medium. The reason for this is that the flows of this type provide ideal benchmark tests for turbulence closures since their behavior is determined more by turbulent transport than by pressure effects. The prediction of the free swirling jets has highlighted defects in nearly all current closure models. This is believed to be primarily

due to the sensitivity of the turbulence in a thin shear layer to streamline curvature. The existing simple eddy-viscosity models are not yet capable of capturing the said sensitivity. There are, to be sure, ad-hoc corrections which lead to one physics/one model situation, i.e., the closure model solves only one problem and rarely perform well in flows other than those which were used in their calibration.

Launder and Morse (1979) have identified shortcomings in a pressure-strain model as one of two major weaknesses in a second-order closure when applied to the prediction of a round jet, with or without swirl. One conclusion Launder and Morse drew from their calculations was that their pressure-strain model would not work satisfactorily and that a more elaborate model of the mean-strain effects would be needed. Gibson and Younis (1986) have arrived at the opposite conclusion. In fact, they have shown that significant improvements may be obtained from the simplest of pressure-strain models (simpler than that used by Launder and Morse) when the model constants are adjusted to give relatively less weight to the mean-strain component, and more to the turbulence component, than had previously been thought necessary. They have shown that the ability of the model to predict the development of simple shear flows is unaffected, provided that ratios of the model constants remain the same. But, that is the problem since it leads to one physics/one model situation when one does not have data to use as a control point to suitably adjust the ratios of the model constants.

Most recently, Younis, Gatski, and Speziale (1996) used the pressure-strain model of Speziale, Sarkar and Gatski (SSG model) which is quadratic in the Reynolds stresses. Furthermore, they have also used the two versions of

45

the Launder, Reece and Rodi model which are linear in the same terms. All models were used as part of a complete second-order closure based on the solution of differential transport equations for the solution of free turbulent jets with and without swirl for a swirl number of S = 0.4. Even though the present investigation dealt with S = 0.265, 0.5, and 0.522, it was thought to be sufficiently interesting to compare the prediction of Younis et al. (1996) with the data obtained in the present investigation for S = 0.265. The case of S = 0.50 was not considered appropriate since it is, as noted earlier, a critical case separating the reverse-flow state from the no-reverse-flow state. It must be emphasized that all comparisons are for the deep-submergence case since there are at present no comparable simulations for the shallow-submergence case.

Figures 105 through 112 show the comparison of the numerical predictions (dashed lines), based on the SSG model, with those obtained experimentally (open circles) in a plane at x/d = 4. Bearing in mind the fact that the experiments are for S = 0.265 and the calculations are for S = 0.4, the normalized velocity components u and v are quite comparable. As far as the u'^2, v'^2, and w'^2 are concerned, the comparisons are not as satisfactory even though the shapes are similar. The w'^2 component is well predicted, at least near the axis of the jet. As to the Reynolds stresses u'v' and v'w', they are not too far off from the measurements considering the fact that they are considerably smaller than u'w' which is rather well simulated, as seen in Fig. 112. Finally, it should be noted that comparisons at other x/d values (x/d = 2, 6, and 10) yielded similar conclusions. It is hoped that it would be possible to carry out numerical simulations with the SSG model for S = 0.265, 0.5, and

0.522 for a more detailed and appropriate comparison. There is a strong motivation for such a comparison for the success of the effort will enable one to attempt to the same for the more challenging and technologically significant case of a swirling jet beneath a free surface.

V. CONCLUSIONS

The investigation described herein dealt with the study of the turbulent flow created by a round swirling jet issuing from a nozzle into a large medium of identical fluid (free swirling jet) and then with that issuing beneath and parallel to a free surface, using a three-component laser Doppler velocimeter and flow visualization (laser-induced fluorescence and shadowgraph techniques). The results have shown that:

1. Swirl leads to the faster spreading and quicker mixing of the jet as evidenced by flow visualization. As the jet develops, viscous dissipation reduces the maximum swirl velocity within the jet. This leads to a relaxation of the radial pressure gradient and hence to the larger outward spreading of the jet relative to the non-swirling jet.

2. The similarity of the velocity profiles is achieved at distances as close as 4d from the nozzle for weak (S = 0.265) and critical (S = 0.50) swirling jets. For strongly swirling jets (S = 0.522), the similarity is not reached within ten diameters downstream.

3. The measurements of turbulent velocity components (u', v', w') have shown that a free swirling jet can be considered to be close to local isotropic turbulence except at the nozzle exit where the free shear layers are still very thin.

4. Both the axial and tangential velocity components decrease outward from the jet axis, naturally leading to centrifugal instabilities. This, in turn, leads to the creation of large scale coherent structures at the periphery

49

of the jet, particularly when it is in the vicinity of the free surface, as seen in photographs.

5.   The turbulence shear stresses (u'v', v'w', u'w') exhibit anisotropic behavior, the largest always being in the plane passing through the jet axis.

6.   For a high swirl number (S = 0.522) where the azimuthal component of velocity is comparable to the axial component, vortex breakdown takes place in the jet core near the nozzle exit (within or outside the nozzle).   The momentum deficit due to the large flow reversal leads to a wake-like velocity profile.

7.   The shear layer growing along the outer periphery of the jet interacts with the vortex bursting and modifies the turbulence field, and leads to the production of high turbulence fluctuations that spread rapidly outward from the vortex core to the shear layer surrounding the jet in the form of weak and very irregular large-scale structures.   It is these particular phenomena that make a swirling jet unique among all shear flows.

8.   The free surface modifies all of the foregoing characteristics of the swirling jet, particularly after a downstream distance of about 10d, within a very thin surface layer, intensifies the anisotropy of the turbulence, and gives rise to numerous clockwise and counter-clockwise rotating vortices attached to the free surface.   The merging of the homostrophic (same sign) vortices lead to reverse energy cascade.

9.   The increase of u' and v' in the surface layer appears to be a low-Froude number phenomenon (F < 1).   At high Froude numbers, u', v' remain (almost uniformly) large near the free surface while w' decreases to small but finite values.   The energy partition to components in the horizontal

plane is still effective, but not as a consequence of the increase of TKE in the surface layer.

10. The change of TKE with S is not monotonic. It is maximum for S = 0.265, smallest for S = 0.50, and has an intermediate value for S = 0.522. This is due to the occurrence of vortex breakdown and the resulting intensification of the turbulence within the jet prior to its exit from the nozzle.

11. The single swirling jet, with or without free-surface effects, embodies all the essential physics, without unnecessary geometric complexities, and provides ideal benchmark tests for turbulence closure models particularly because their behavior is determined more by turbulent transport than by pressure effects. Thus, computational fluid dynamics (CFD) has a major role to play in the free-surface/turbulence interaction, but the simple isotropic eddy viscosity models are not likely to deal with free surface effects. The use of non-isotropic turbulence models (e.g., the SSG model) is now underway.

APPENDIX
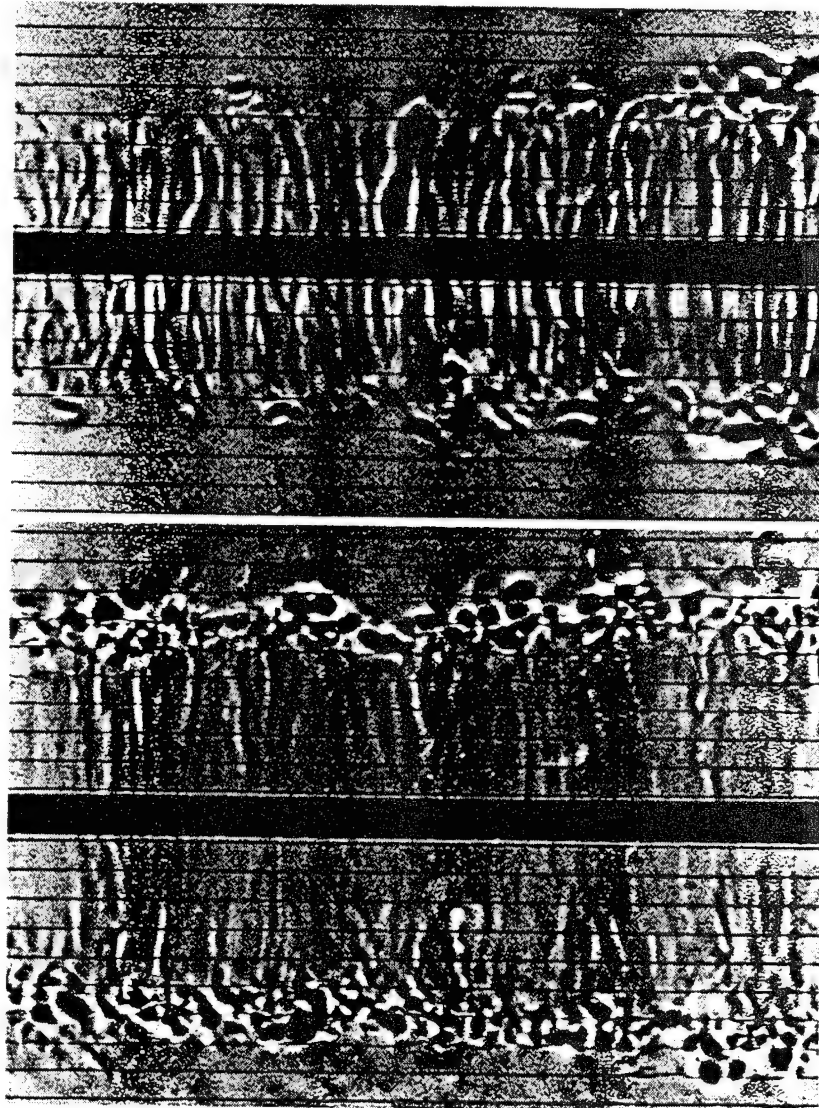
Figure 1.   Scars and striations on a free surface
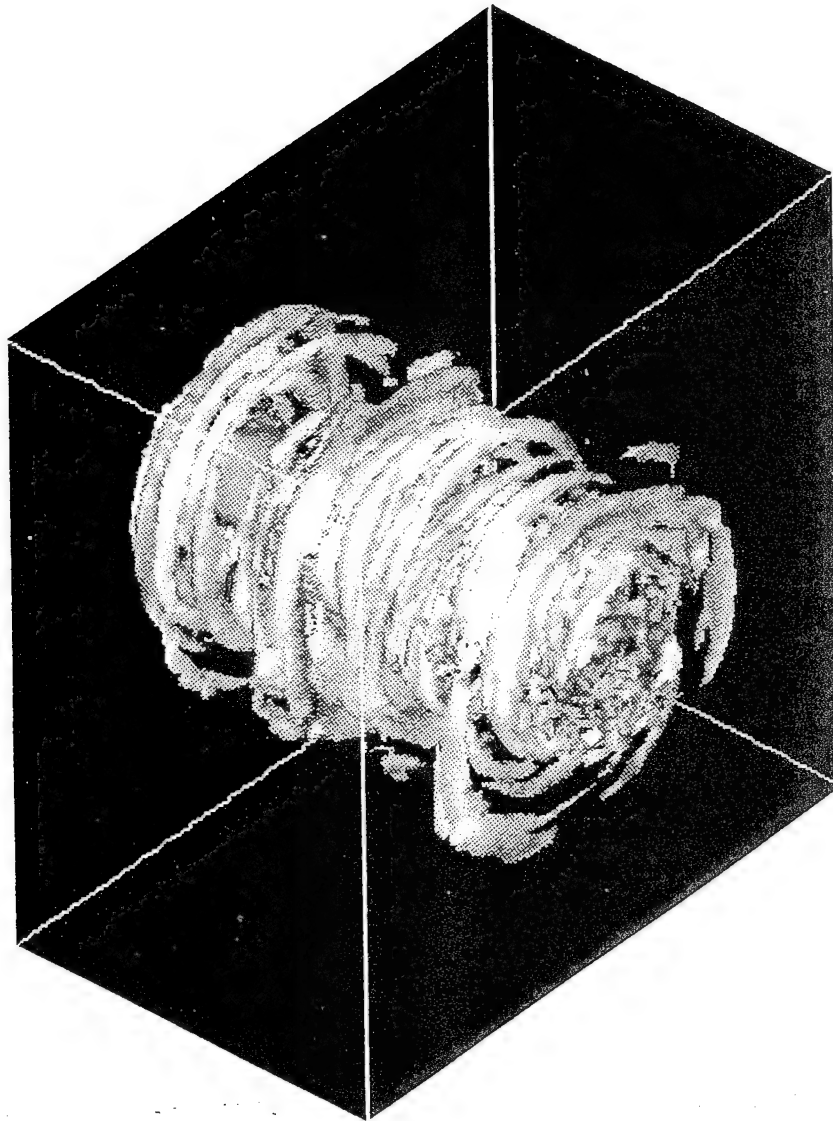
Figure 2.   Development of large-scale helical structures around
              a swirling jet (Sreedhar and Ragab, 1994)
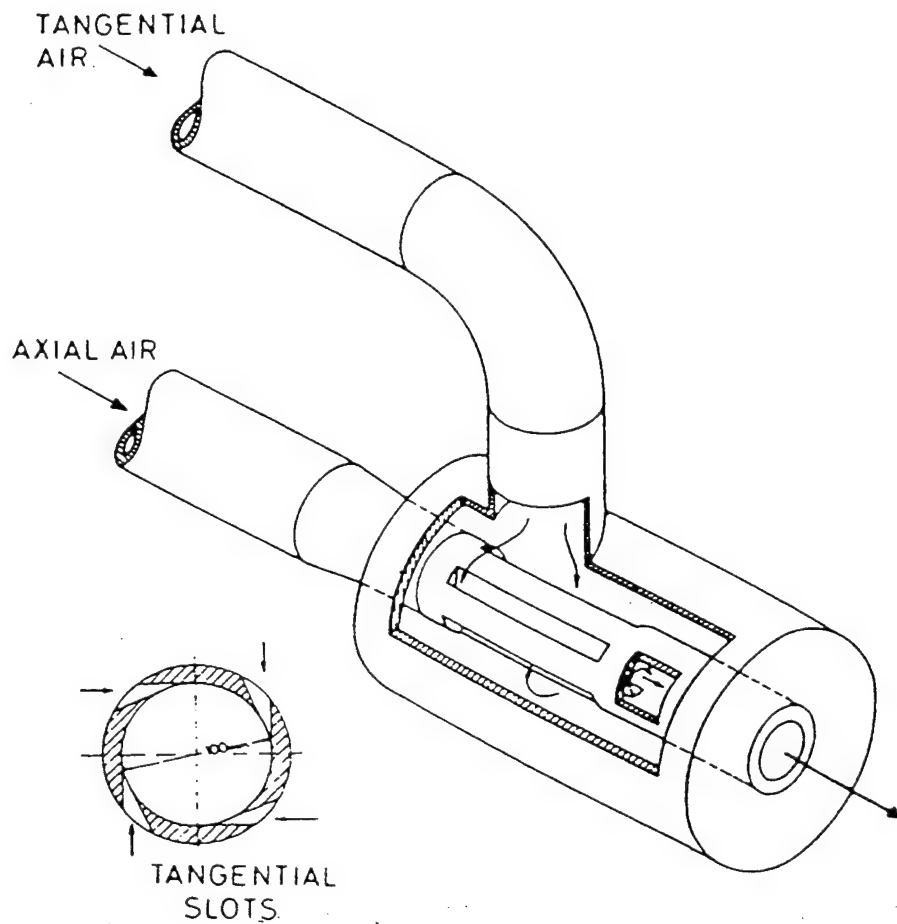
Figure 3.   Axial-plus-tangential-entry swirl generator (Chigier and Chervinsky (1967))

.250 [6.35]

1.625 [41.27]

.450 [11.43]

.875 [22.23]

.625 [15.88]

.341 [8.66]

.063 [1.59]

.250 [6.35]
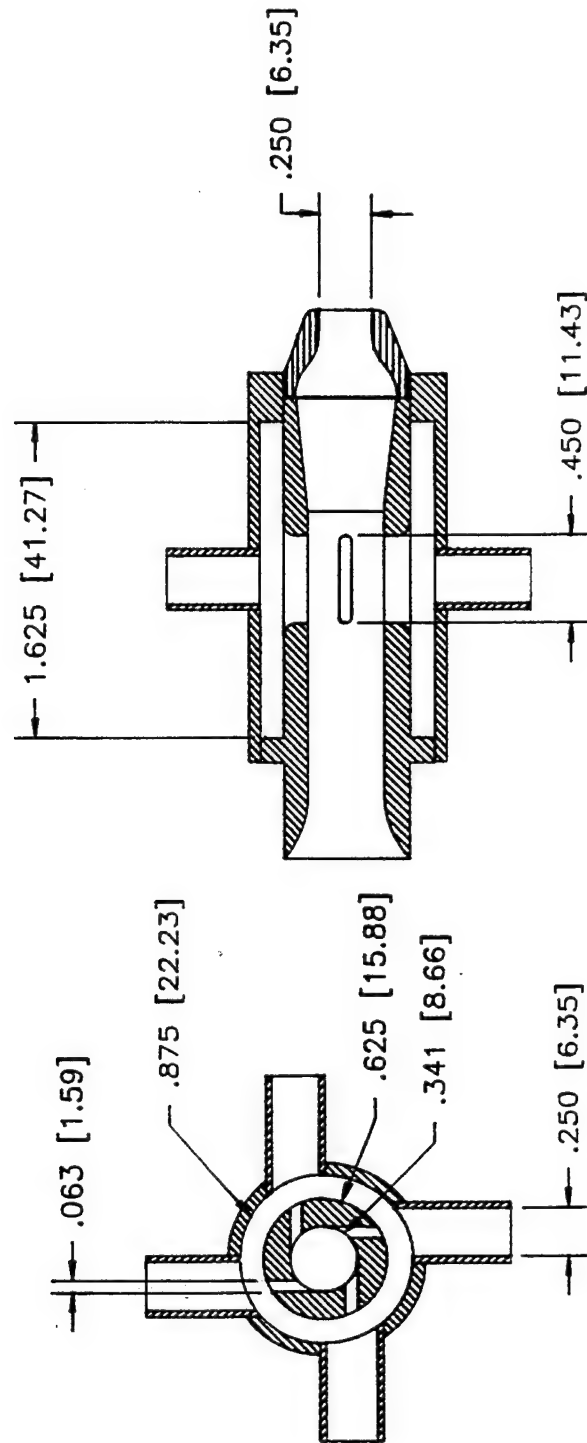
Figure 4.   Axial-plus-tangential-entry swirl generator

56
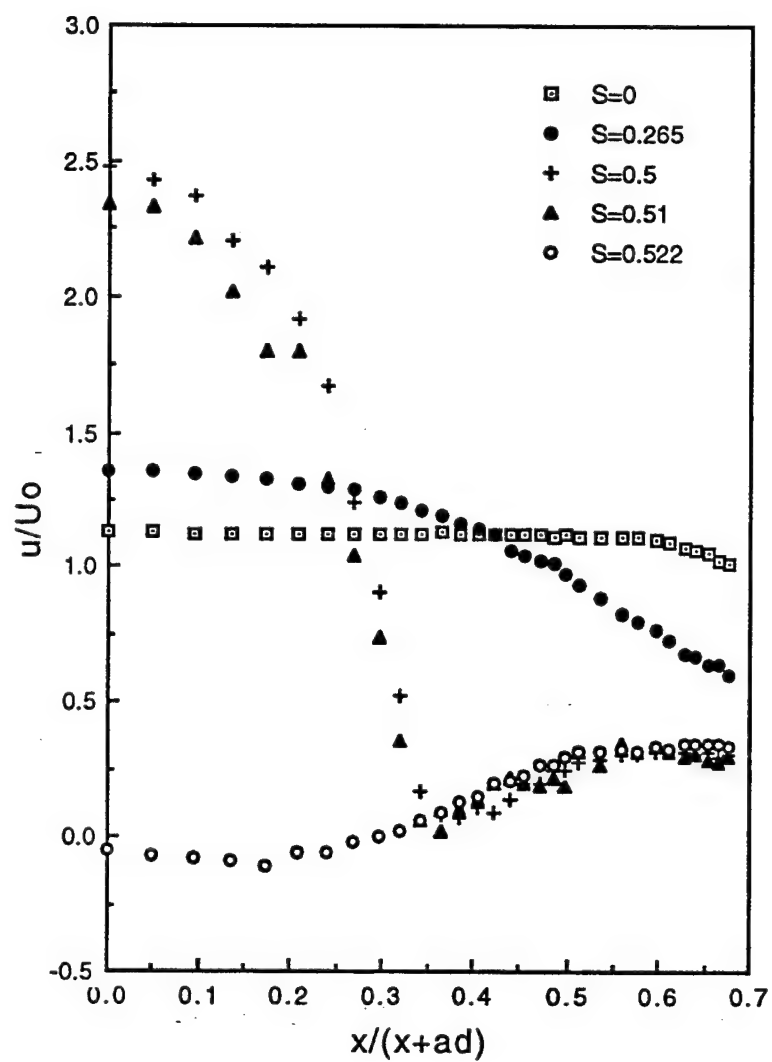
Figure 5.   u/Uo versus x/(x+ad) in the deep mode for
various swirl numbers

57
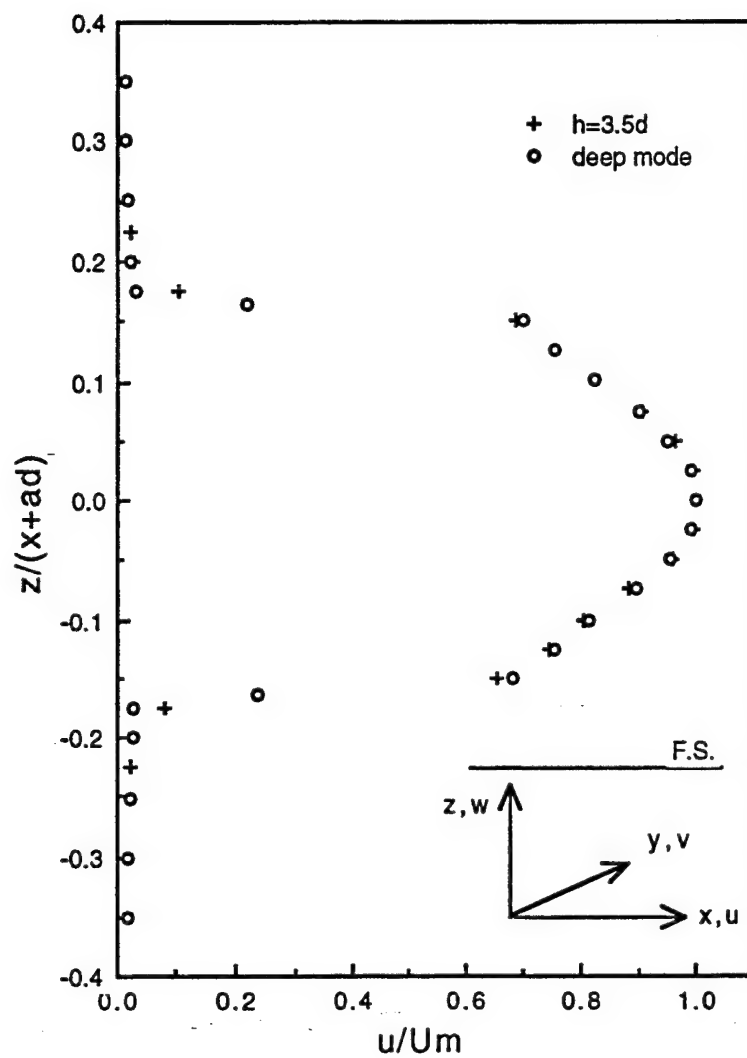
Figure 6.   u/Um versus z* in the deep and shallow modes for
            S = 0.265 at x/d = 0.14
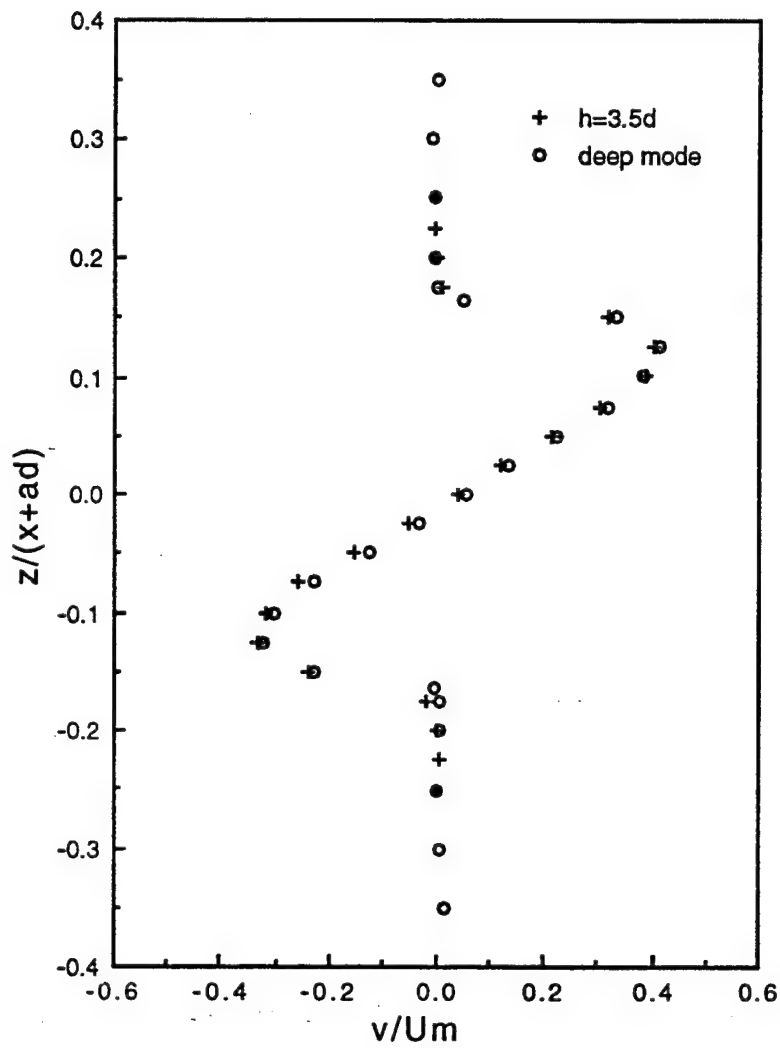
Figure 7. v/Um versus z* in the deep and shallow modes for
S = 0.265 at x/d = 0.14
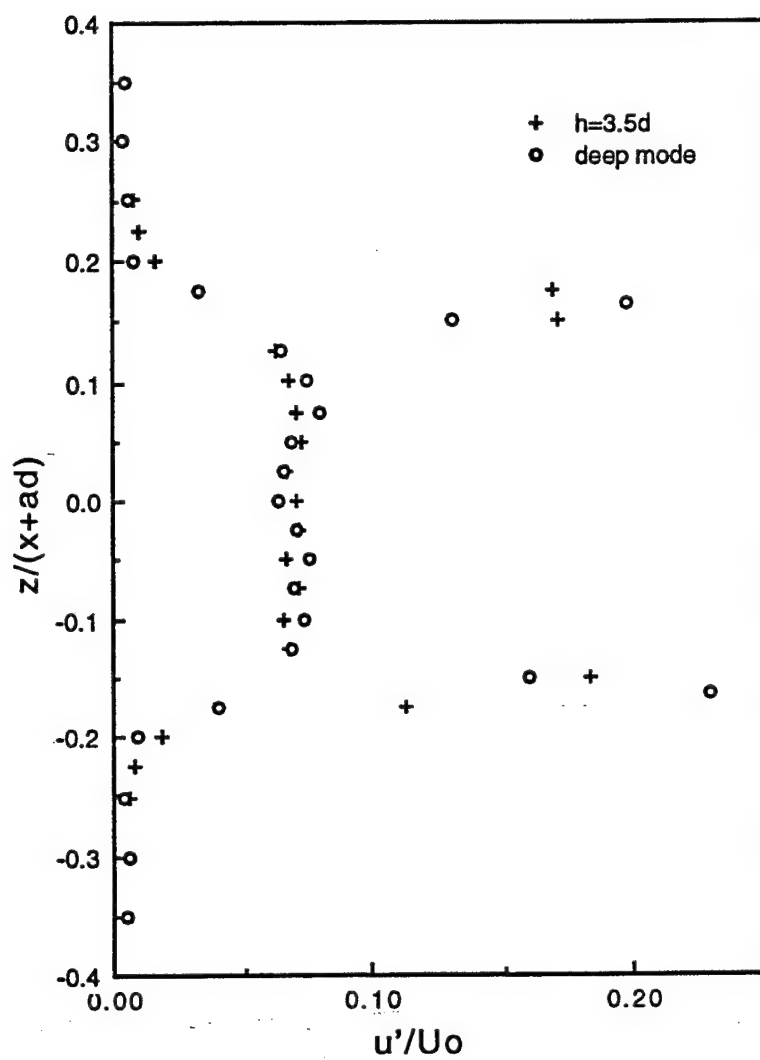
Figure 8.   u'/Uo versus z* in the deep and shallow modes for
S = 0.265 at x/d = 0.14
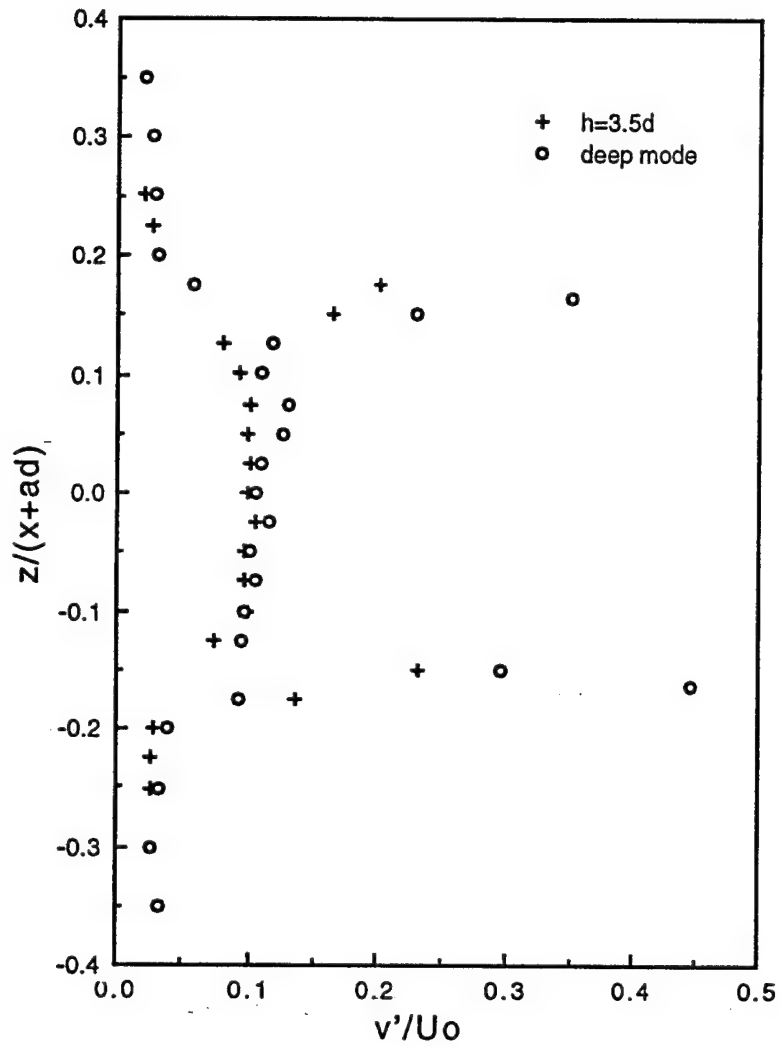
Figure 9.   v'/Uo versus z* in the deep and shallow modes for
S = 0.265 for x/d = 0.14

61
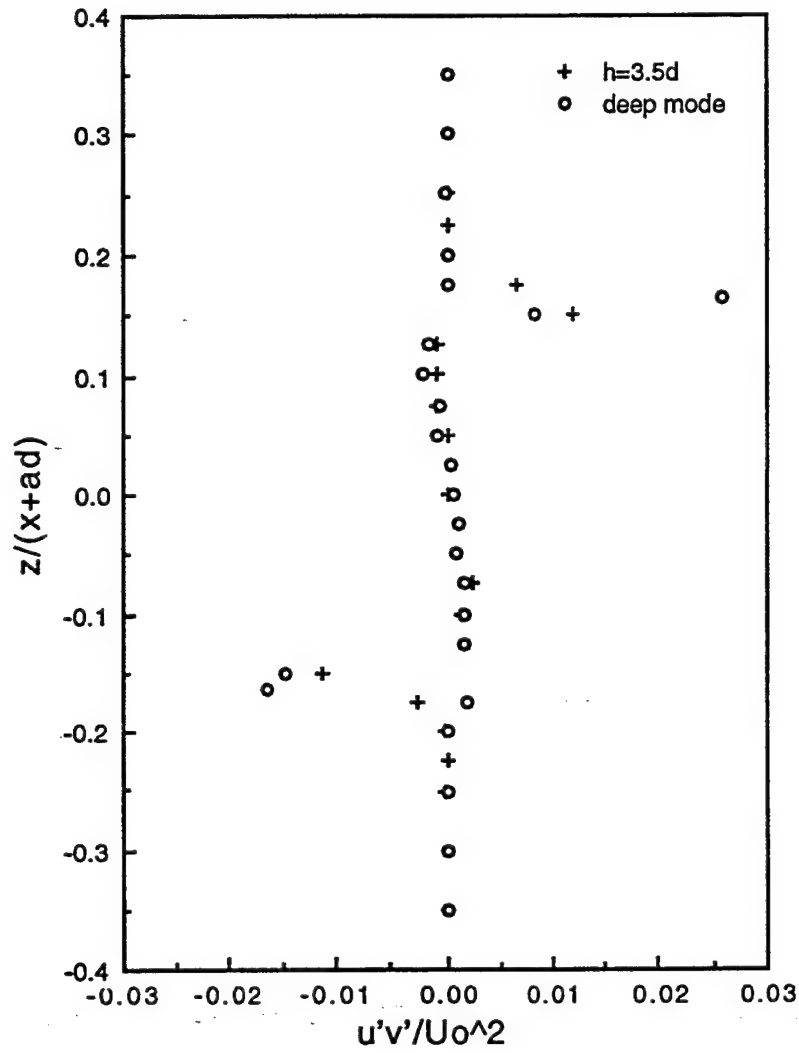
Figure 10. $u'v'/U_0^2$ versus z^* in the deep and shallow modes
for $S = 0.265$ at $x/d = 0.14$

62
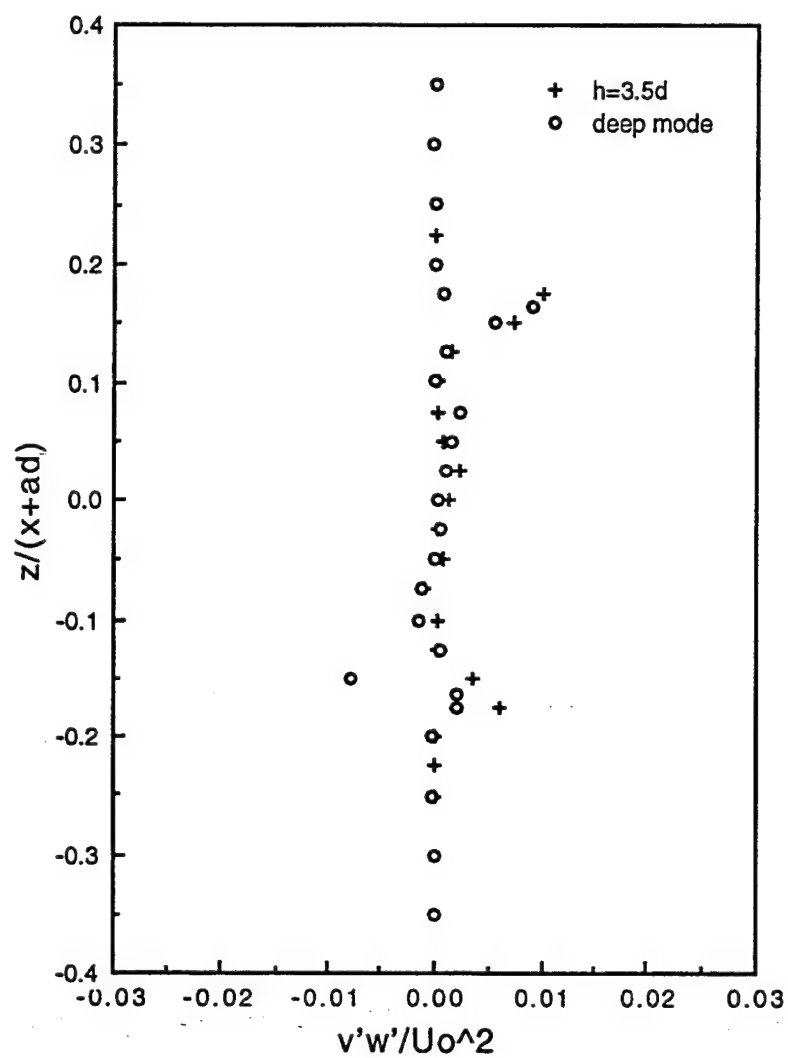
Figure 11. $v'w'/U_0^2$ versus z^* in the deep and shallow modes
for S = 0.265 at x/d = 0.14

63
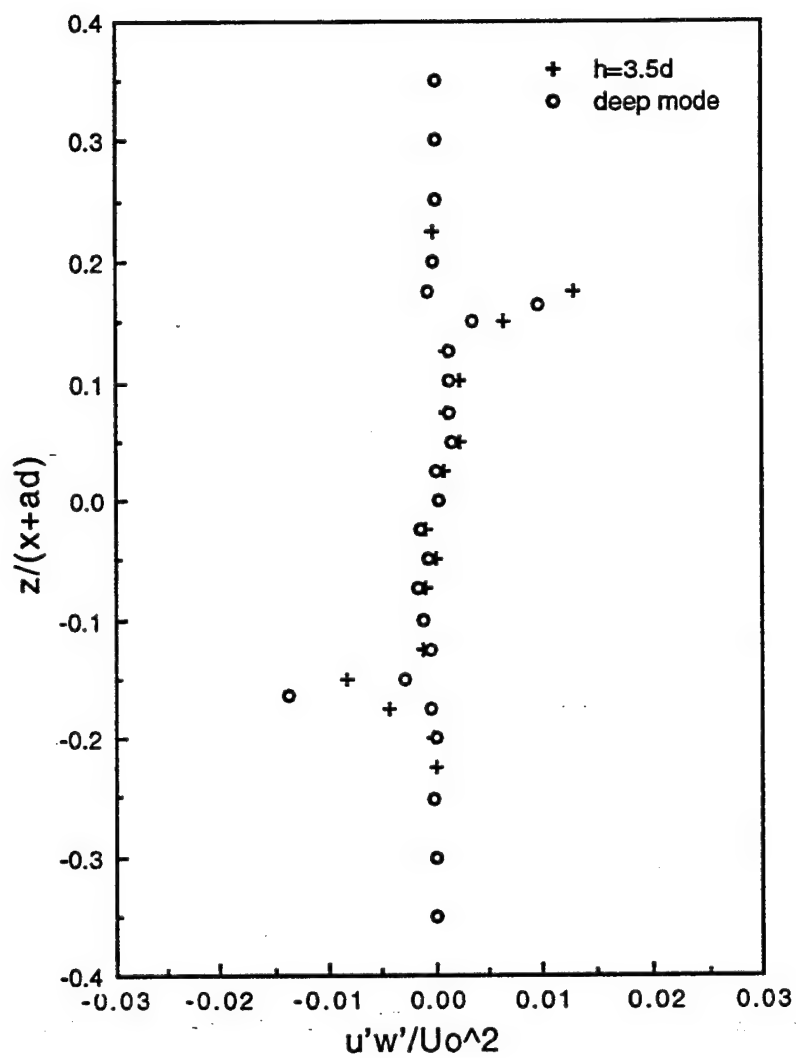
Figure 12. $u'w'/U_0^2$ versus z* in the deep and shallow modes for S = 0.265 at x/d = 0.14
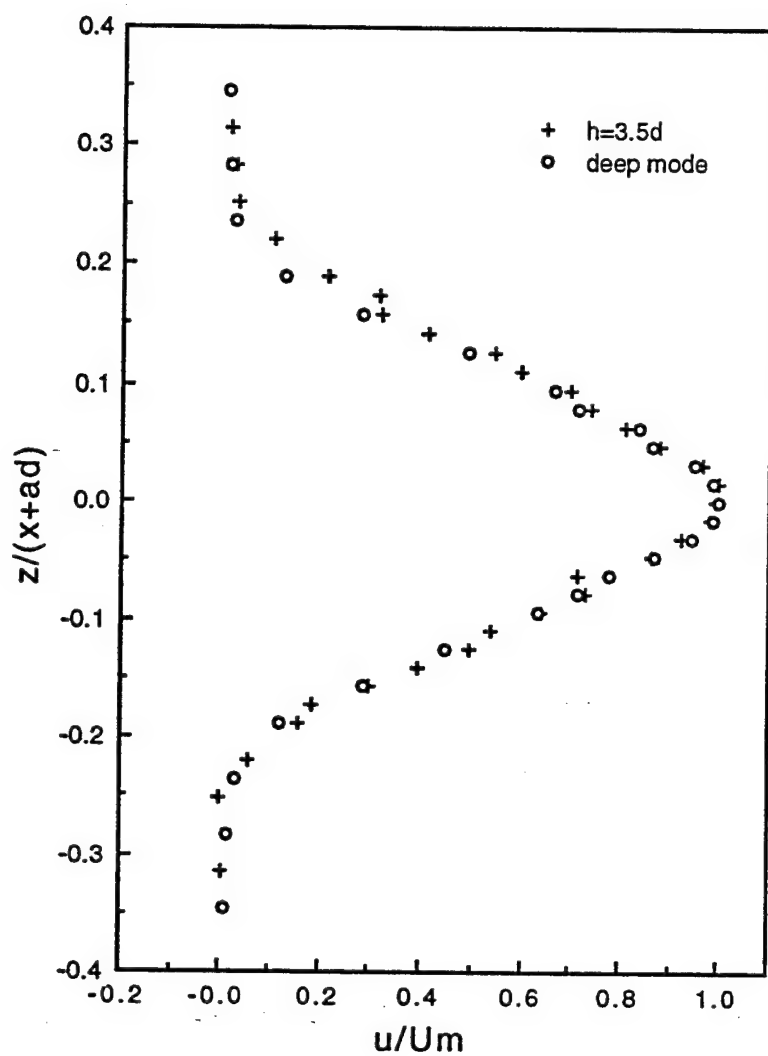
Figure 13.   u/Um versus z* in the deep and shallow modes for
              S = 0.265 at x/d = 2
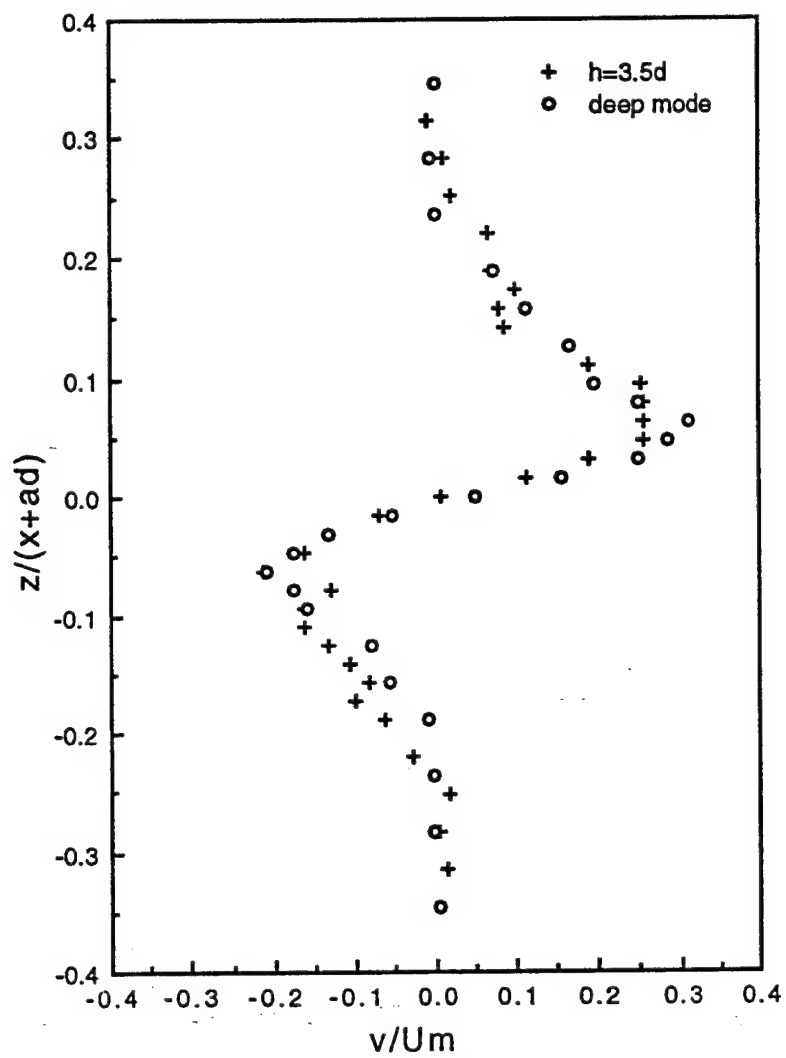
Figure 14.   v/Um versus z* in the deep and shallow modes for
               S = 0.265 at x/d = 2
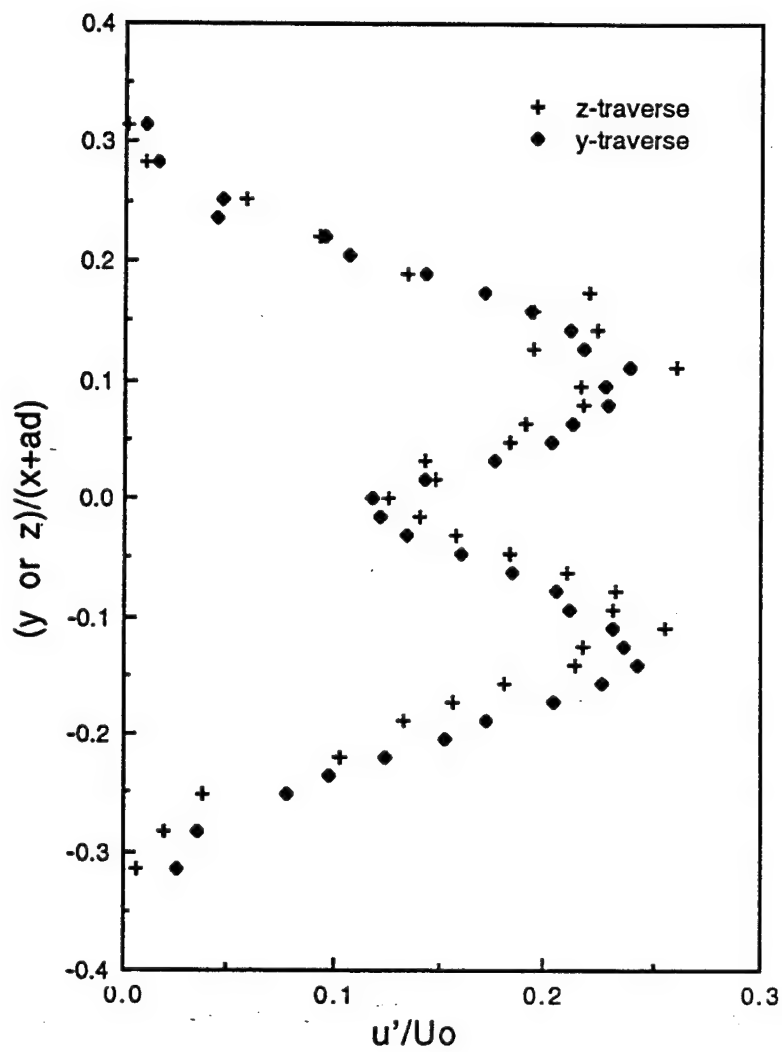
Figure 15.   u'/Uo versus y* and z* in the shallow mode for
              S = 0.265 at x/d = 2

67
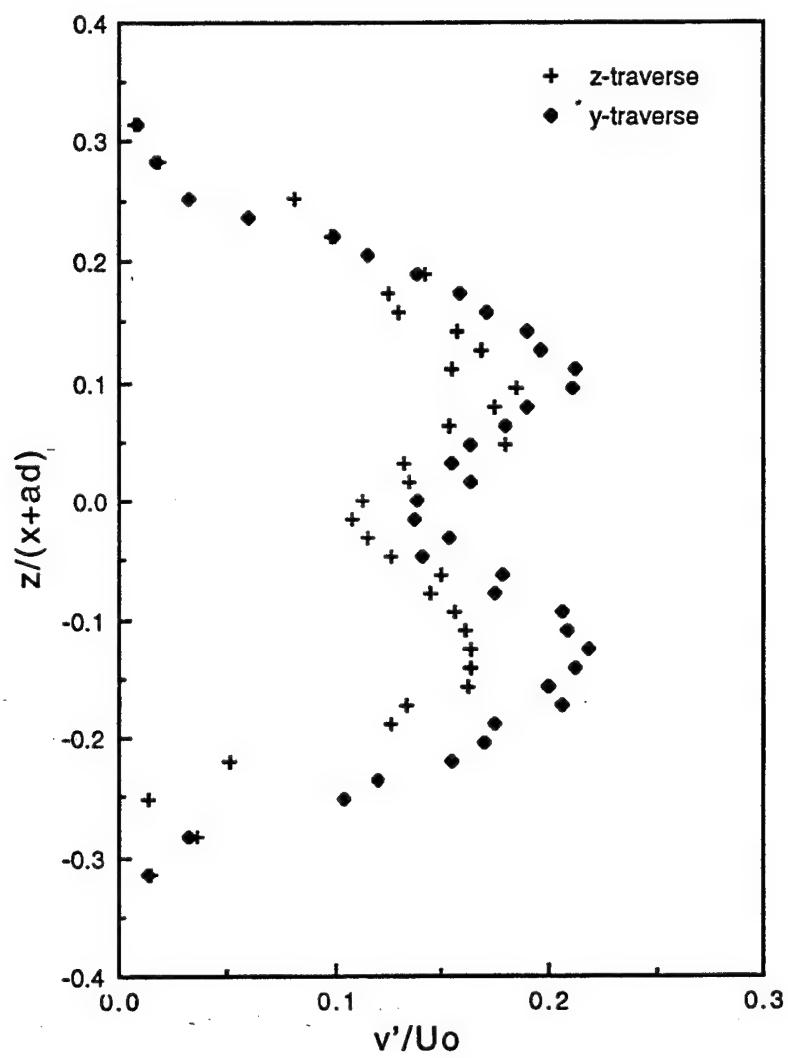
Figure 16.   v'/Uo versus y* and z* in the shallow mode for
S = 0.265 at x/d = 2
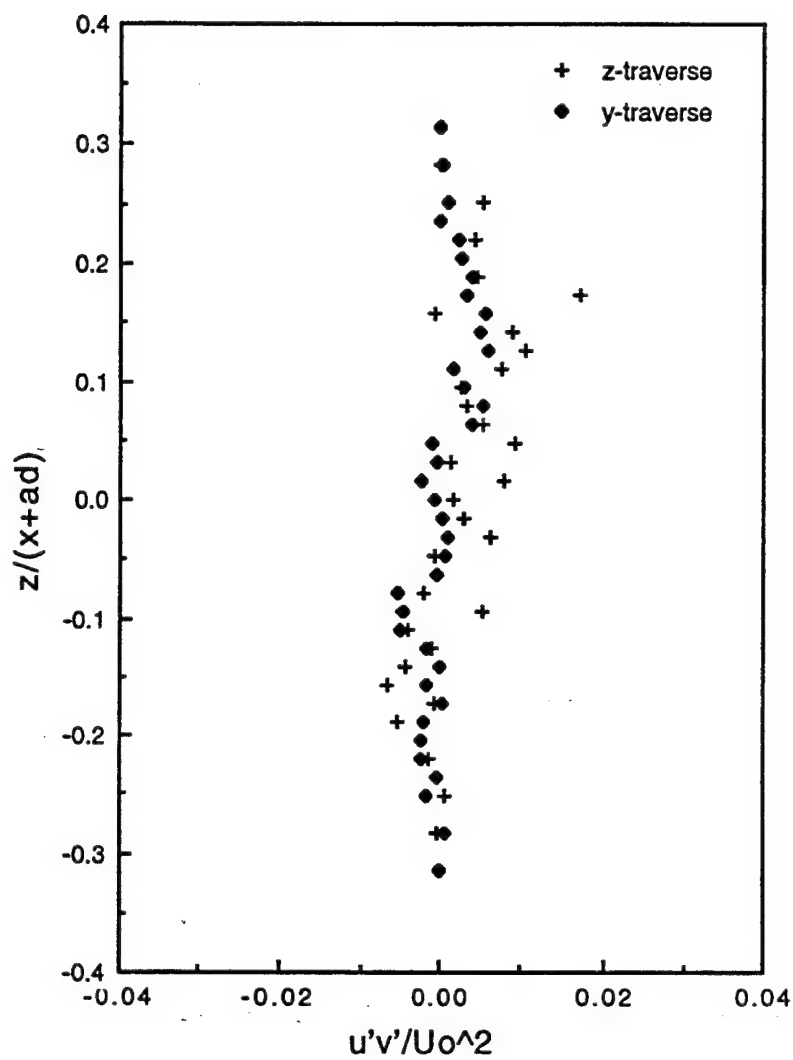
Figure 17. $u'v'/U_0^2$ versus y^* and z^* in the shallow mode for
S = 0.265 at x/d = 2

69
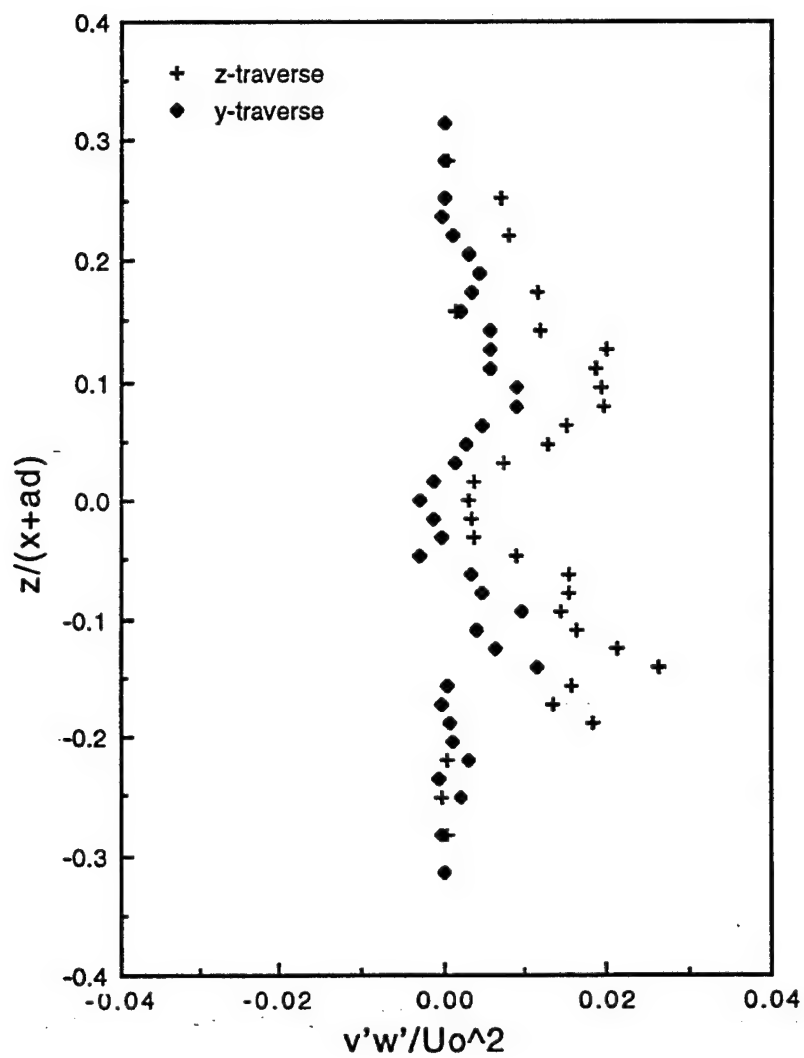
Figure 18. $v'w'/U_0^2$ versus y^* and z^* in the shallow mode for
S = 0.265 at x/d = 2
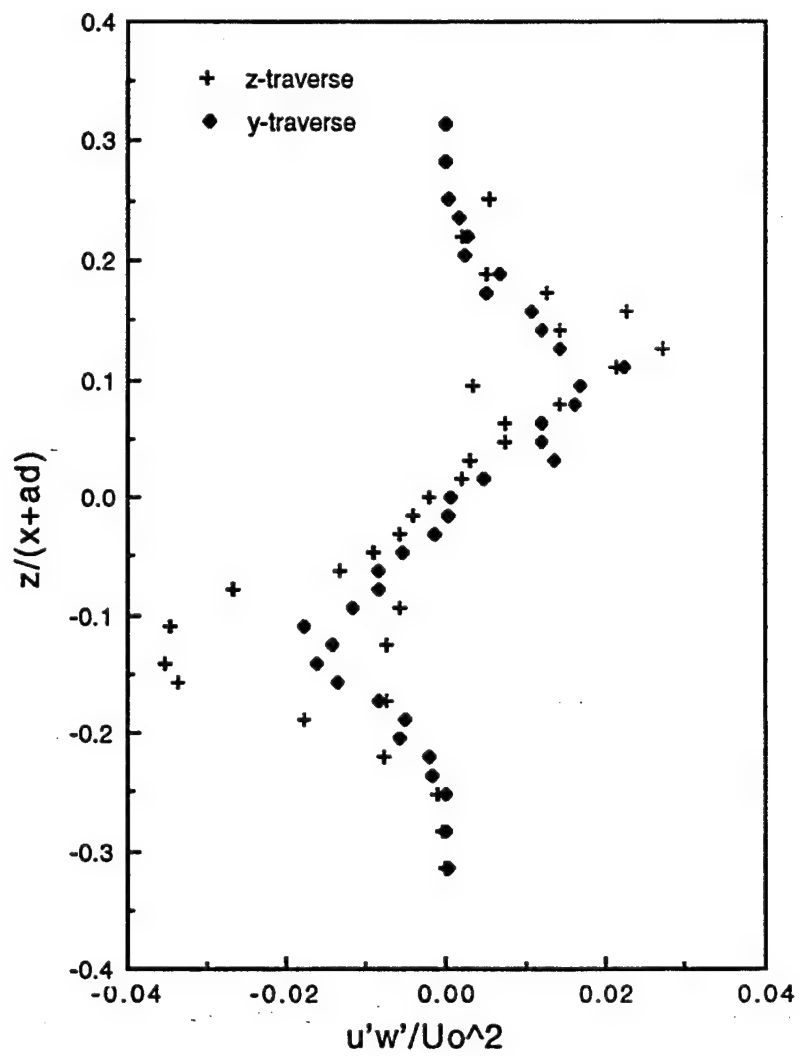
Figure 19. $u'w'/U_0^2$ versus y^* and z^* in the shallow mode for
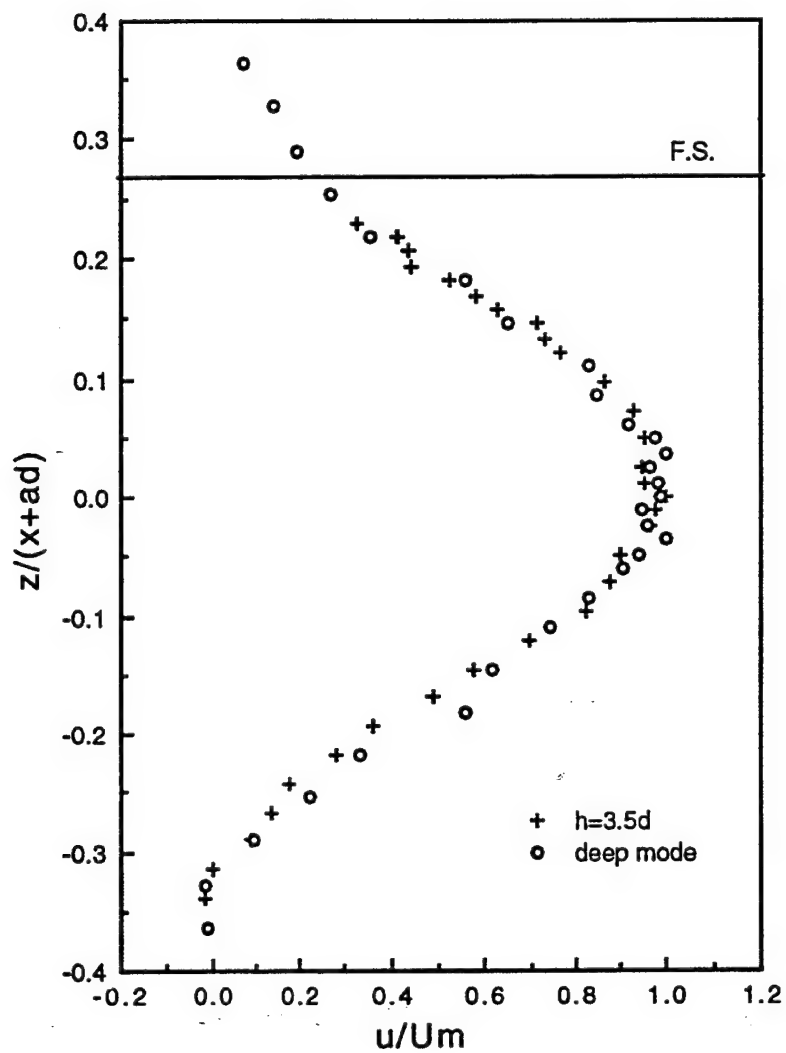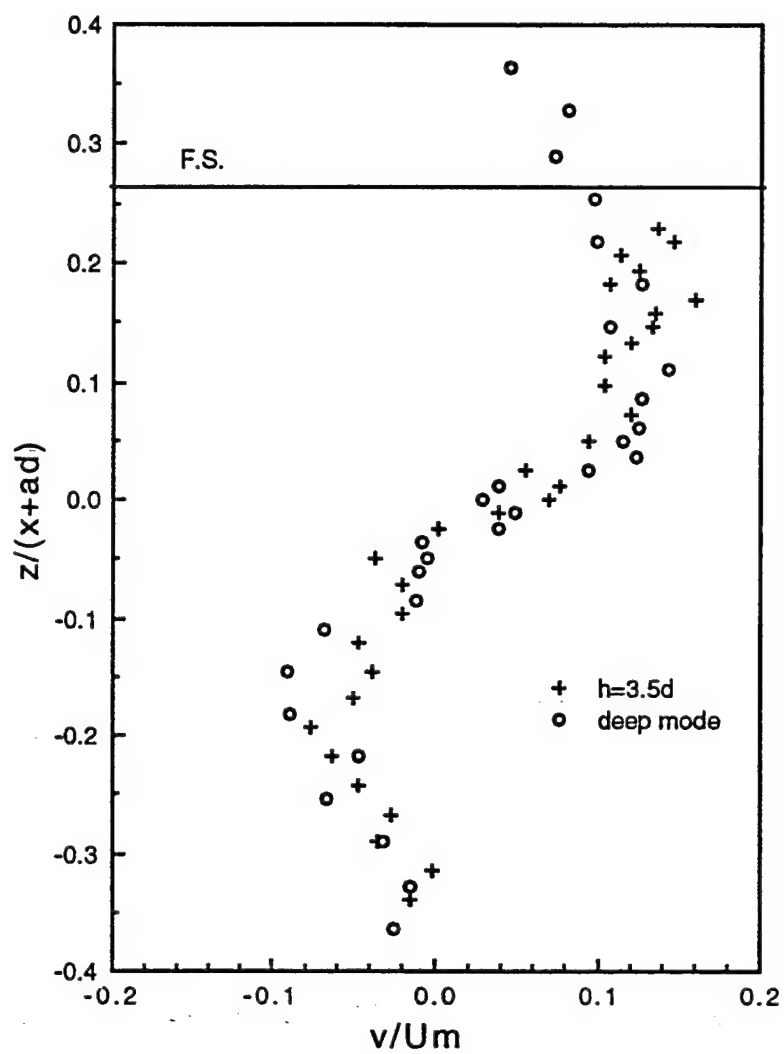S = 0.265 at x/d = 2
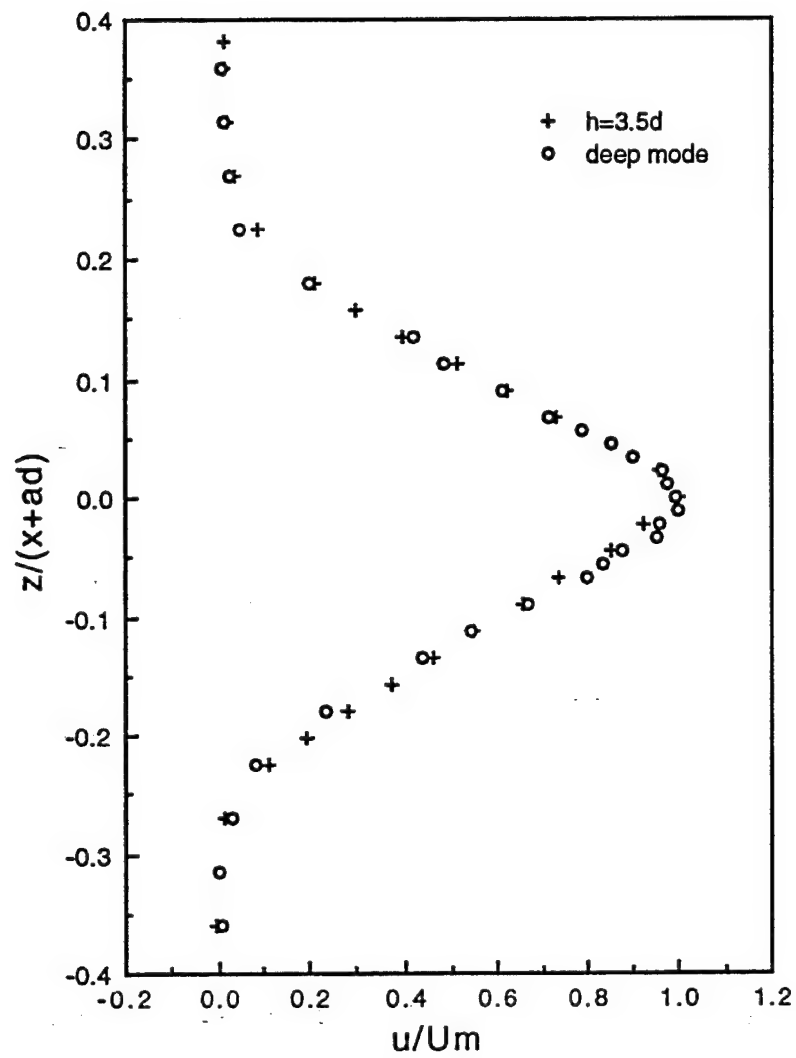
Figure 20.   u/Um versus z* in the deep and shallow modes for
S = 0.265 at x/d = 4

Figure 21.   v/Um versus z* in the deep and shallow modes for
             S = 0.265 at x/d = 4
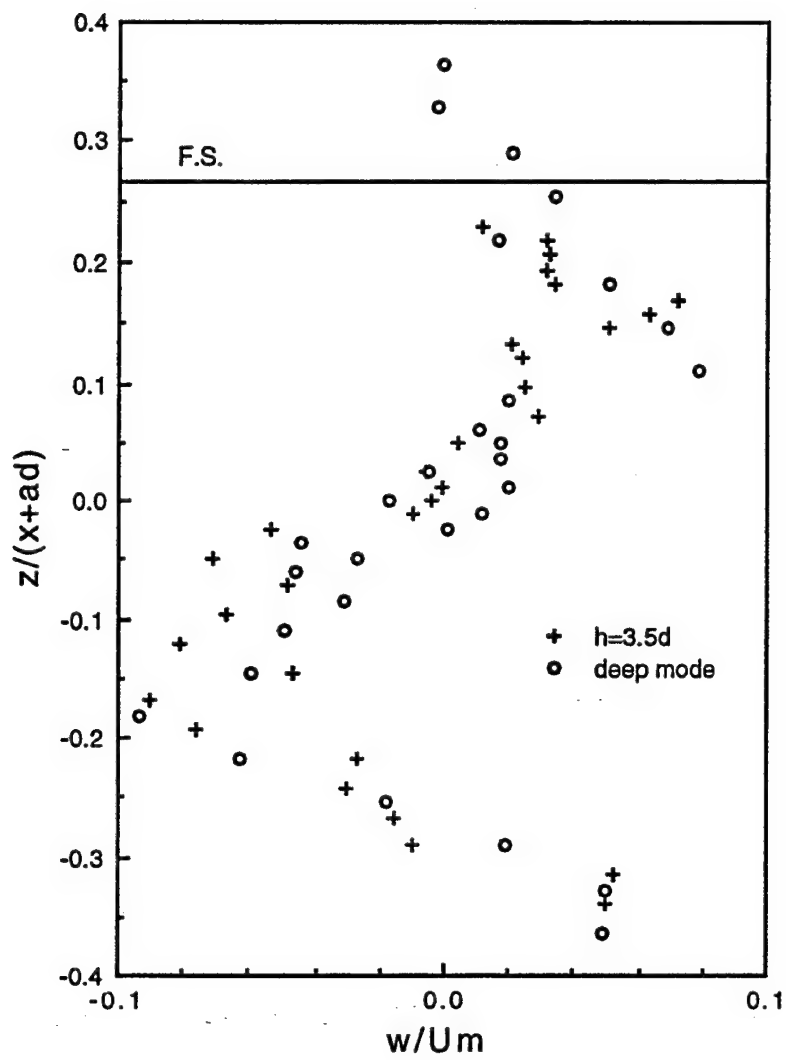
Figure 22.   u'/Uo versus z* in the deep and shallow modes for S = 0.265 at x/d = 4

74

Figure 23.   v'/Uo versus z* in the deep and shallow modes for
S = 0.265 at x/d = 4

75
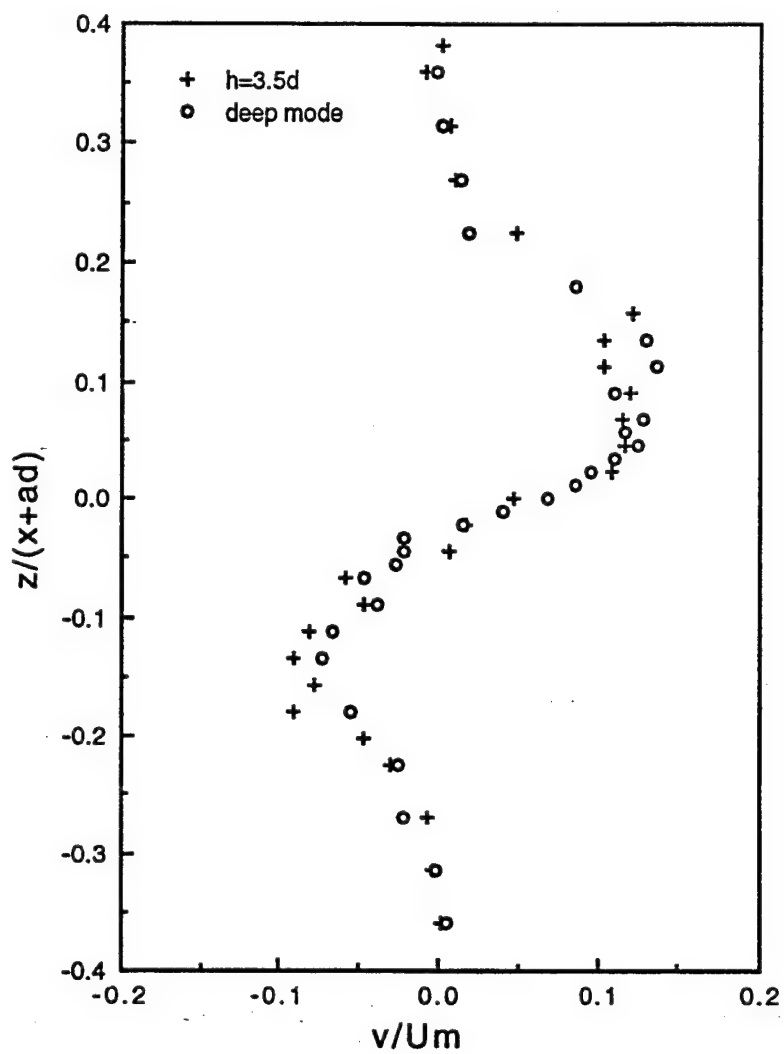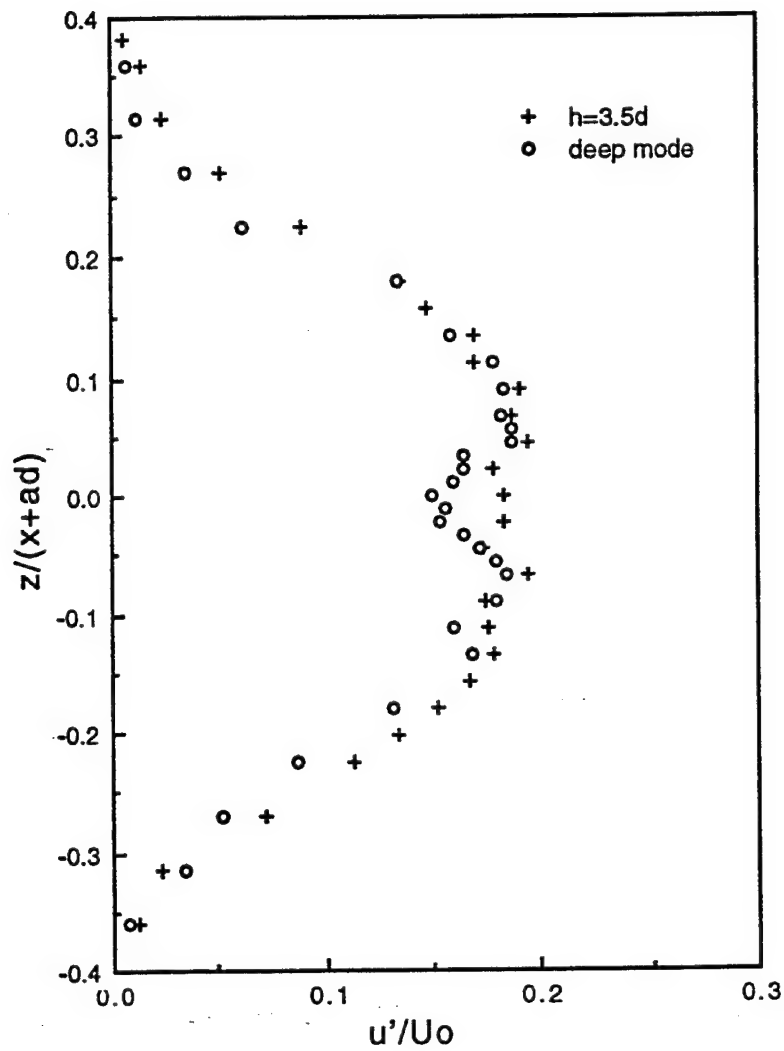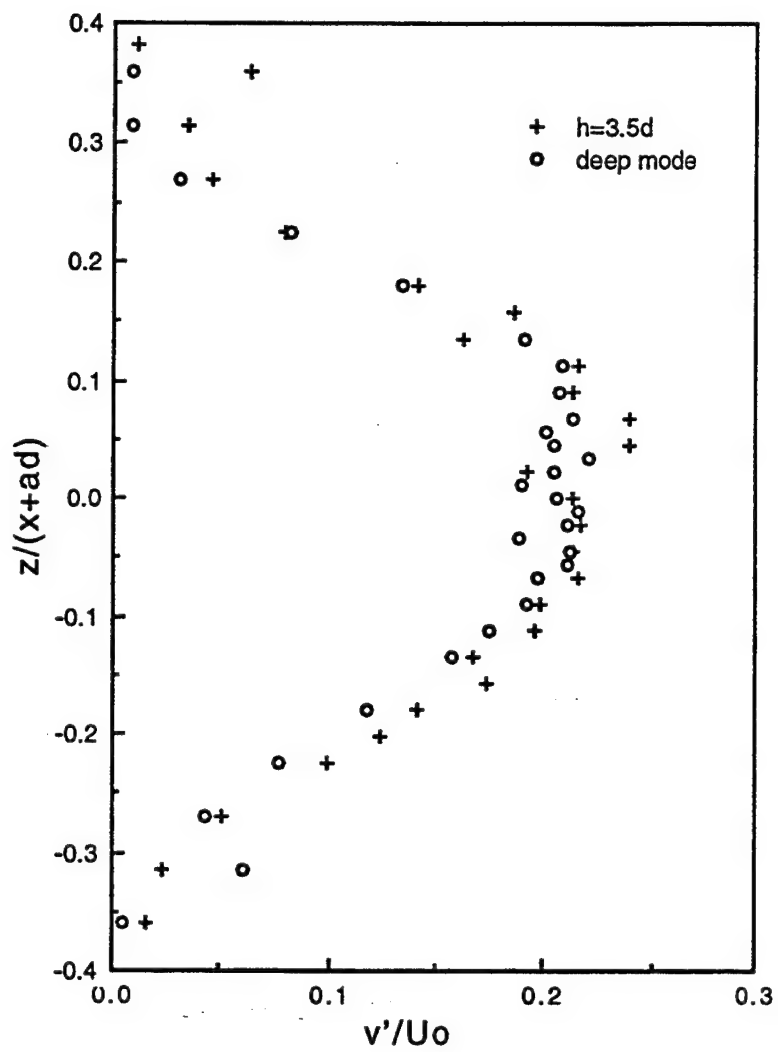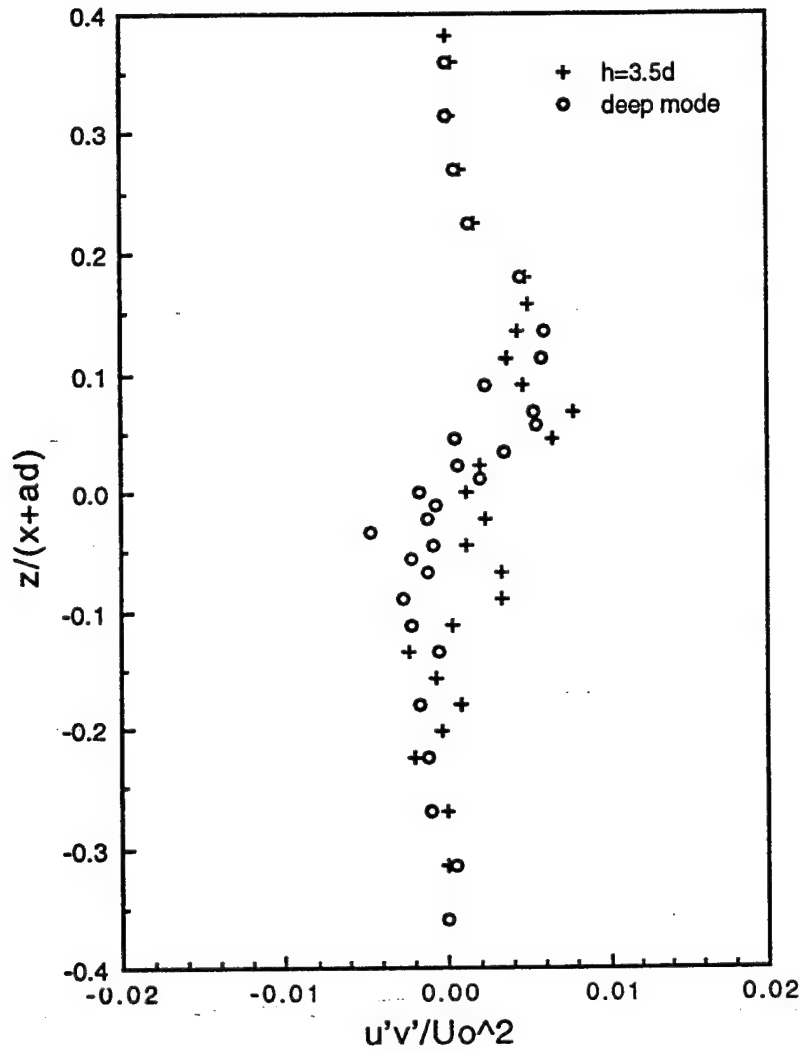
Figure 24. $u'v'/U_0^2$ versus z* in the deep and shallow modes
                for S = 0.265 at x/d = 4
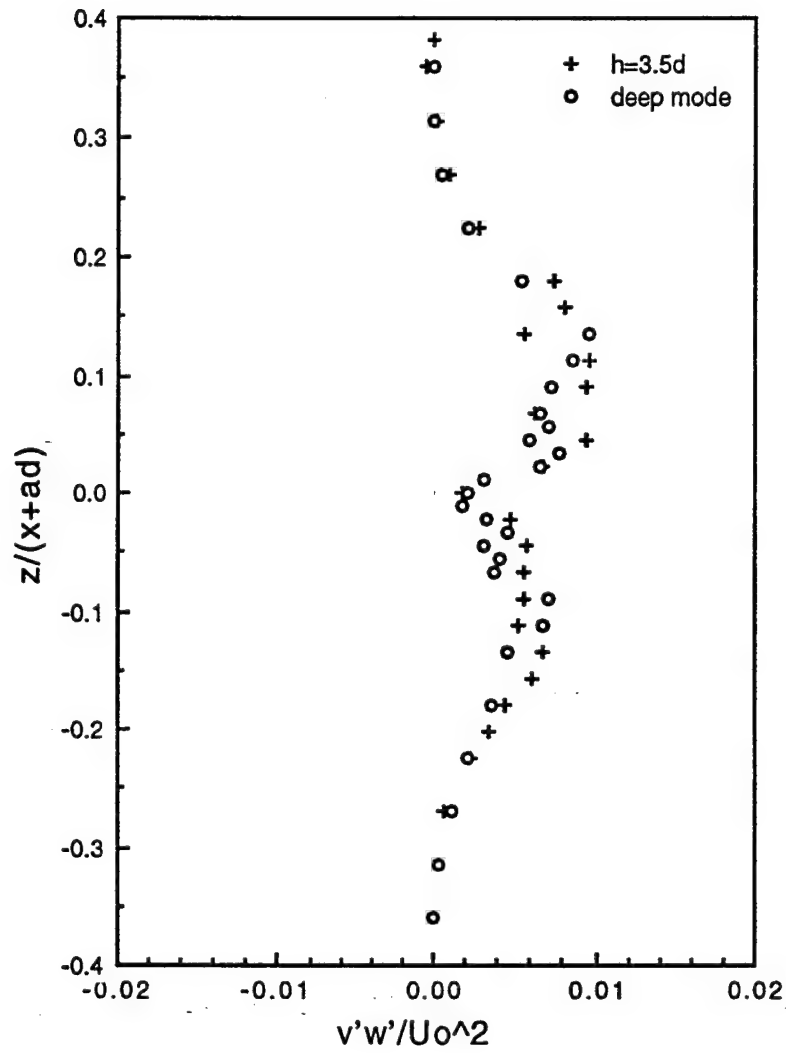
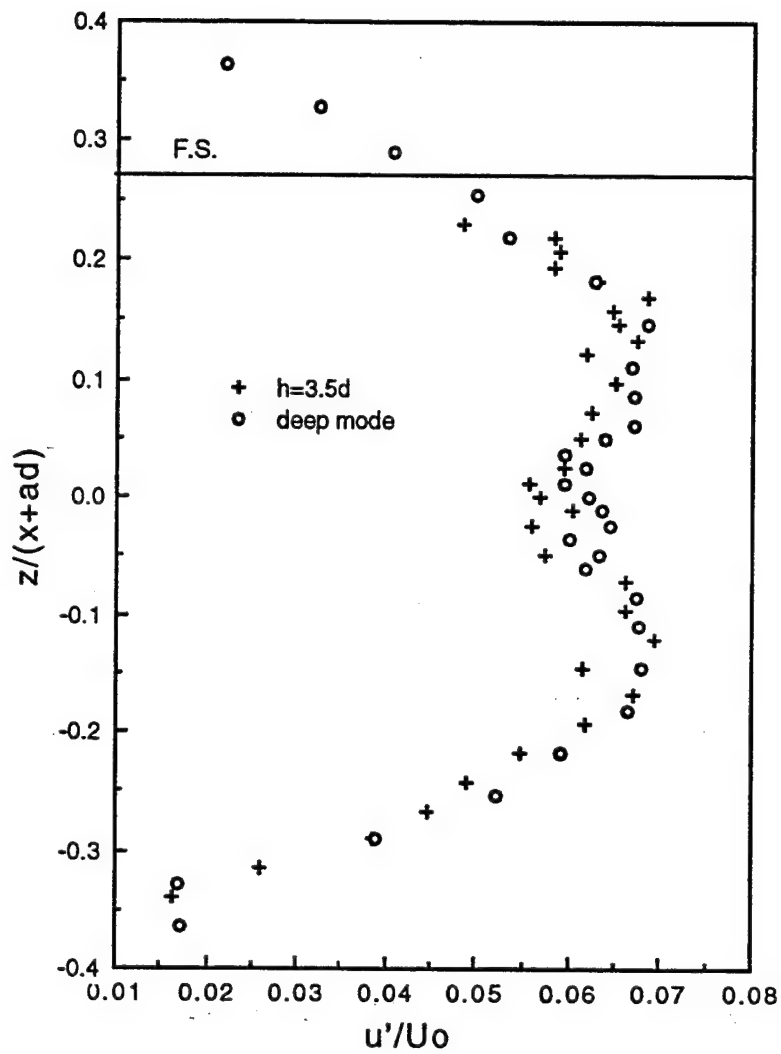Figure 25. $v'w'/U_0^2$ versus z* in the deep and shallow modes
for S = 0.265 at x/d = 4
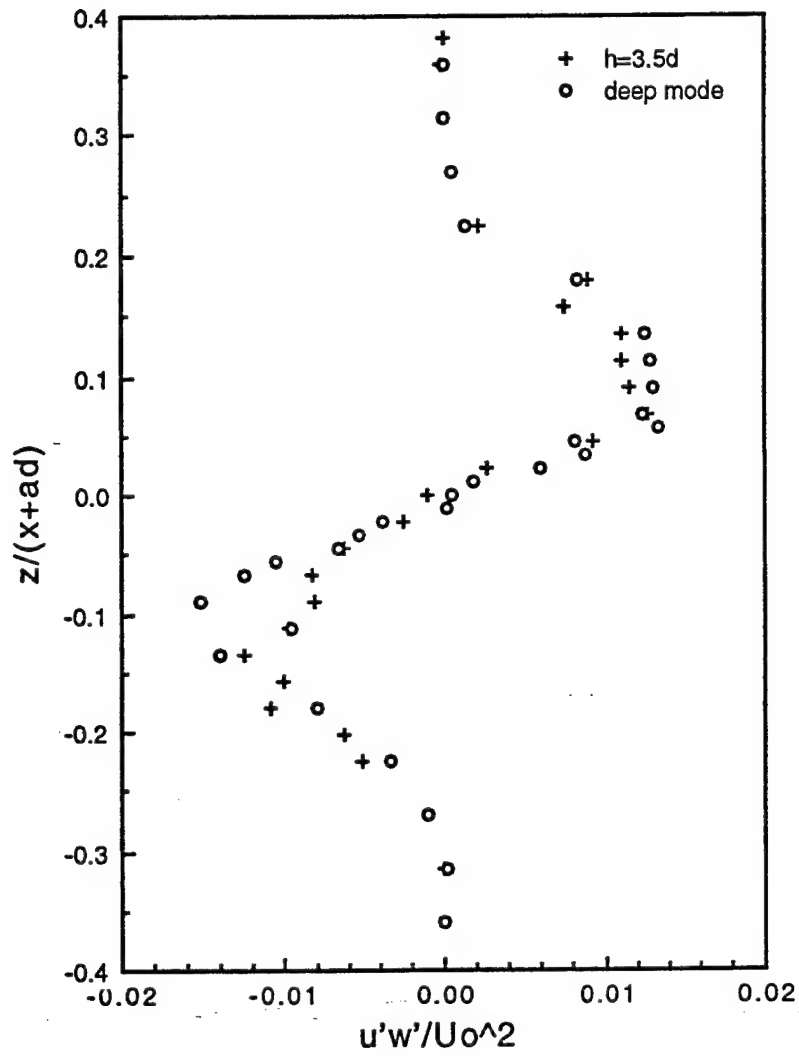
Figure 26. $u'w'/U_o^2$ versus z^* in the deep and shallow modes for $S = 0.265$ at $x/d = 4$
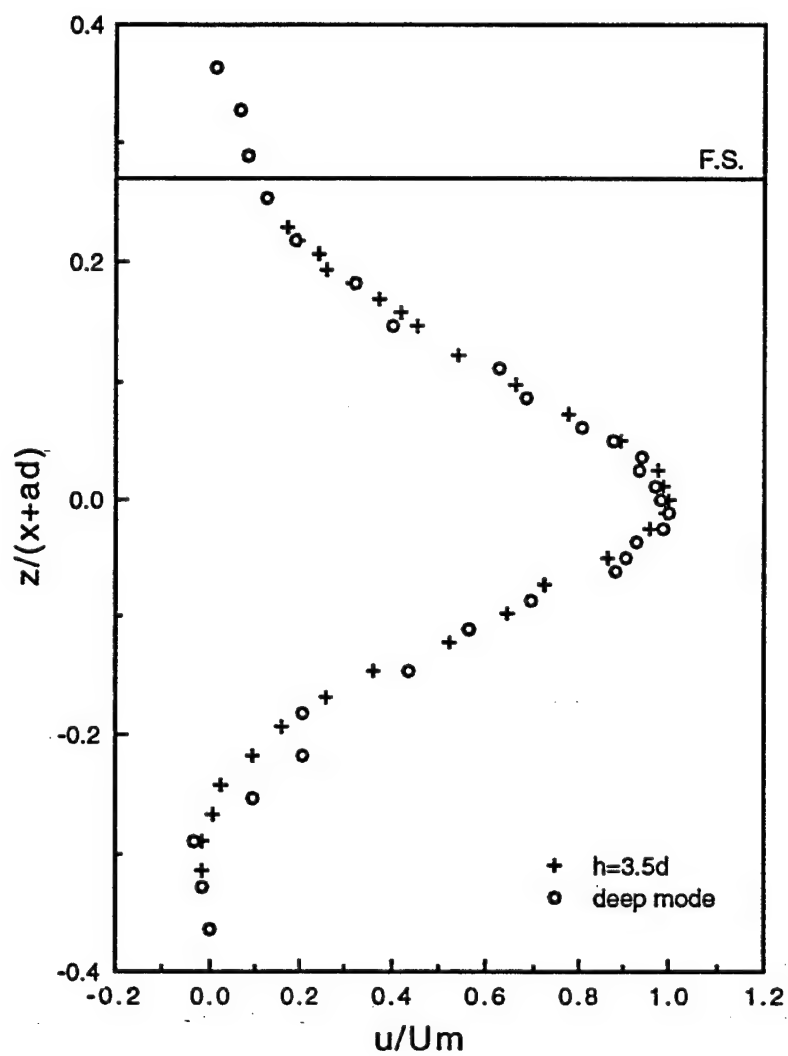
Figure 27.   u/Um versus z^* in the deep and shallow modes for
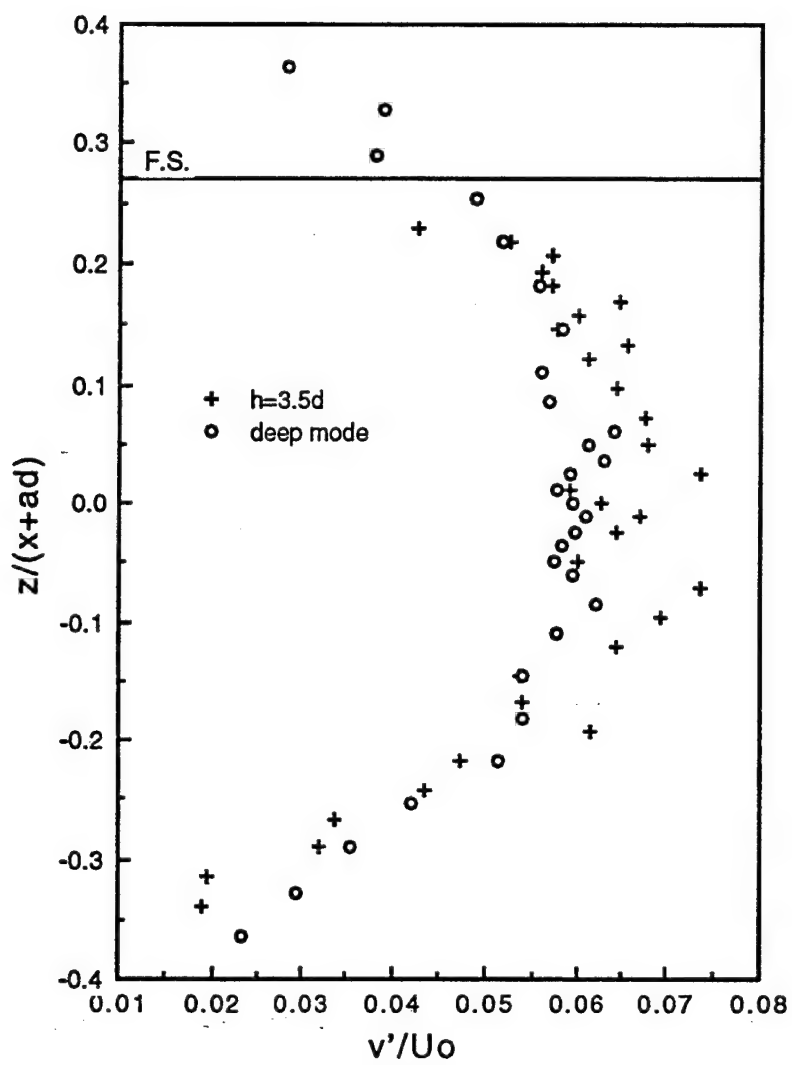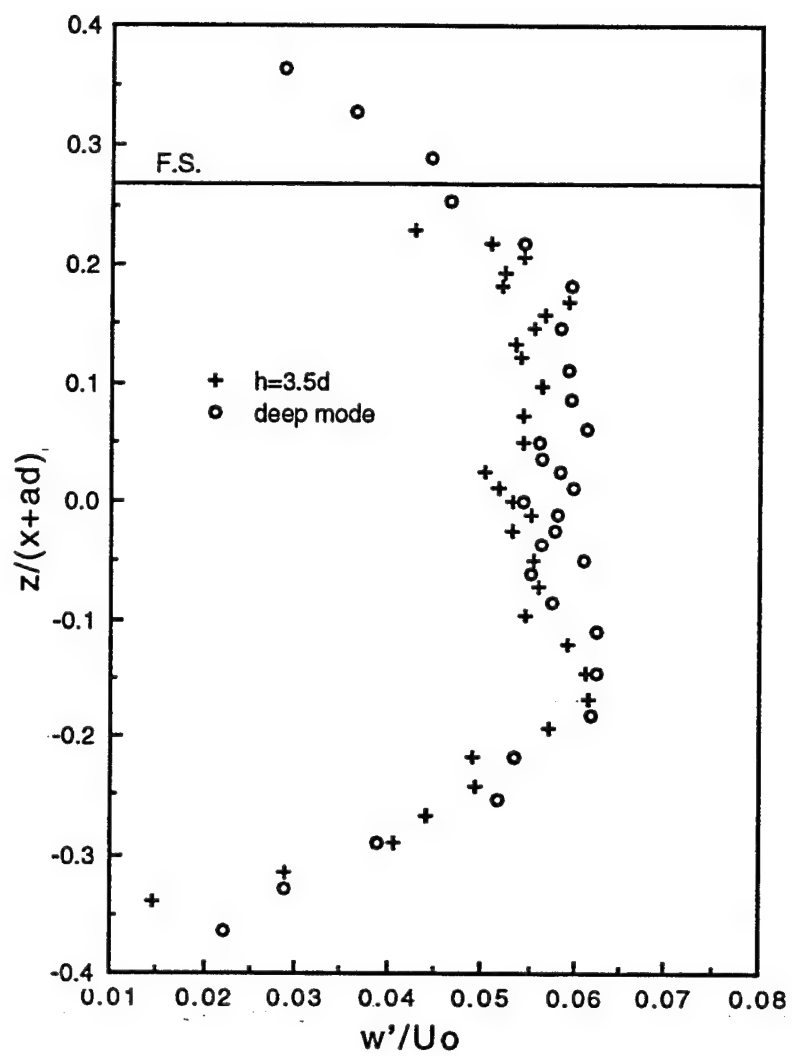   S = 0.265 at x/d = 10
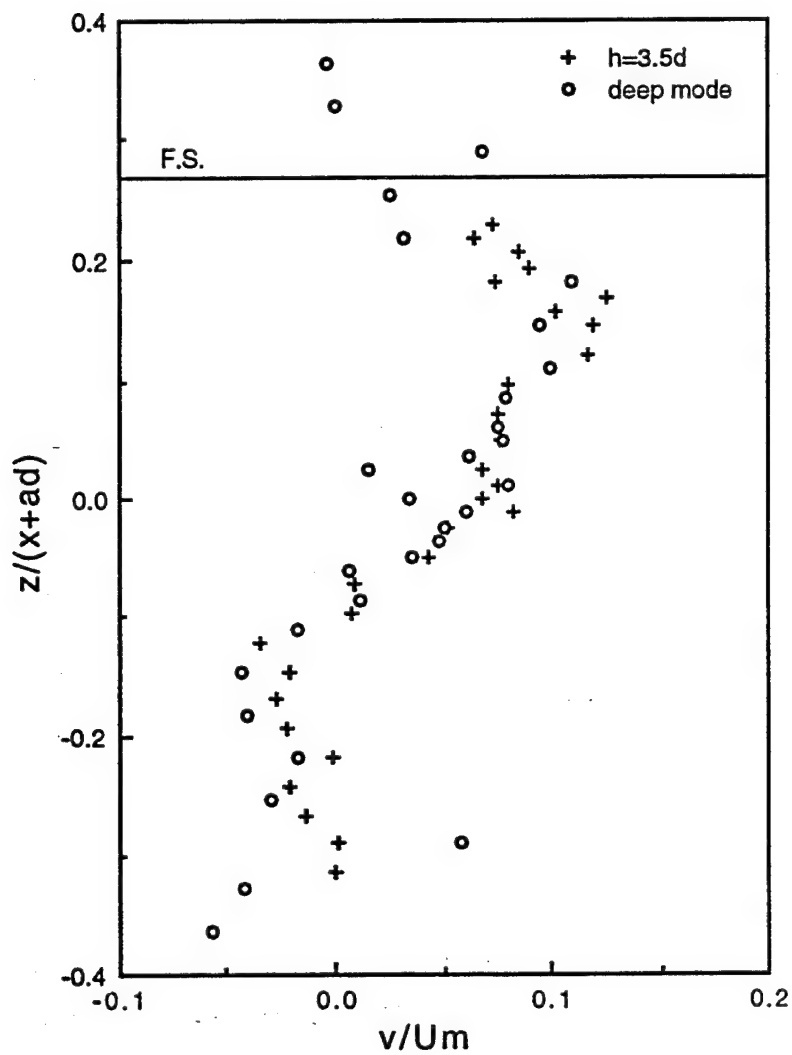
Figure 28.   v/Um versus z* in the deep and shallow modes for
              S = 0.265 at x/d = 10
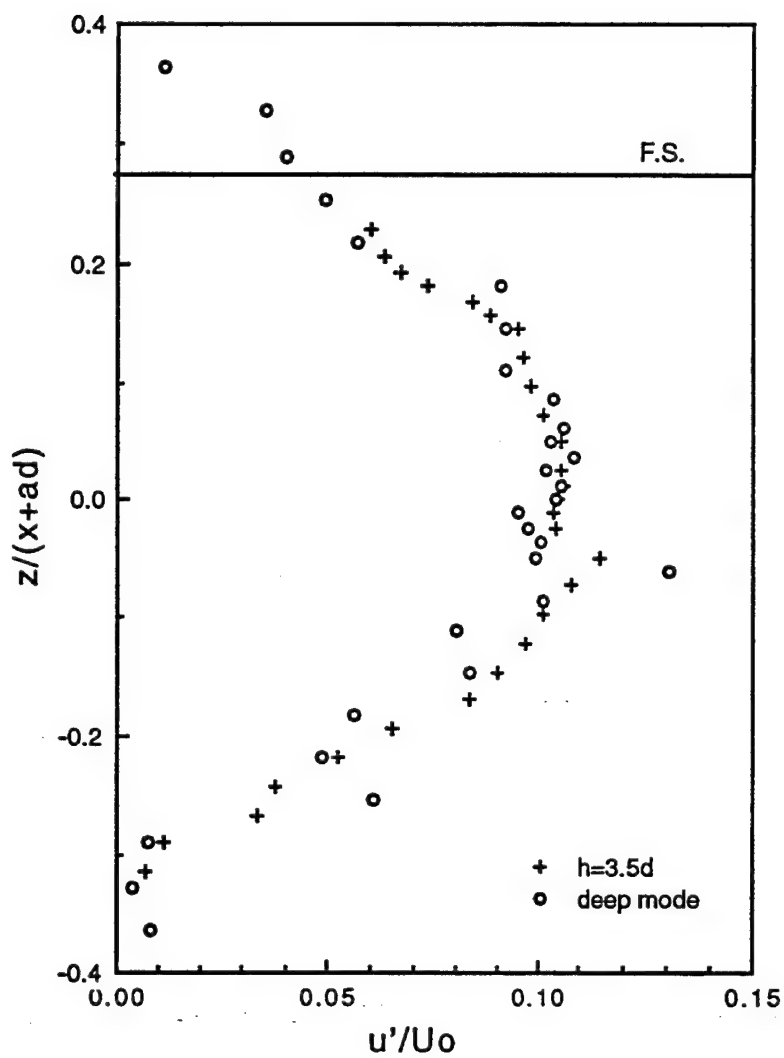
Figure 29.   u'/Uo versus z* in the deep and shallow modes for
              S = 0.265 at x/d = 10

81
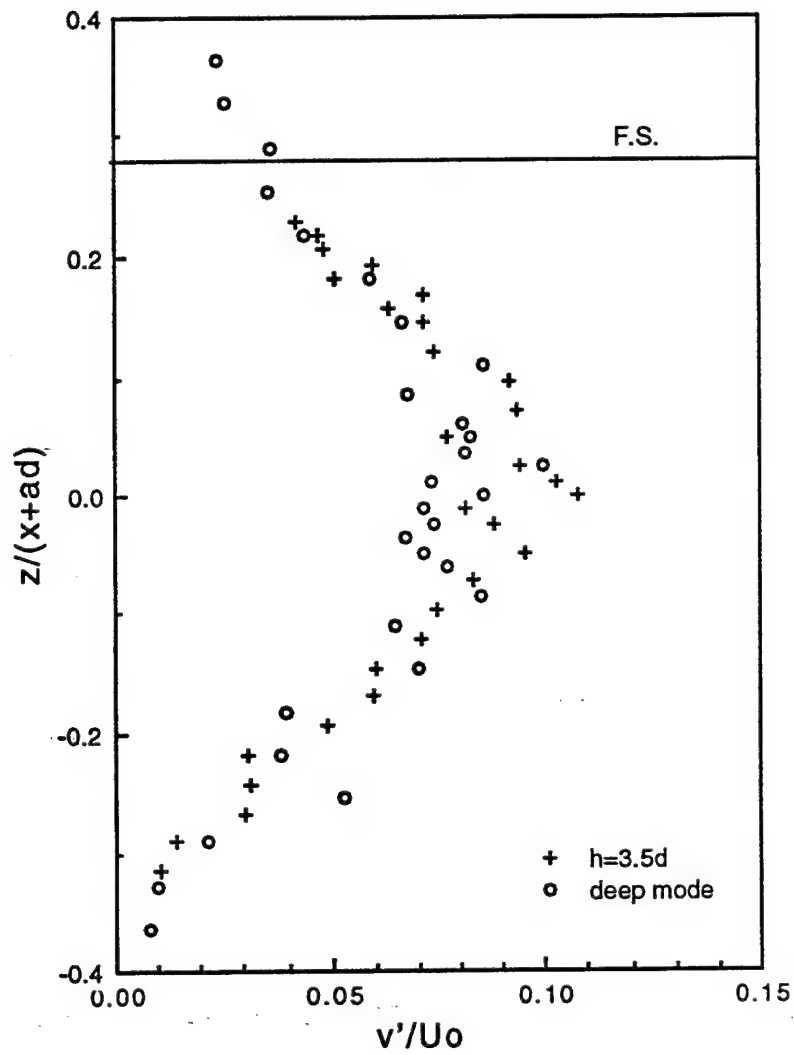
Figure 30. v'/Uo versus z* in the deep and shallow modes for S = 0.265 at x/d = 10
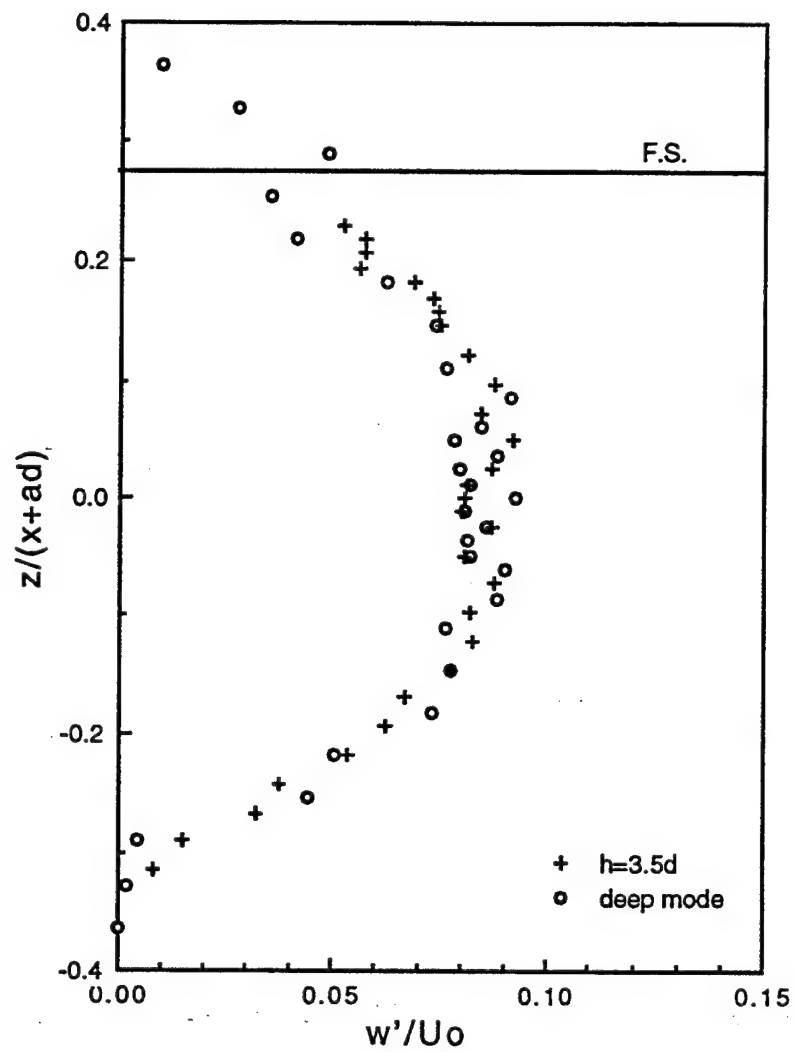
Figure 31.   w'/Uo versus z* in the deep and shallow modes for
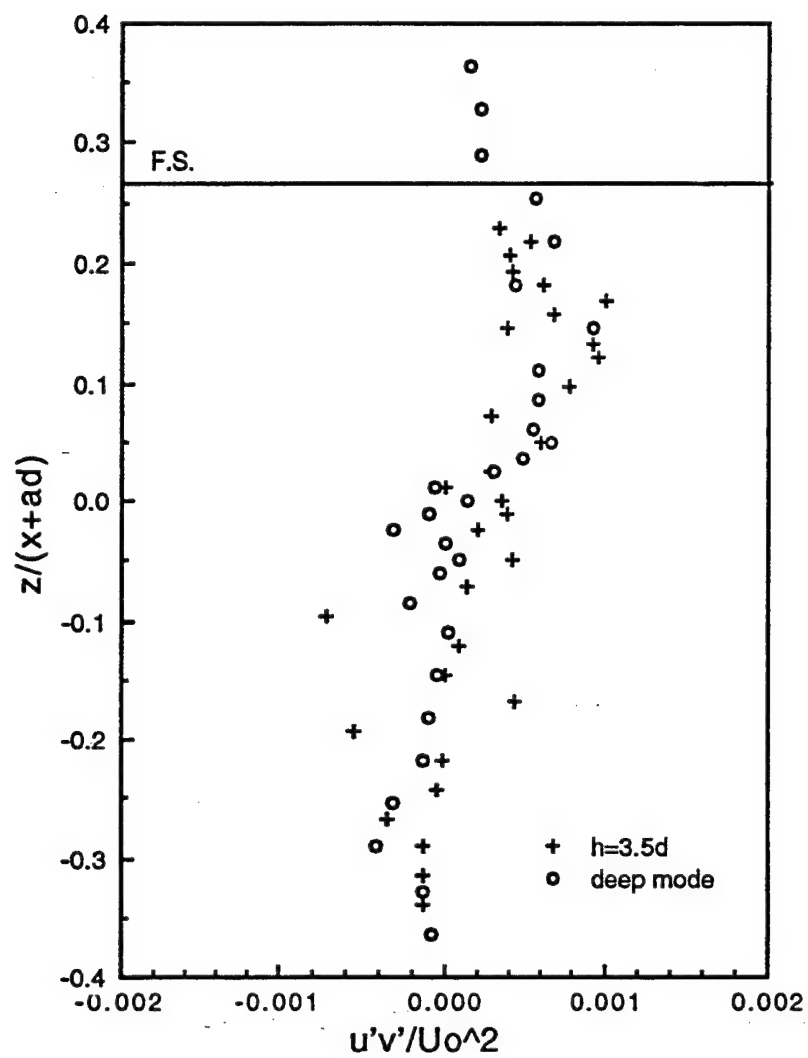S = 0.265 at x/d = 10
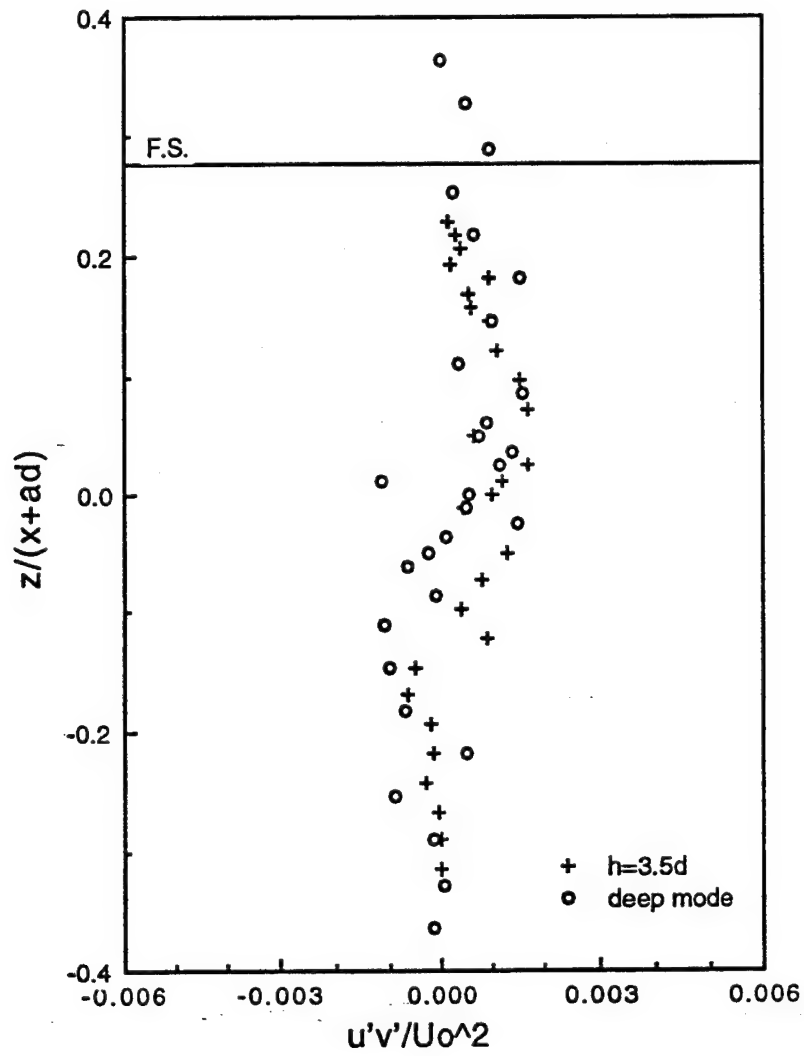
Figure 32. $u'v'/U_o^2$ versus z* in the deep and shallow modes
               for S = 0.265 at x/d = 10
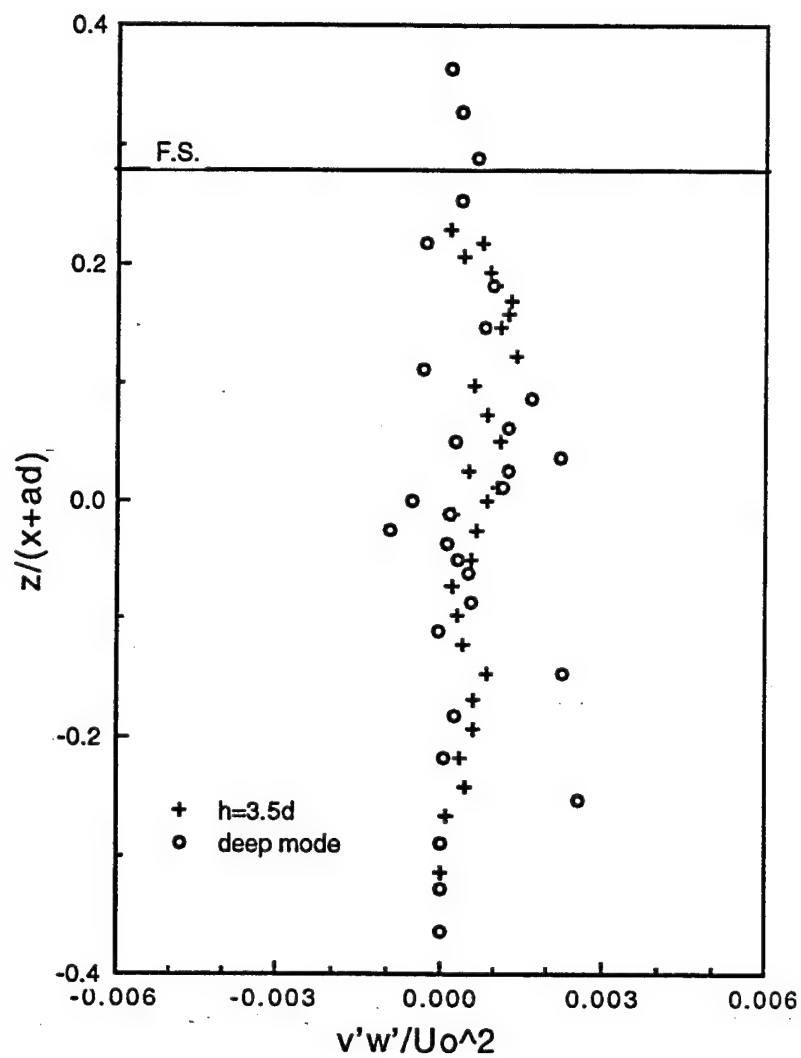
Figure 33. $v'w'/U_0^2$ versus z^* in the deep and shallow modes
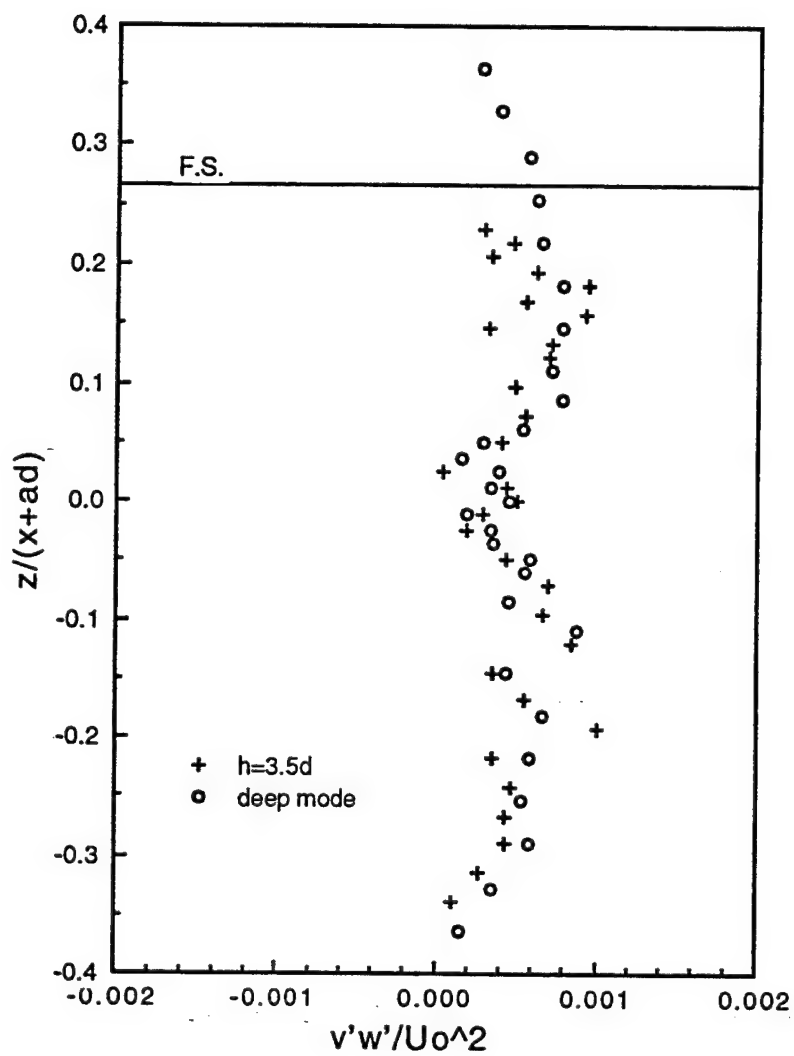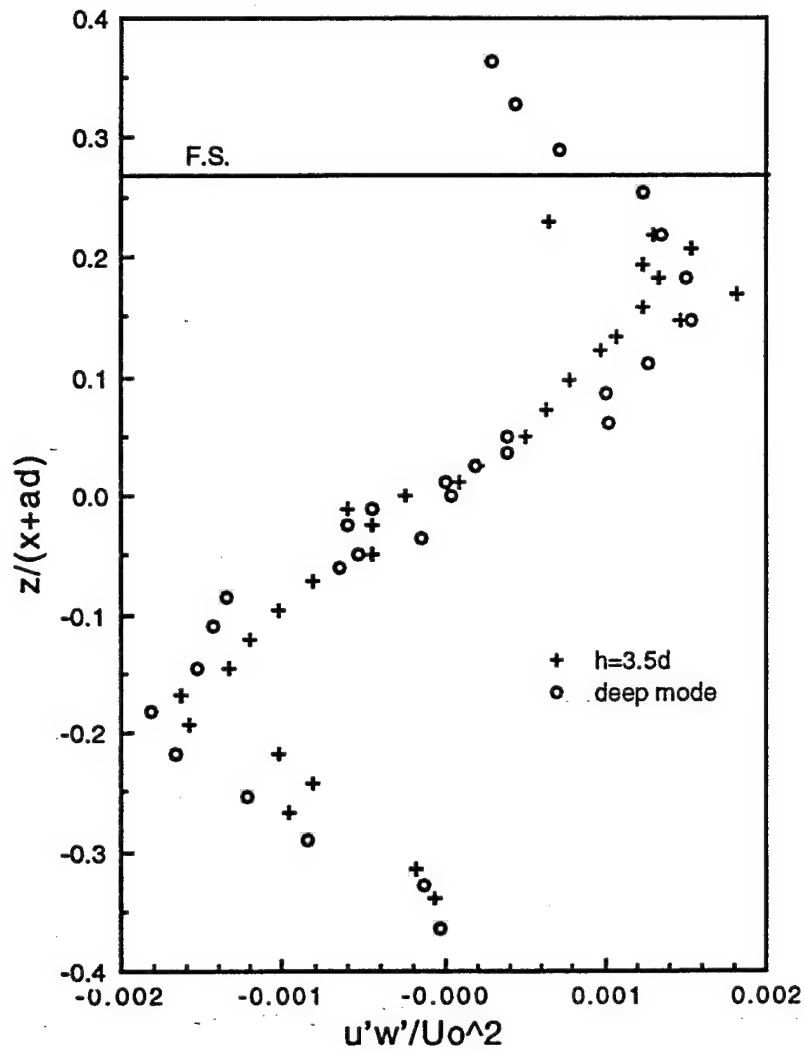for $S = 0.265$ at $x/d = 10$
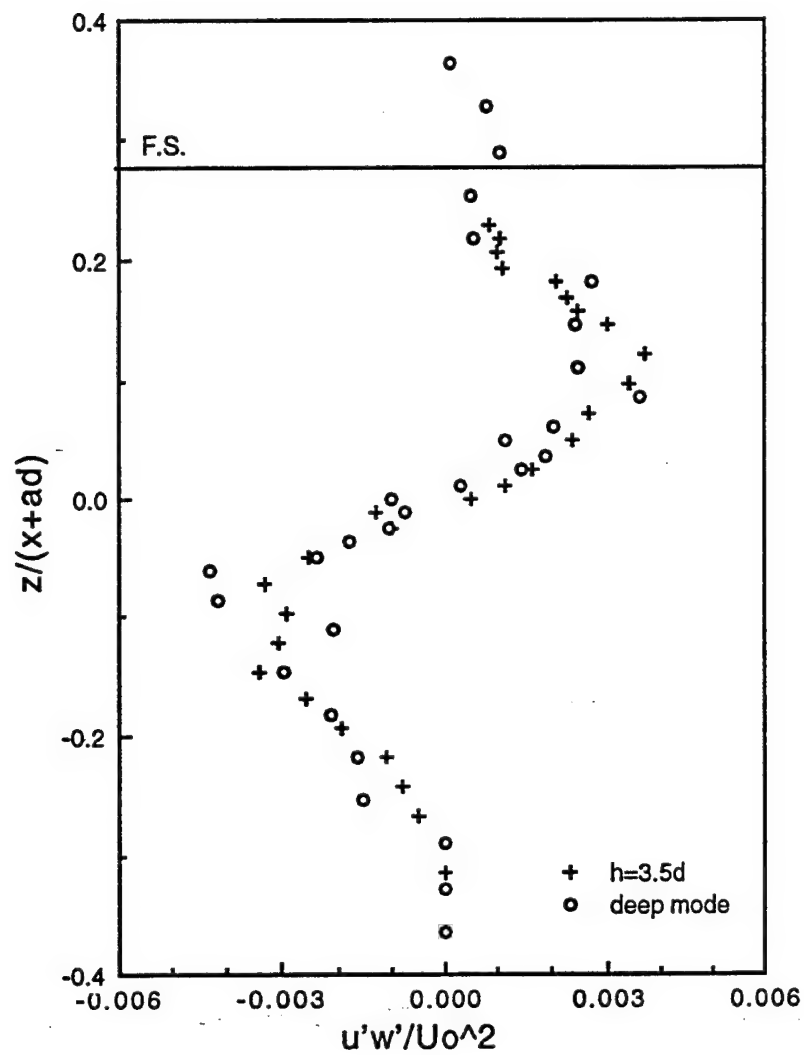
Figure 34. $u'w'/U_o^2$ versus z^* in the deep and shallow modes
for S = 0.265 at x/d = 10

86
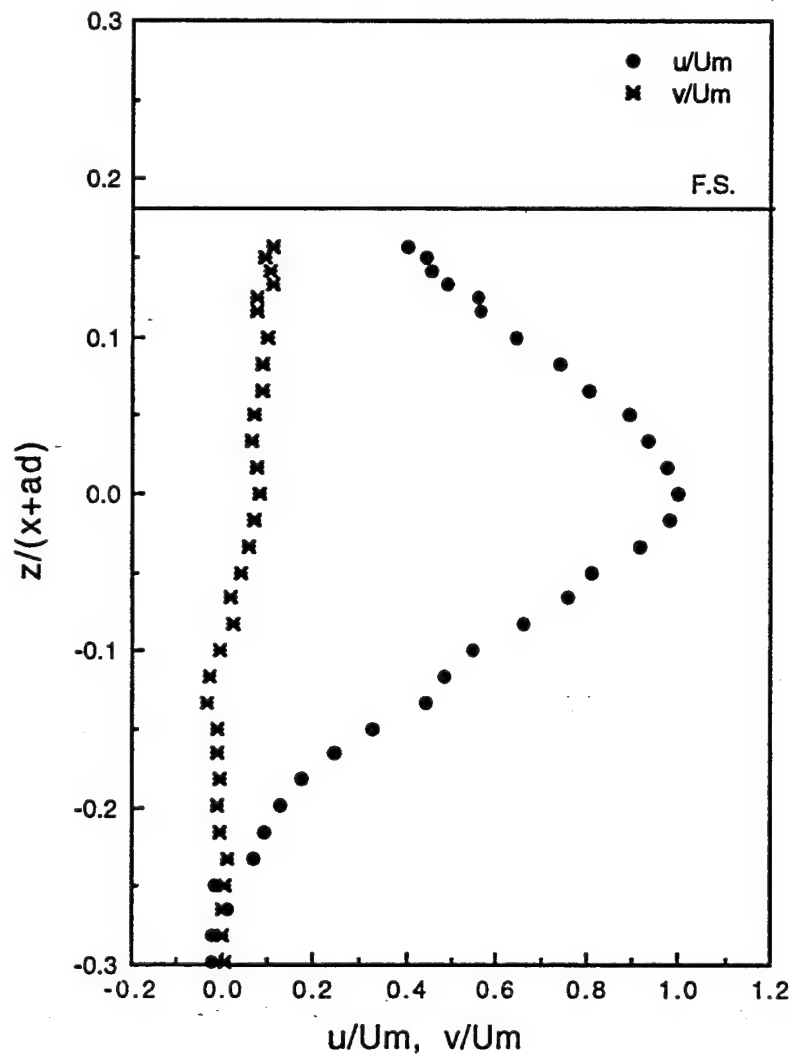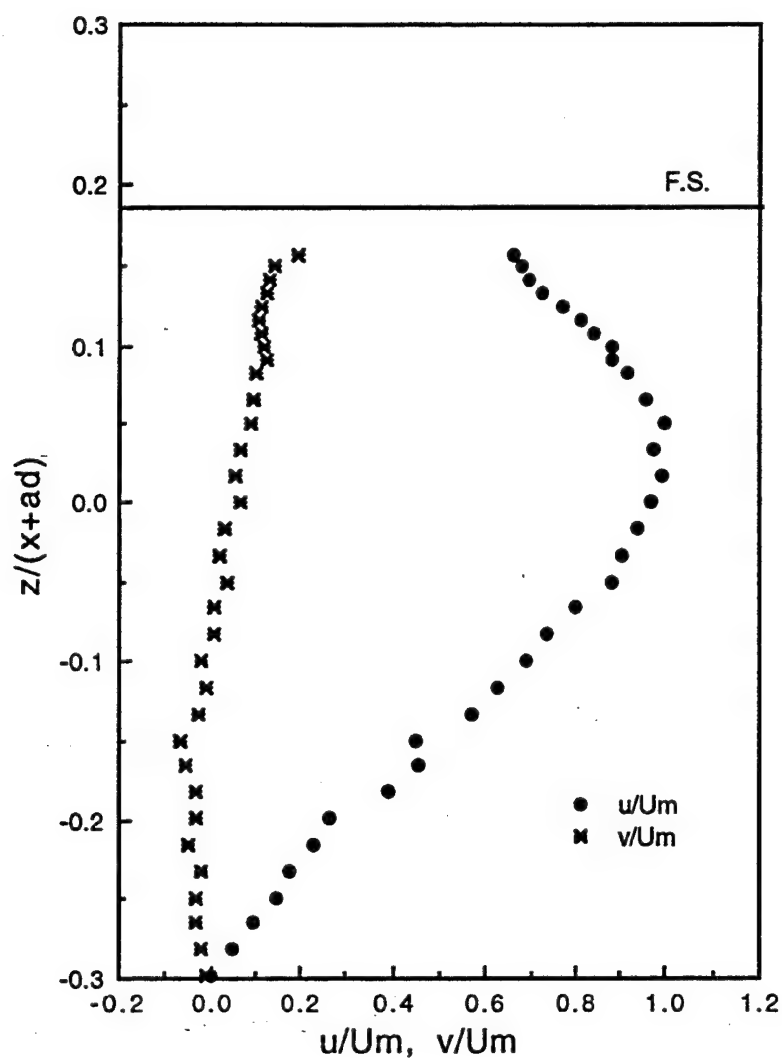
Figure 35.   u/Um and v/Um versus z* in the shallow mode for
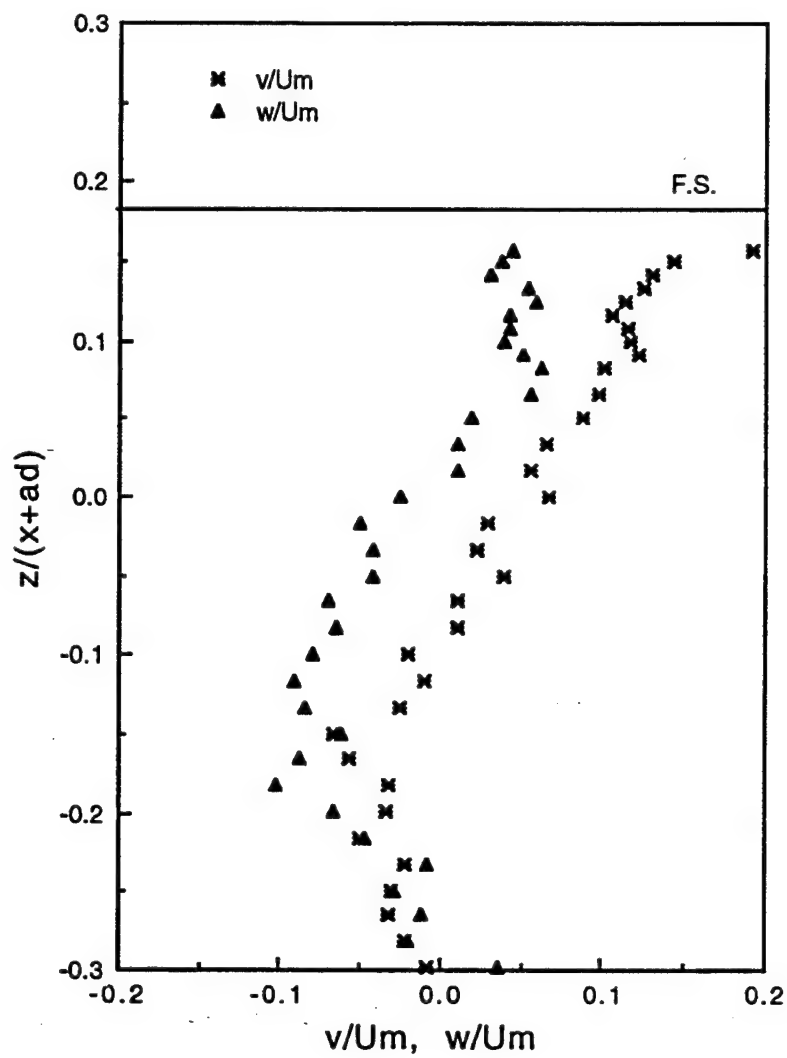S = 0.265 at x/d = 16
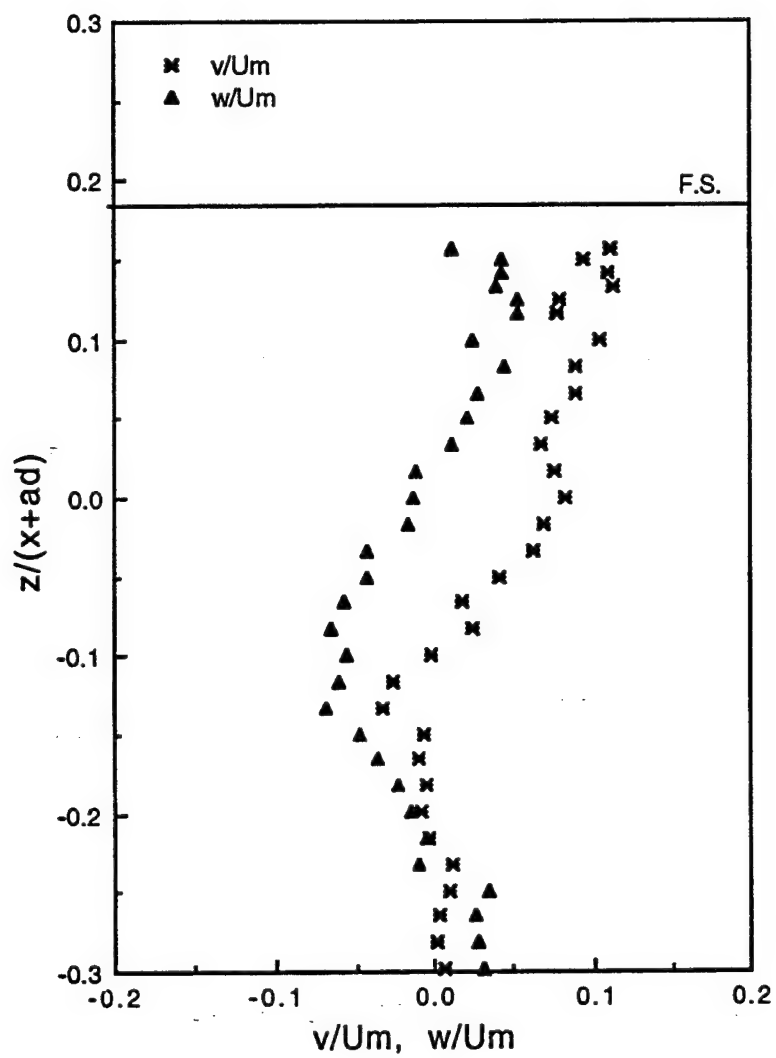
Figure 36. v/Um and w/Um versus z* in the shallow mode for
S = 0.265 at x/d = 16
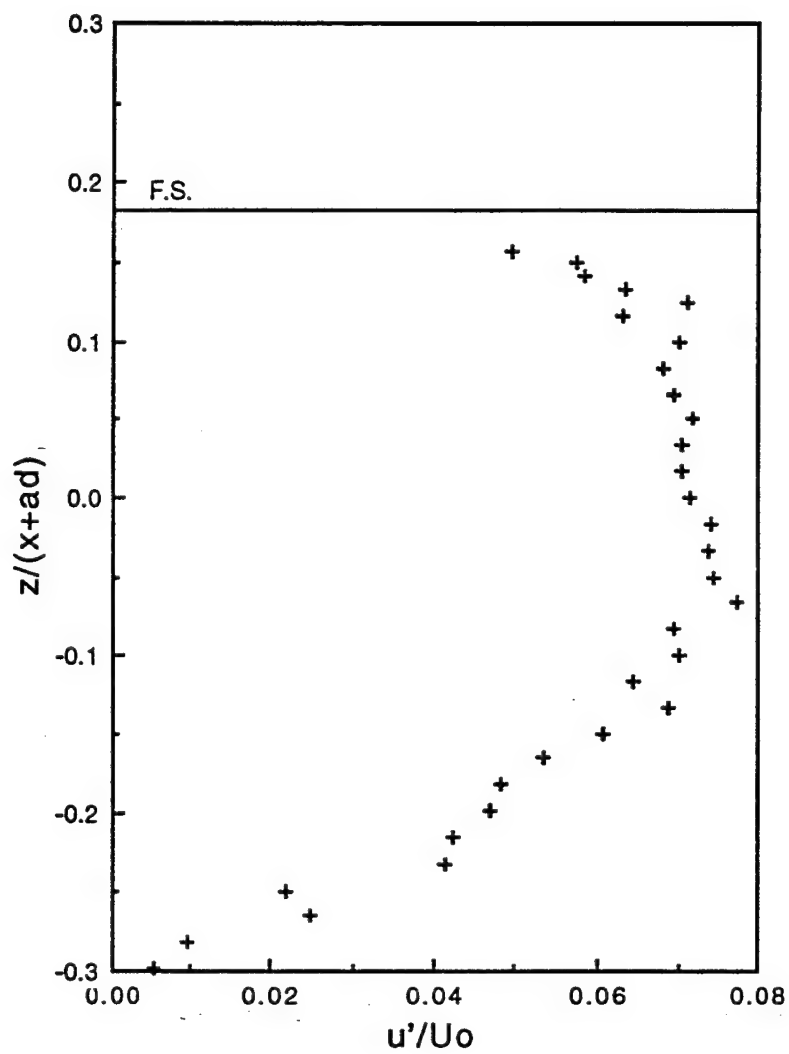
Figure 37.   u'/Uo versus z* in the shallow mode for S = 0.265
             at x/d = 16
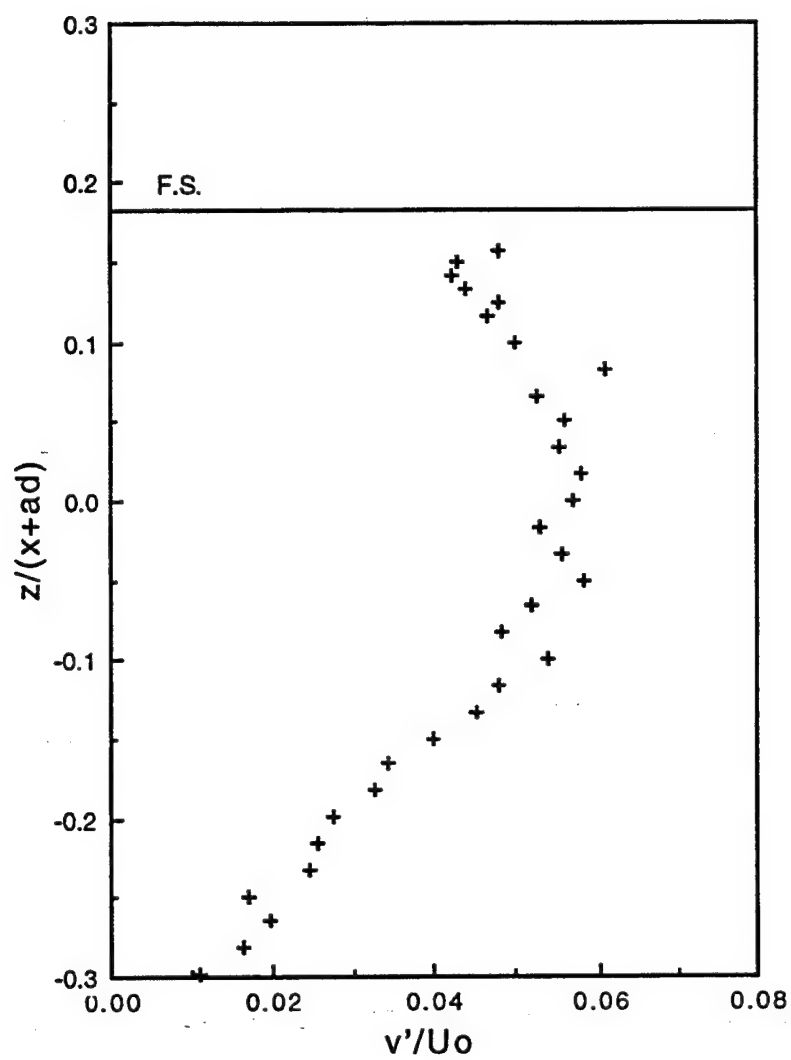
Figure 38.   v'/Uo versus z* in the shallow mode for S = 0.265
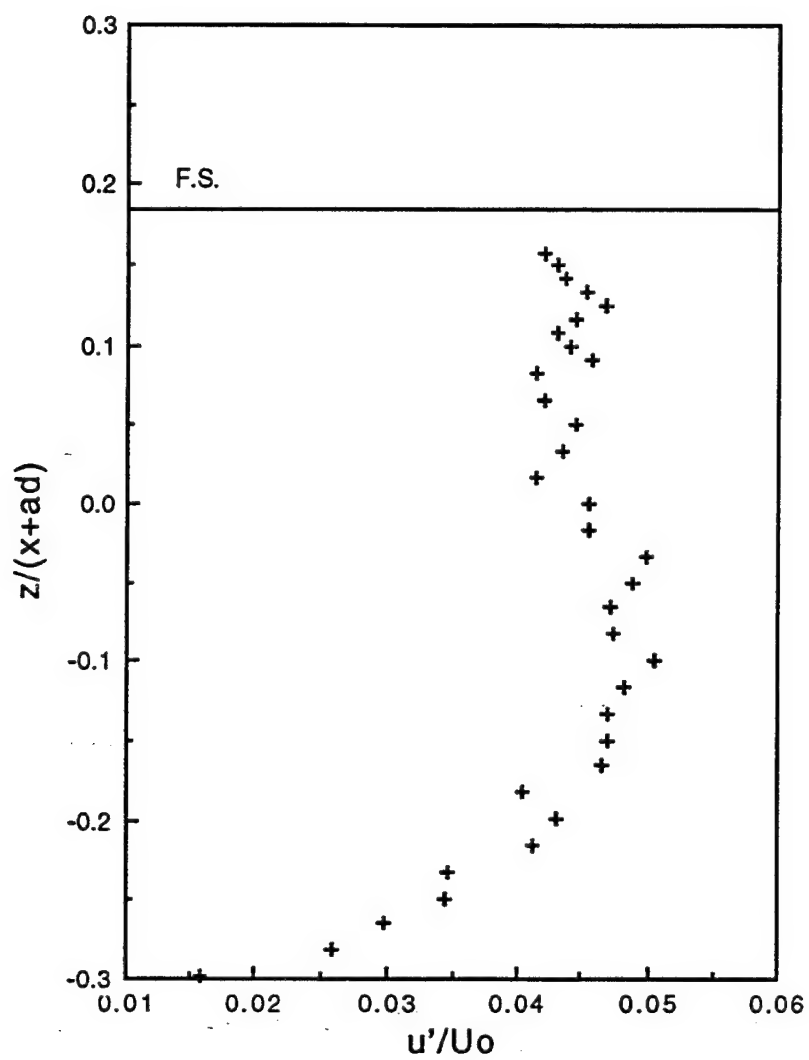   at x/d = 16

90
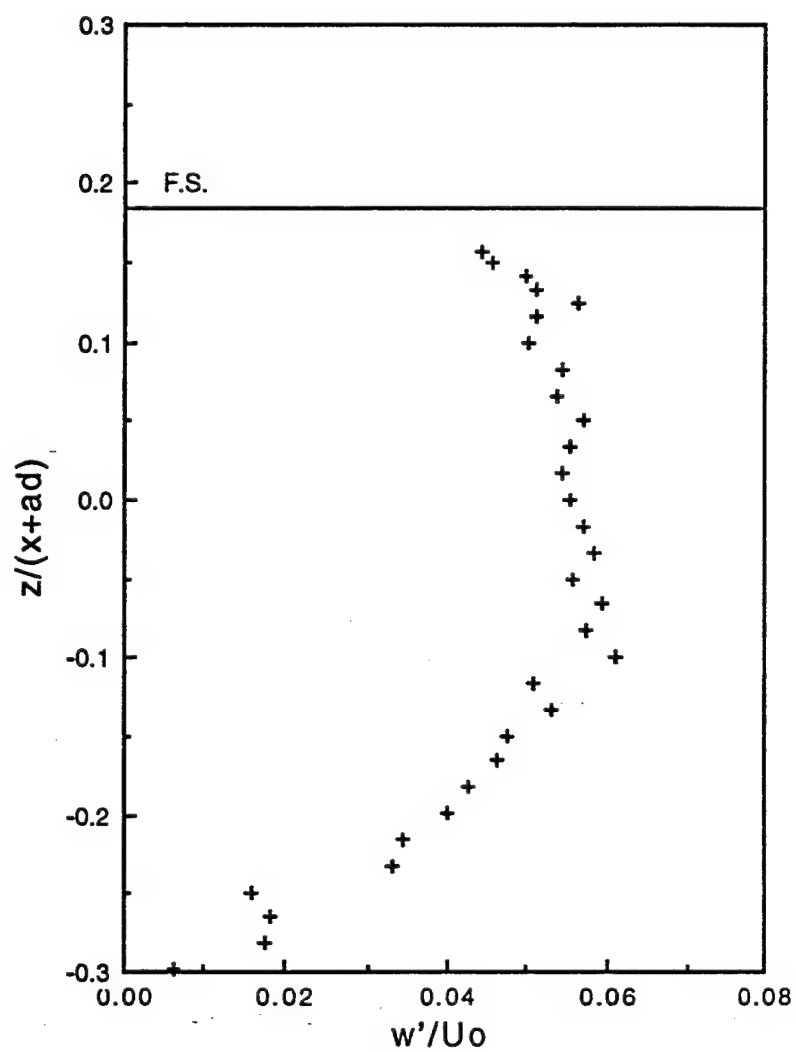
Figure 39.   w'/Uo versus z* in the shallow mode for S = 0.265
at x/d = 16
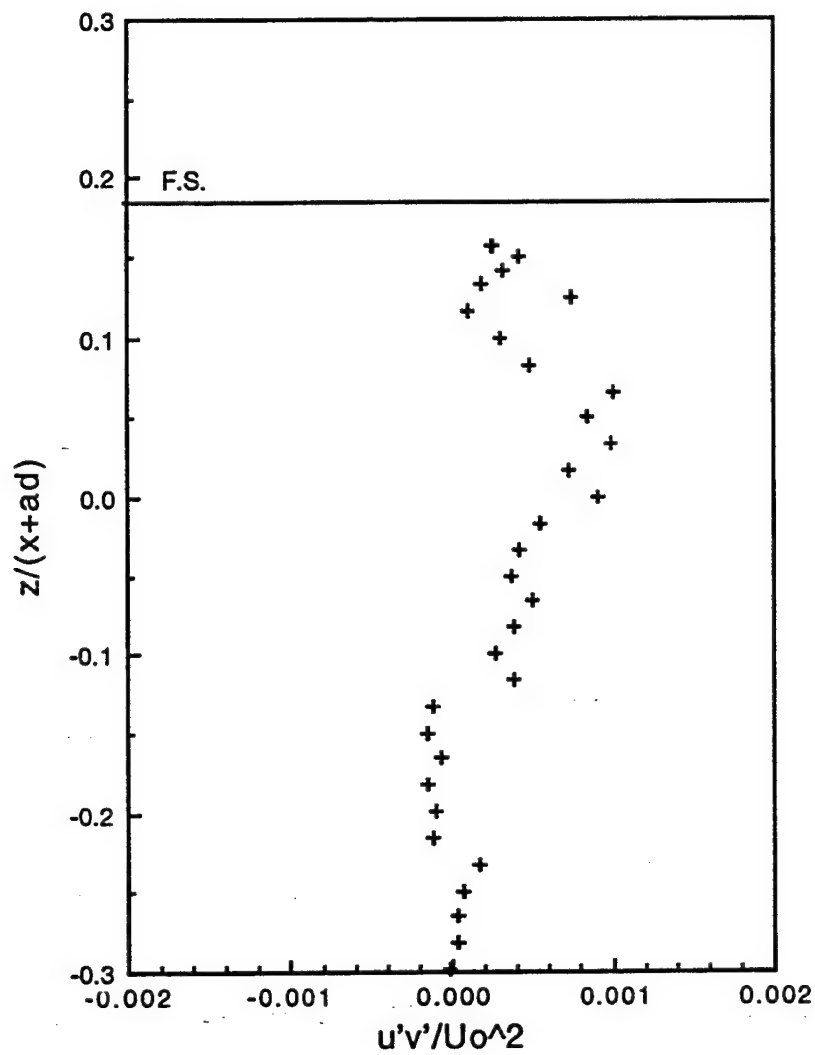
Figure 40. $u'v'/U_0^2$ versus z* in the shallow mode for S = 0.265 at x/d = 16
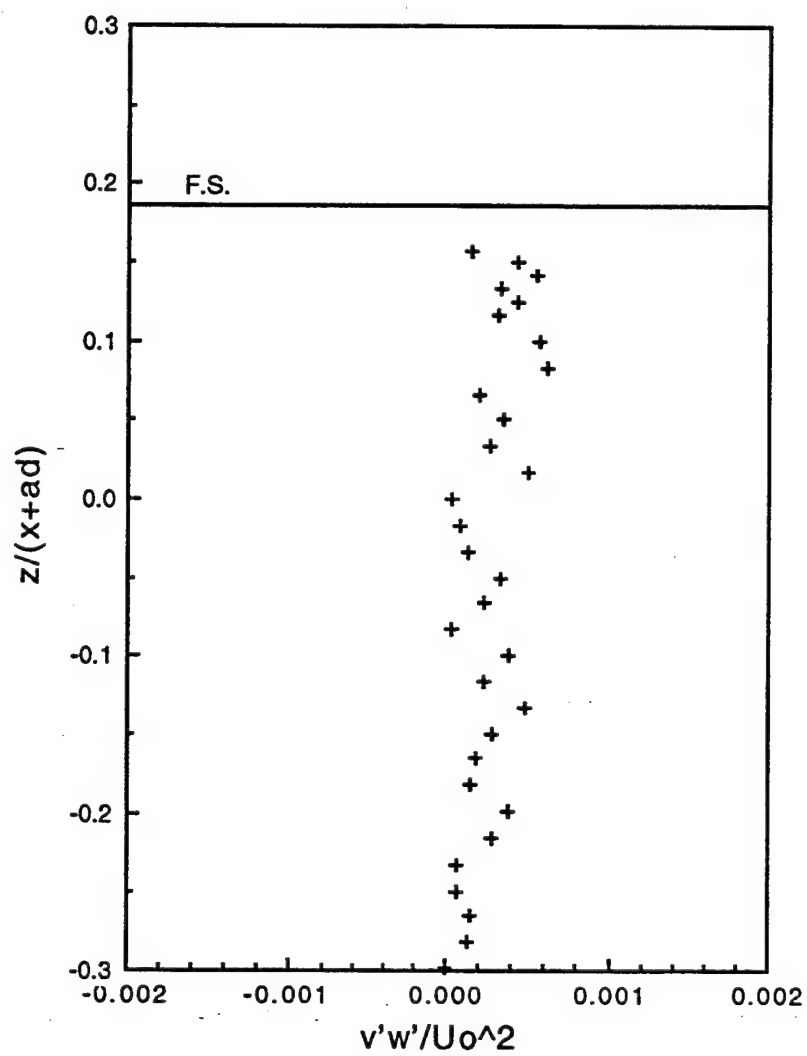
92

Figure 41. $v'w'/U_o^2$ versus z^* in the shallow mode for S = 0.265 at x/d = 16

93
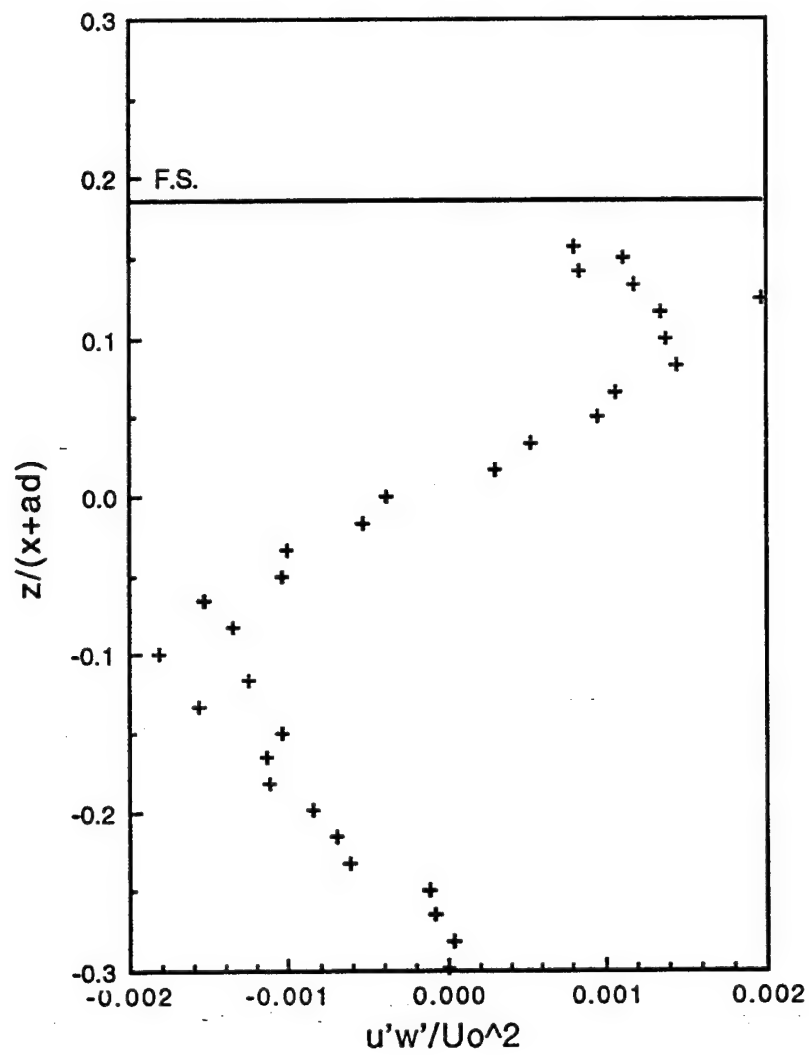
Figure 42. $u'w'/U_o^2$ versus z^* in the shallow mode for $S = 0.265$ at $x/d = 16$
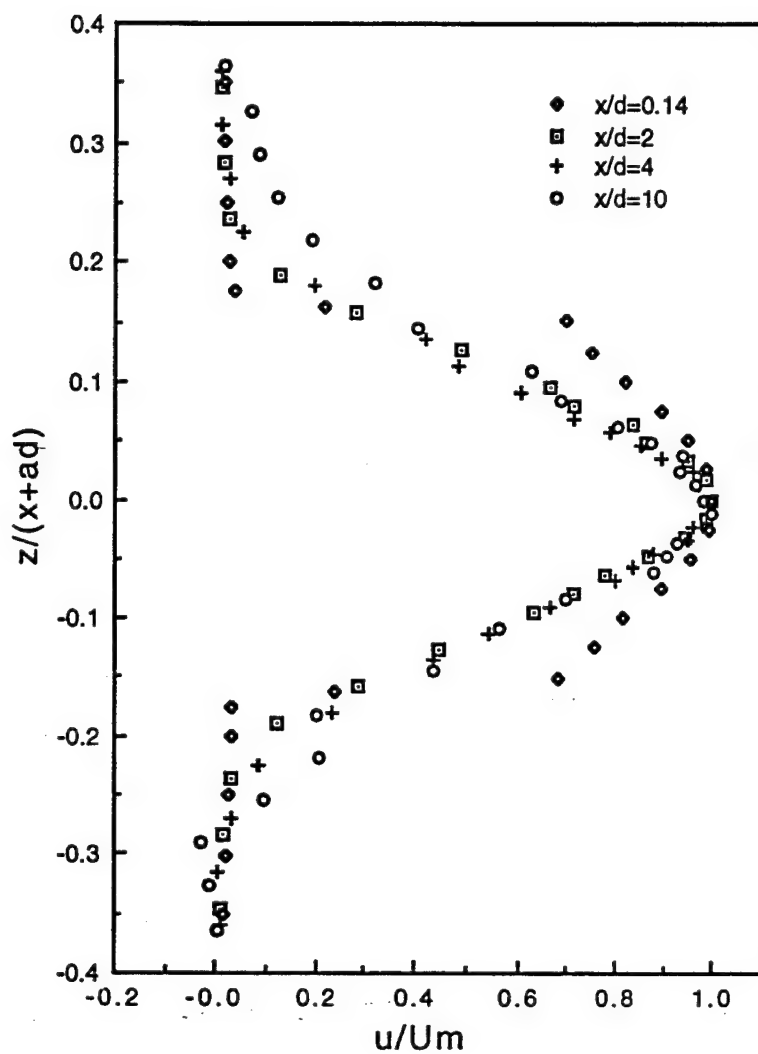
Figure 43.   u/Um versus z* in the deep mode for S = 0.265 at various axial distances
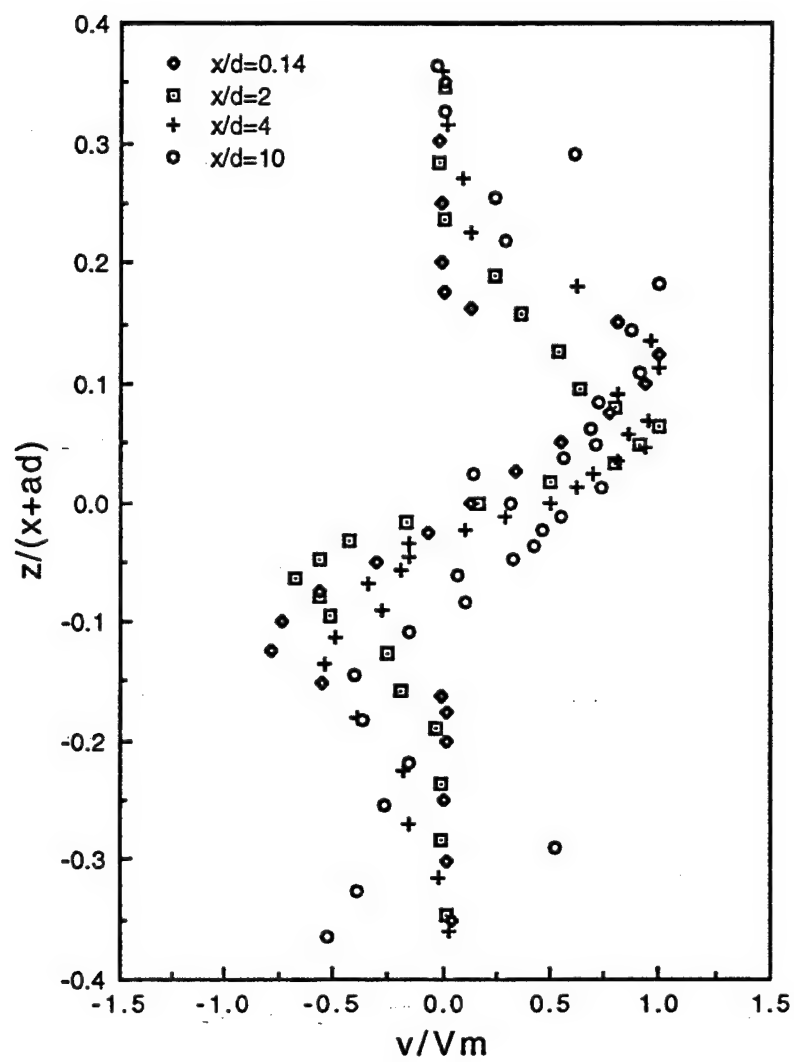
Figure 44.   v/Vm versus z* in the deep mode for S = 0.265 at various axial distances
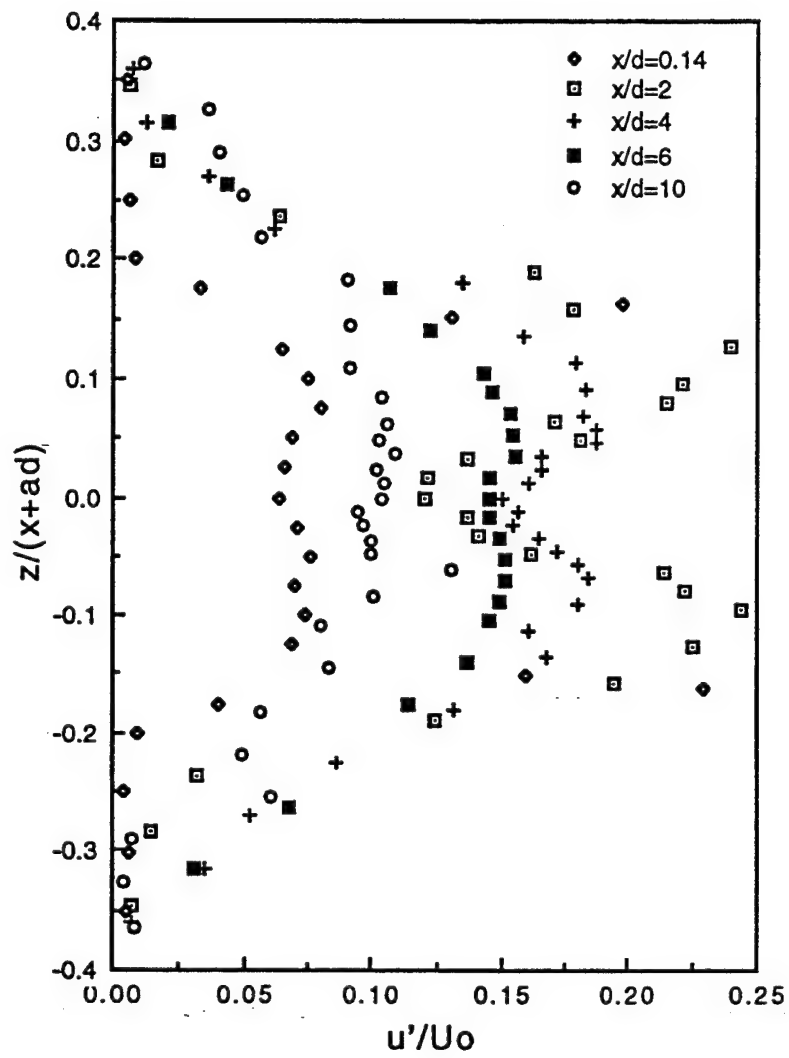
Figure 45a.   u'/Uo versus z* in the deep mode for S = 0.265 at various axial distances

97
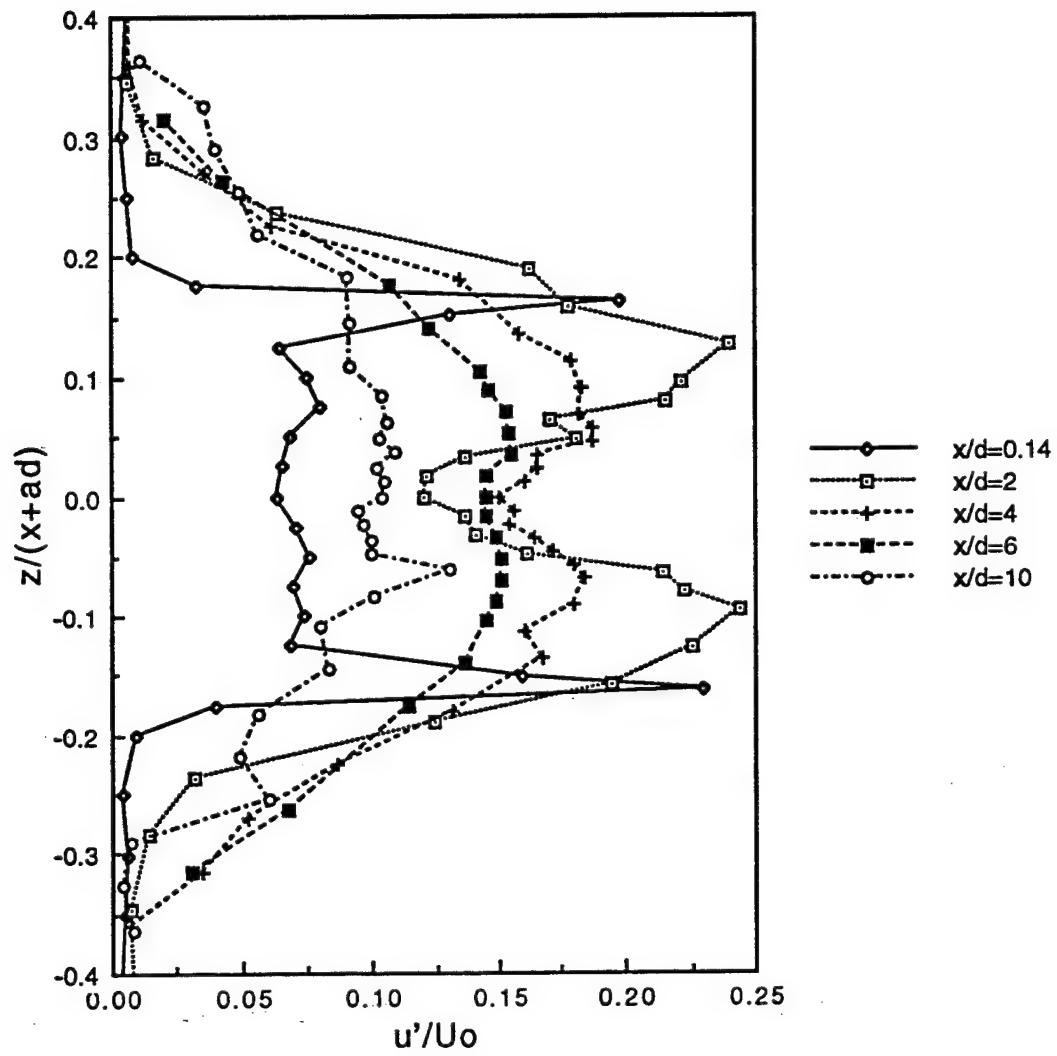
Figure 45b.   u'/Uo versus z* in the deep mode for S = 0.265 at various axial distances
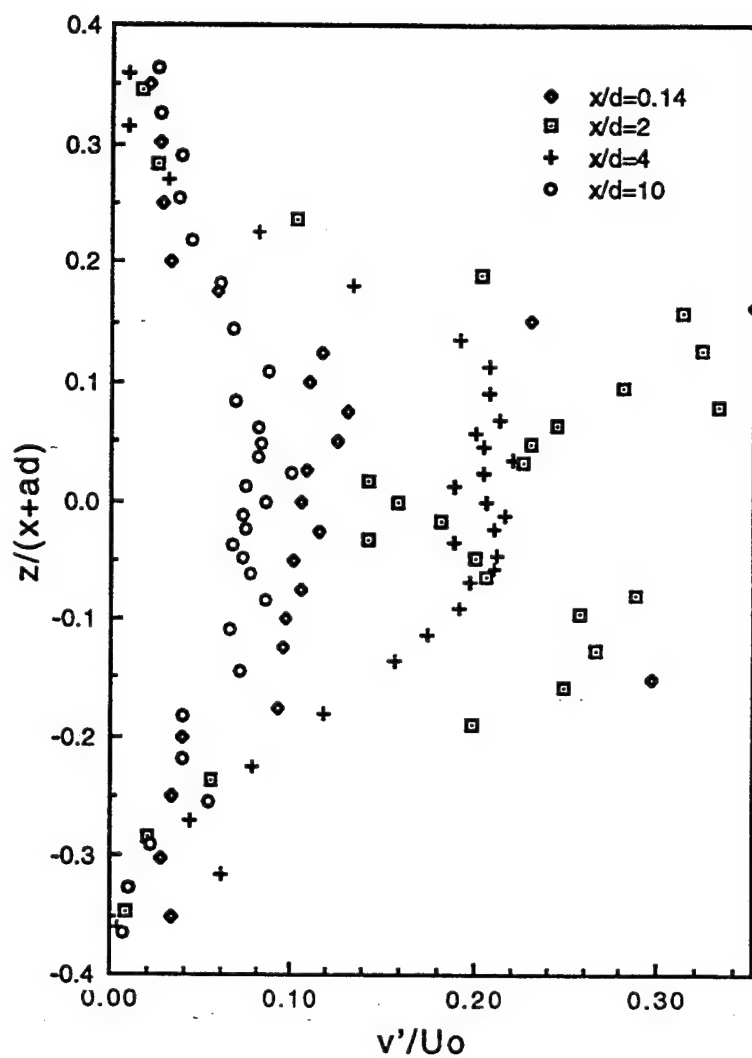
Figure 46a.   v'/Uo versus z* in the deep mode for S = 0.265 at various axial distances
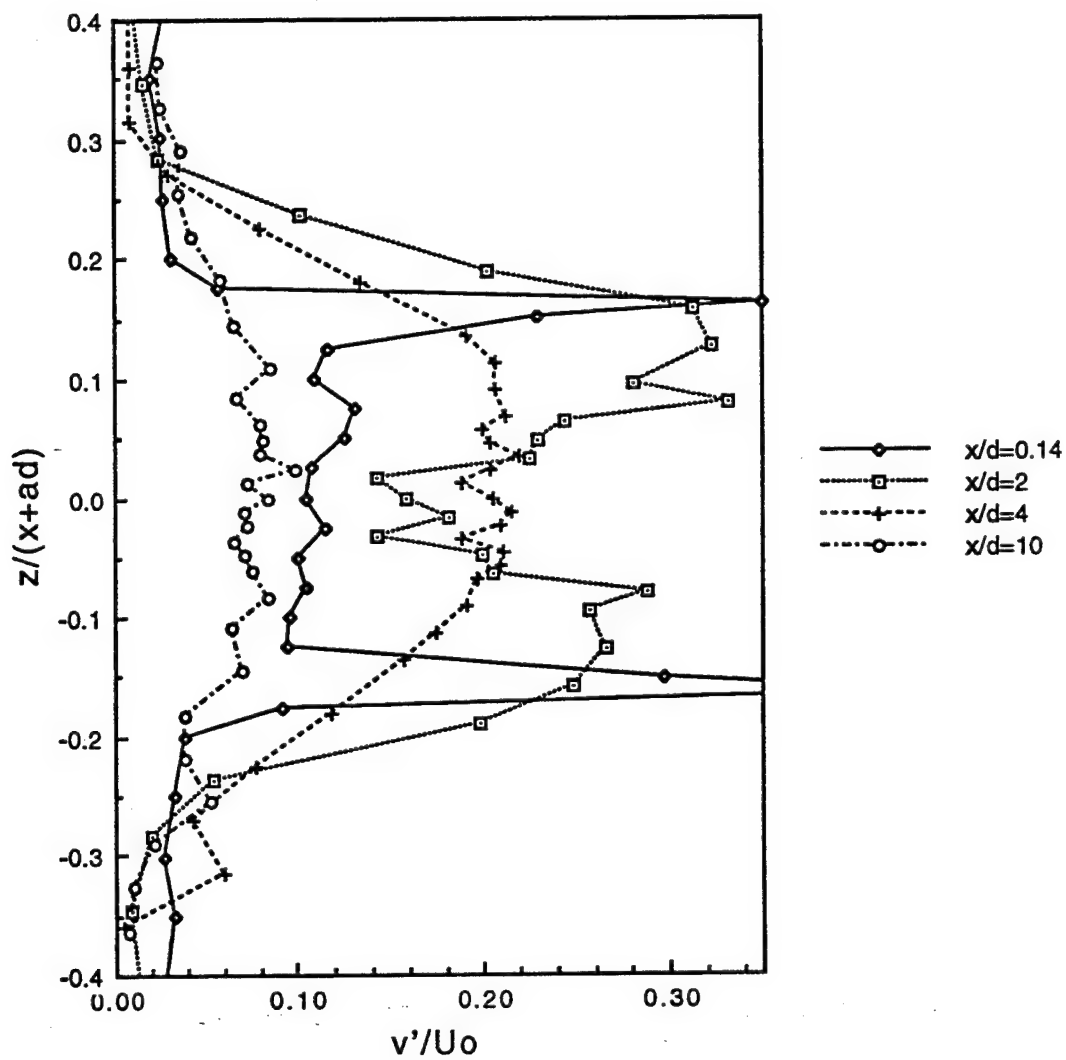
Figure 46b.   v'.Uo versus z* in the deep mode for S = 0.265 at
various axial distances
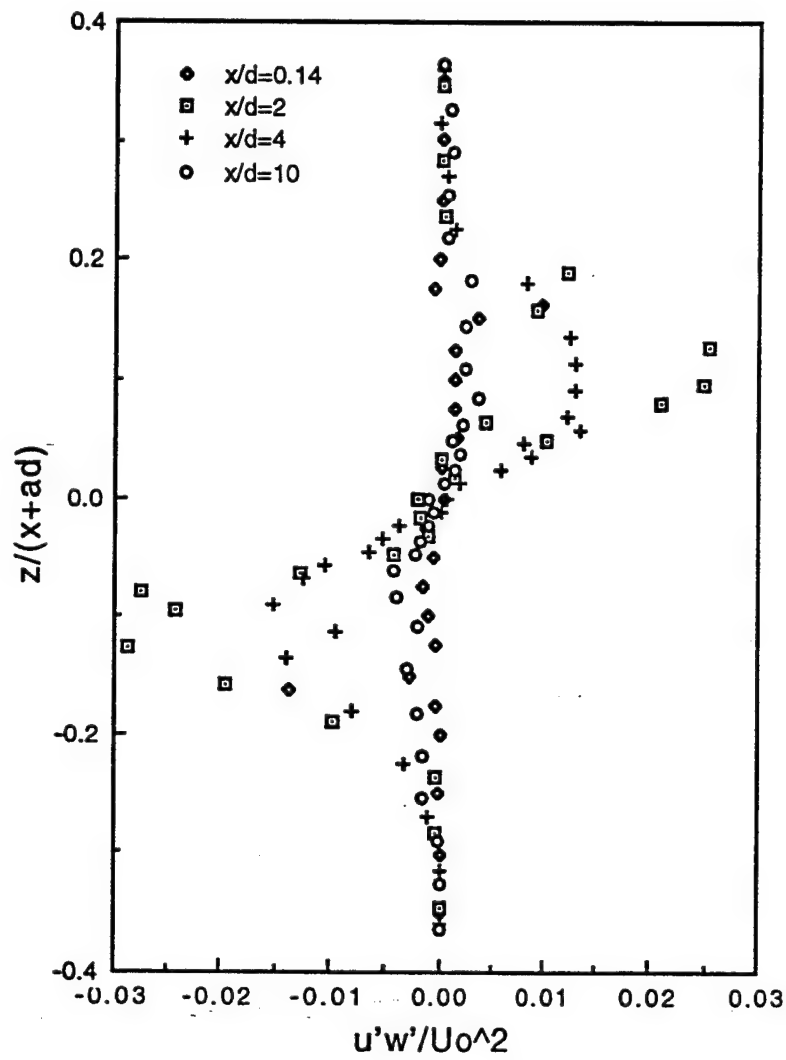
Figure 47.   u'w'/U_0^2 versus z* in the deep mode for S = 0.265 at various axial distances
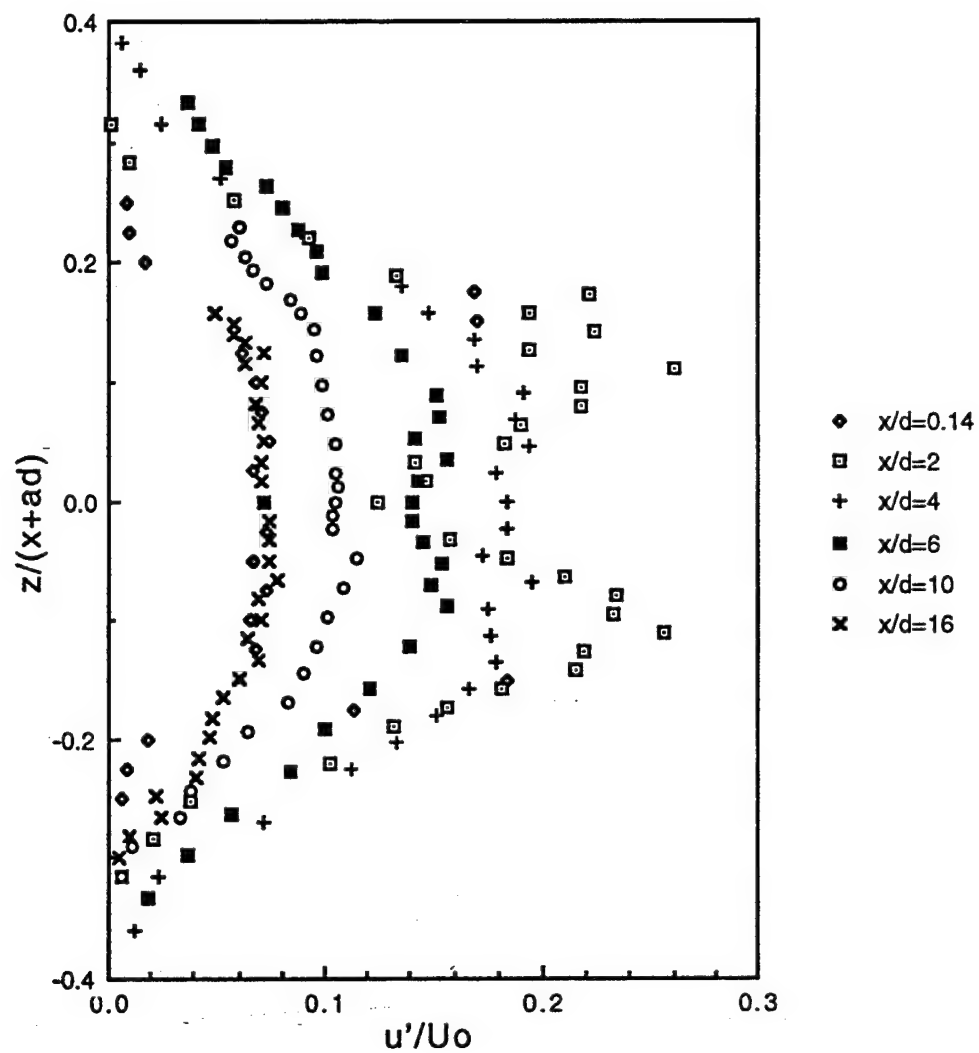
Figure48a.   u'/Uo versus z* in the shallow mode for S = 0.265
              at various axial distances

102
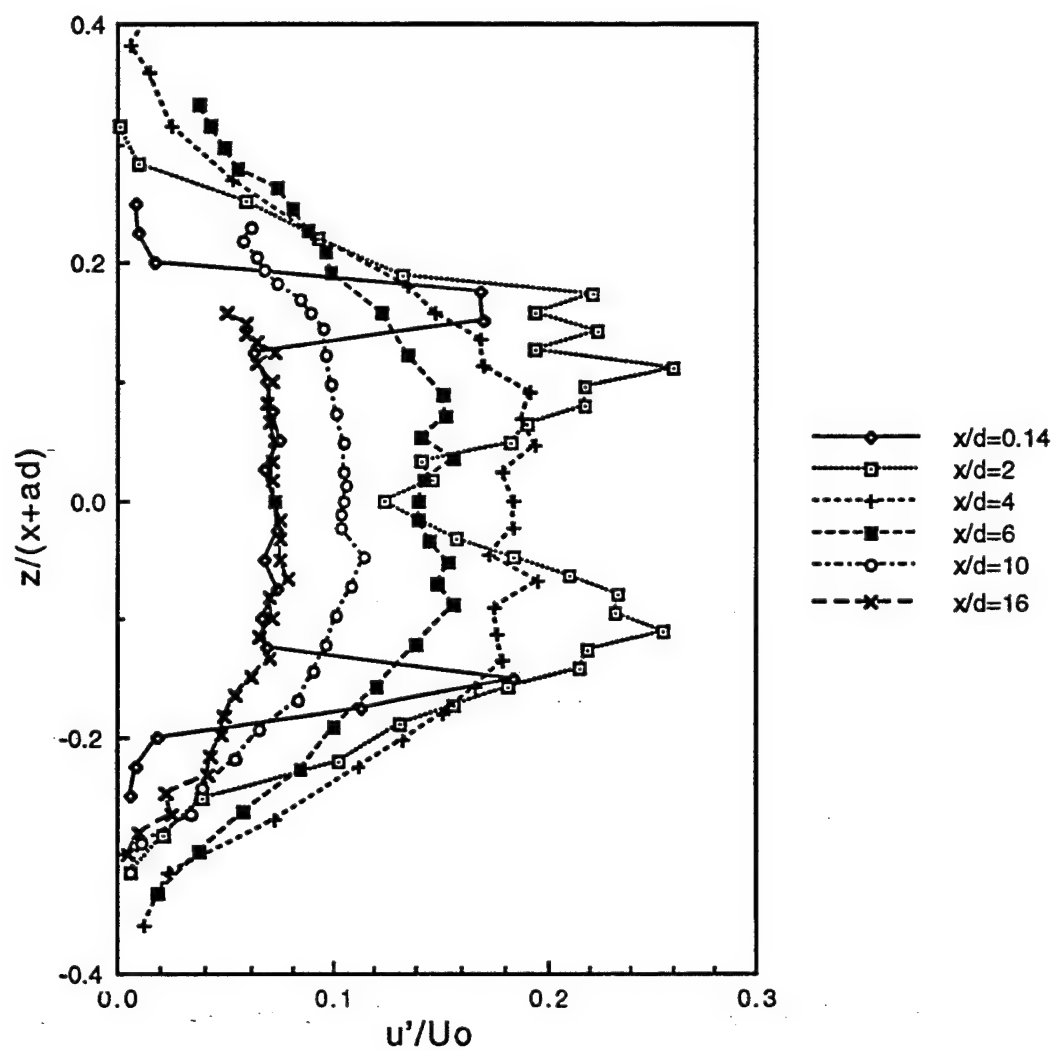
Figure 48b.   u'/Uo versus z* in the shallow mode for S = 0.265
              at various axial distances
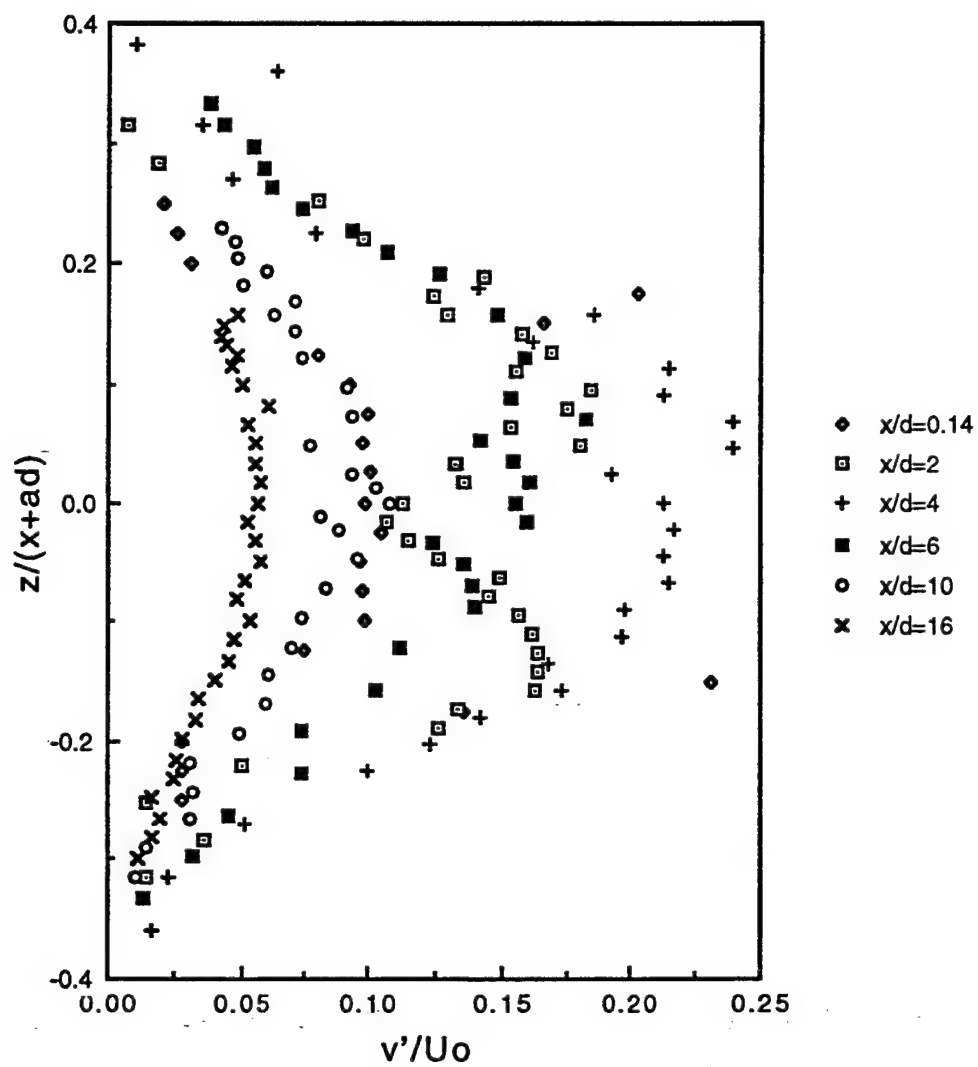
Figure 49a.   v'/Uo versus z* in the shallow mode for S = 0.265
at various axial distances
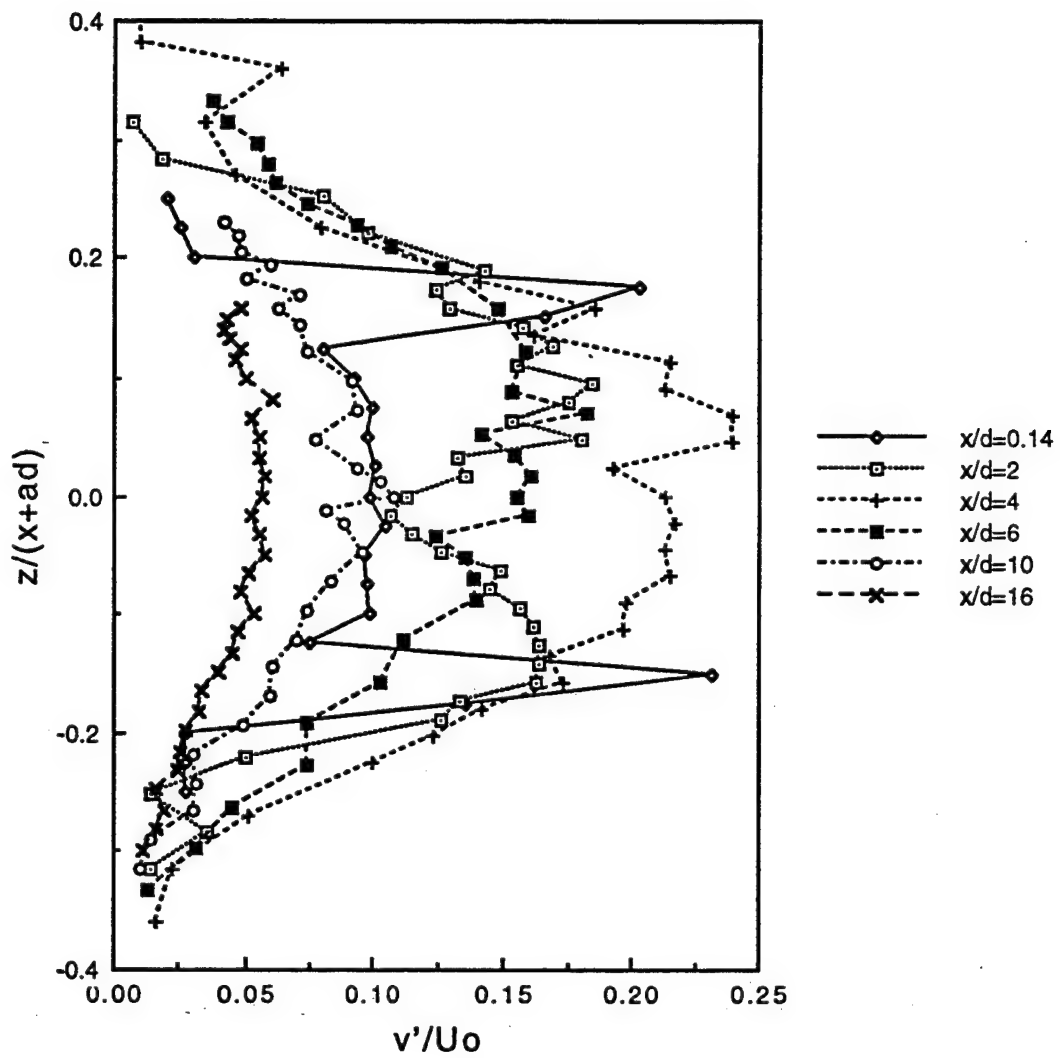
Figure 49b.   v'/Uo versus z* in the shallow mode for S = 0.265
               at various axial distances
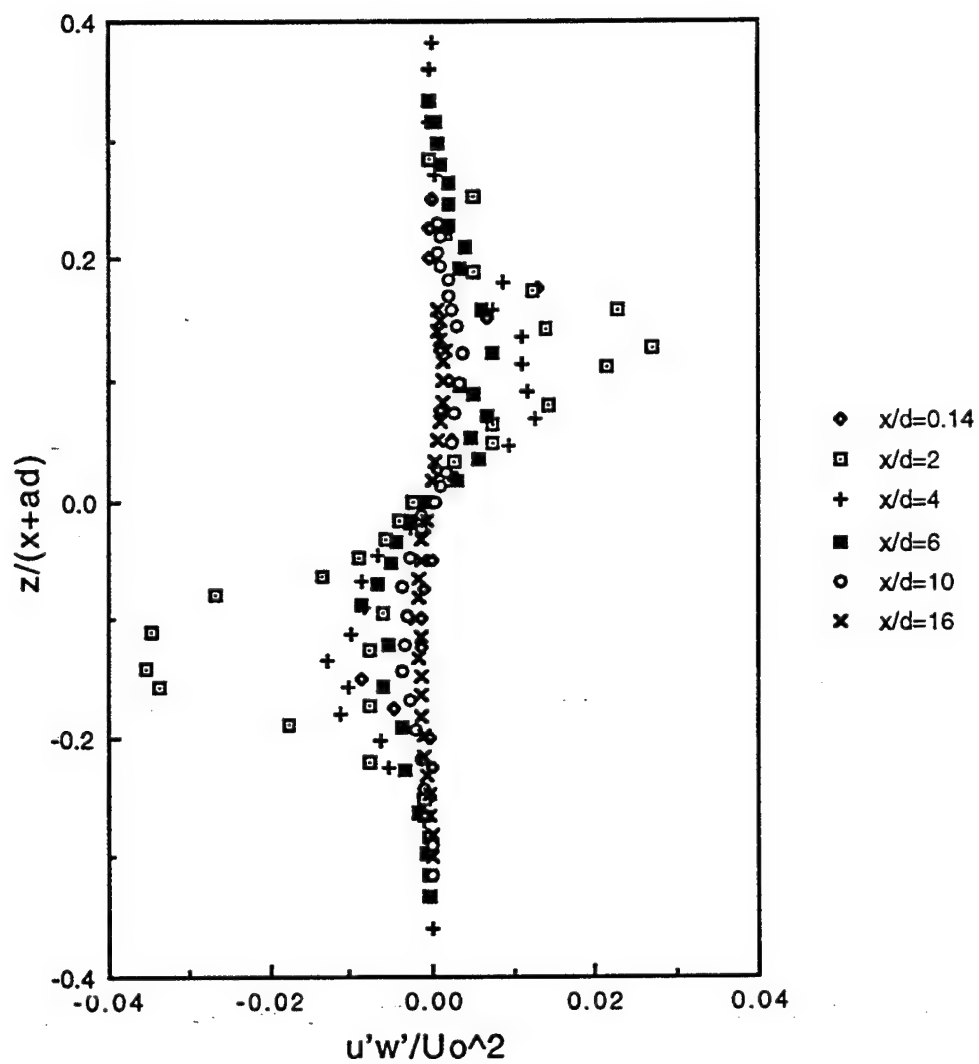
105

Figure 50a. $u'w'/U_o^2$ versus z^* in the shallow mode for
                $S = 0.265$ at various axial distances

106
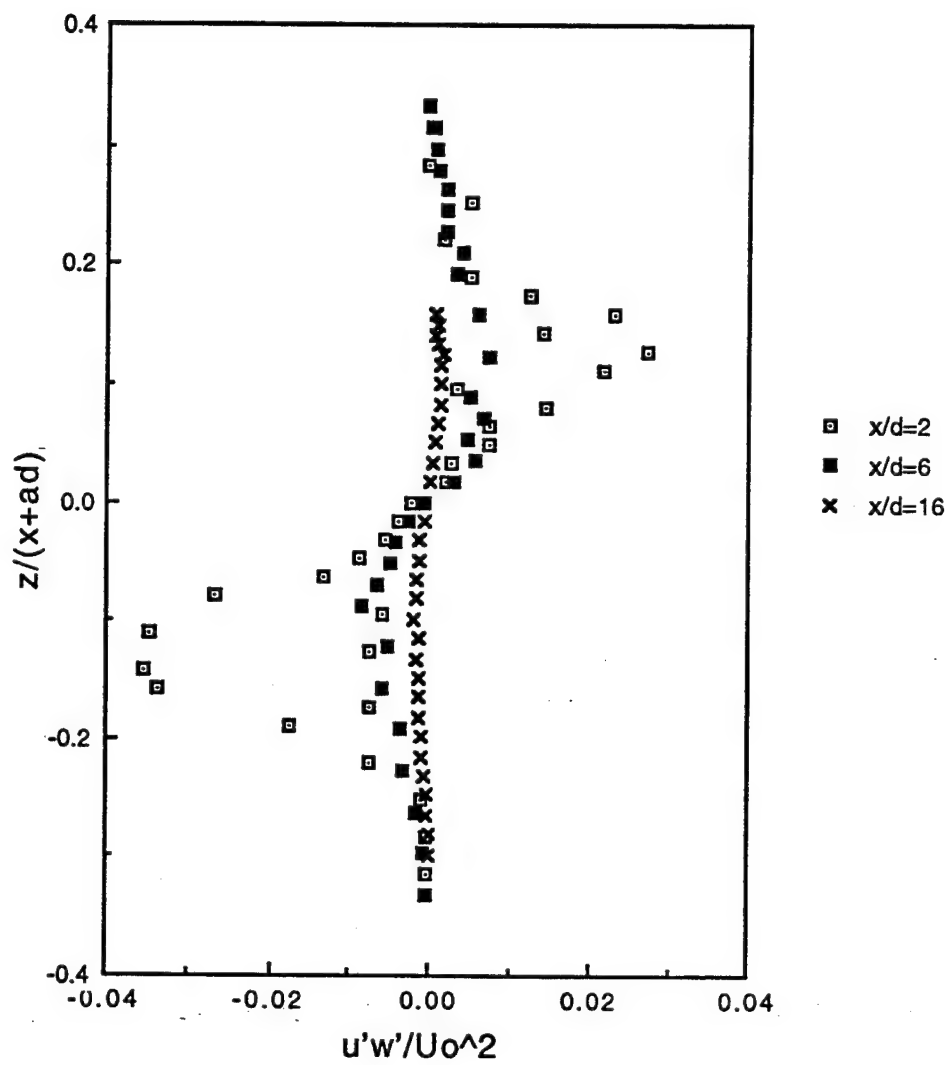
Figure 50b. $u'w'/U_0^2$ versus z^* in the shallow mode for
             S = 0.265 at various axial distances

107
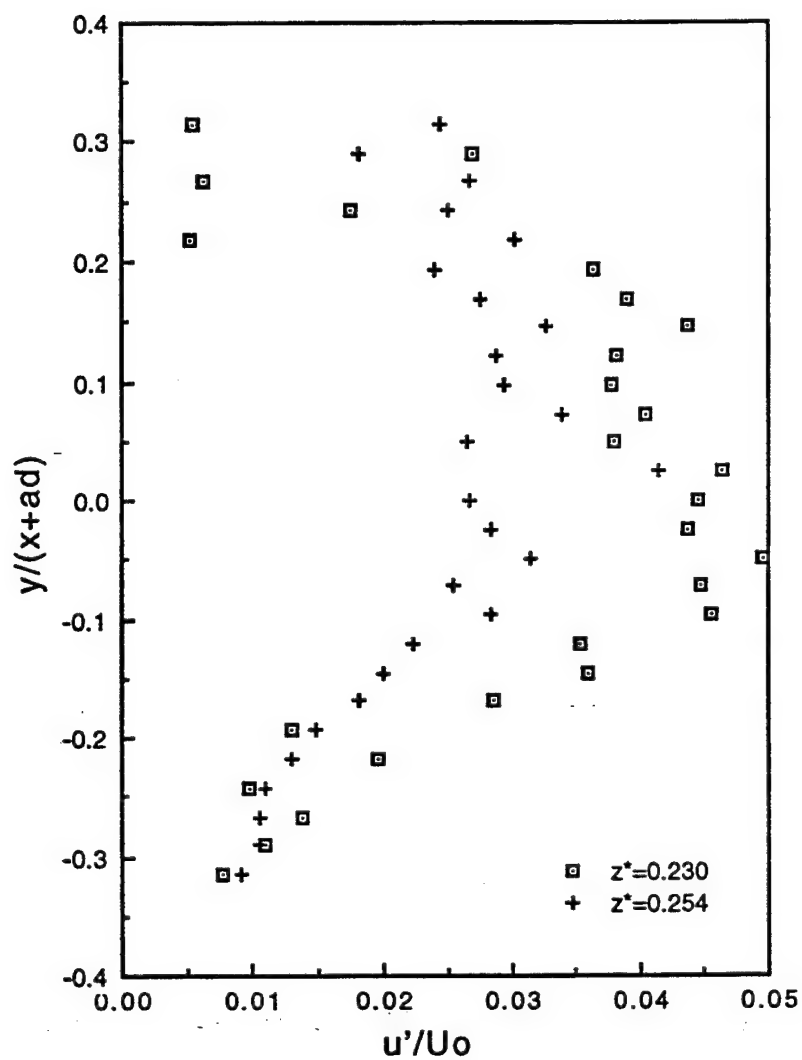
Figure 51.   u'/Uo versus y* near the free surface for S = 0.265
              at x/d = 10
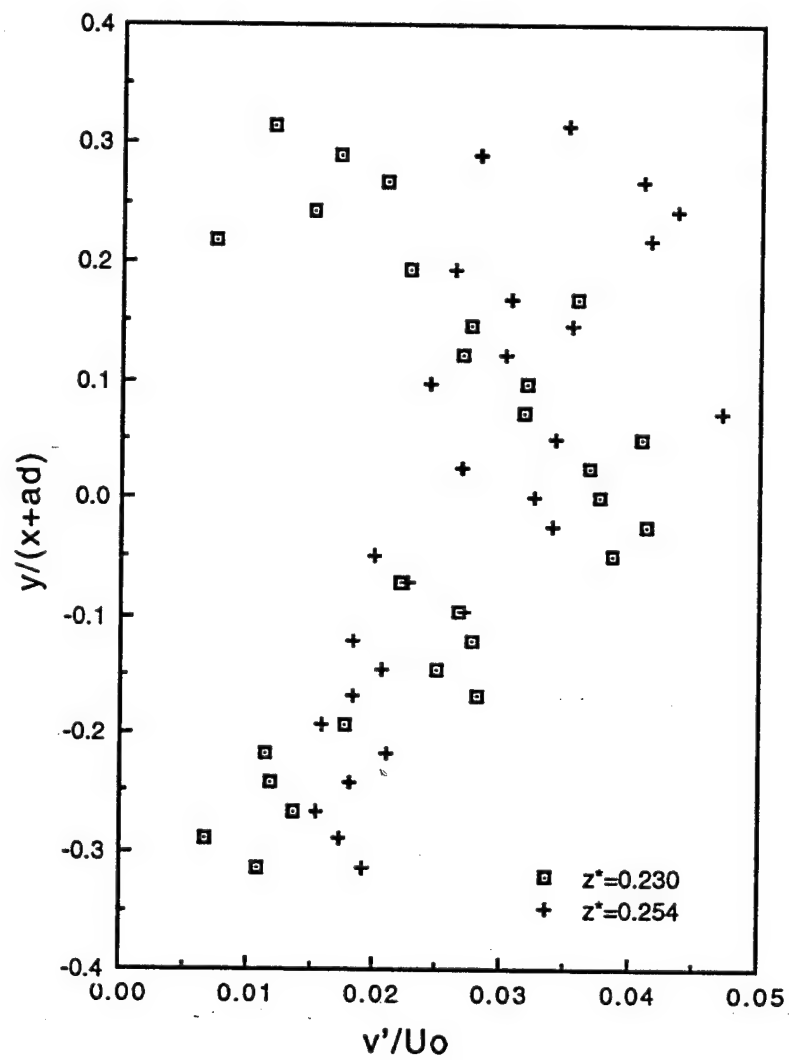
Figure 52.   v'/Uo versus y* near the free surface for S = 0.265 at x/d = 10
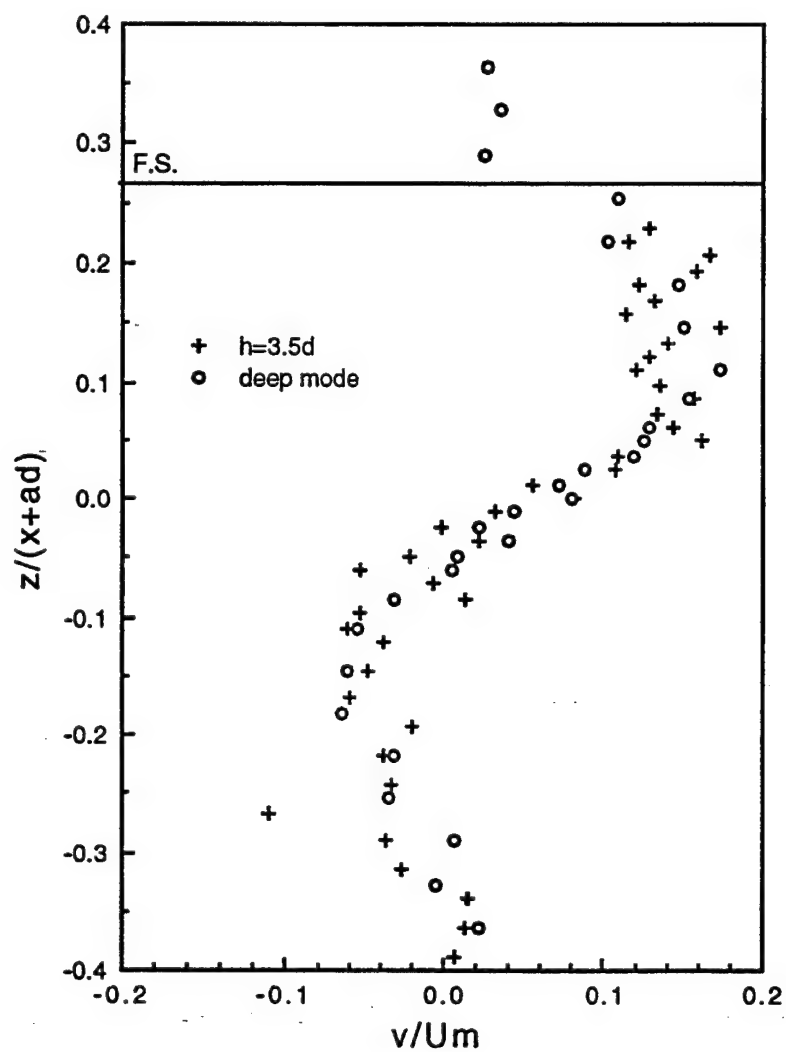
Figure 53.   u/Um versus z* in the deep and shallow modes
for S = 0.5 at x/d = 10

Figure 54.   v/Um versus z* in the deep and shallow modes
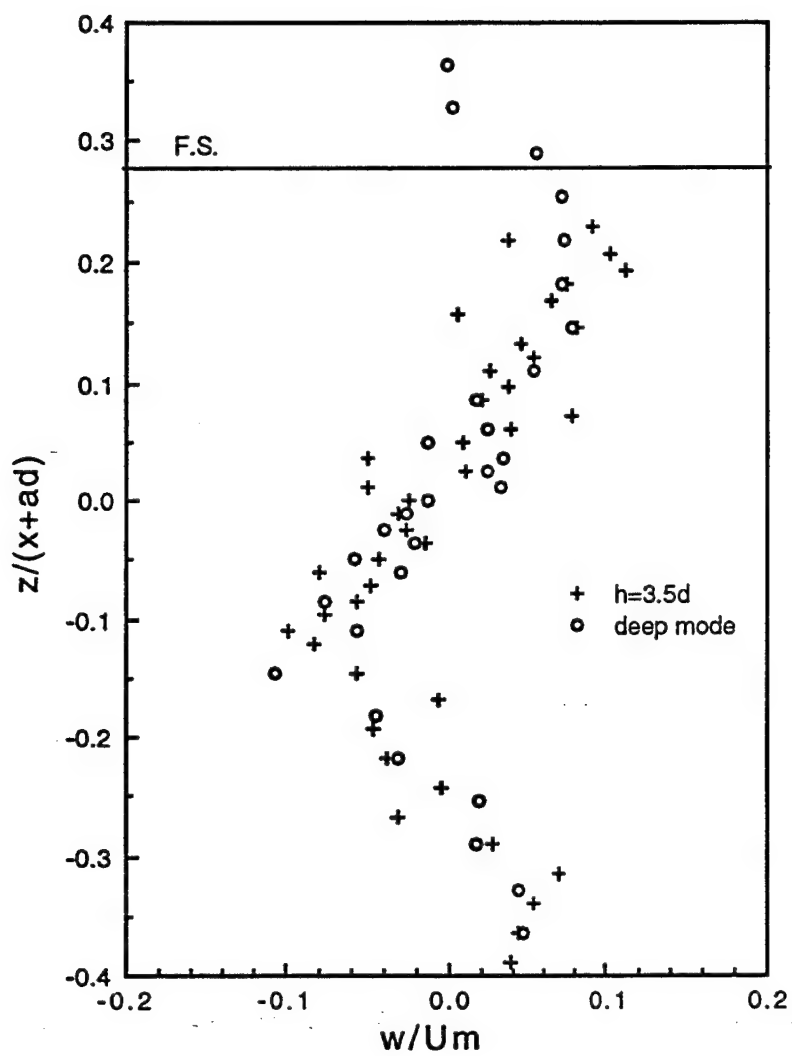   for S = 0.5 at x/d = 10

Figure 55.   w/Um versus z* in the deep and shallow modes
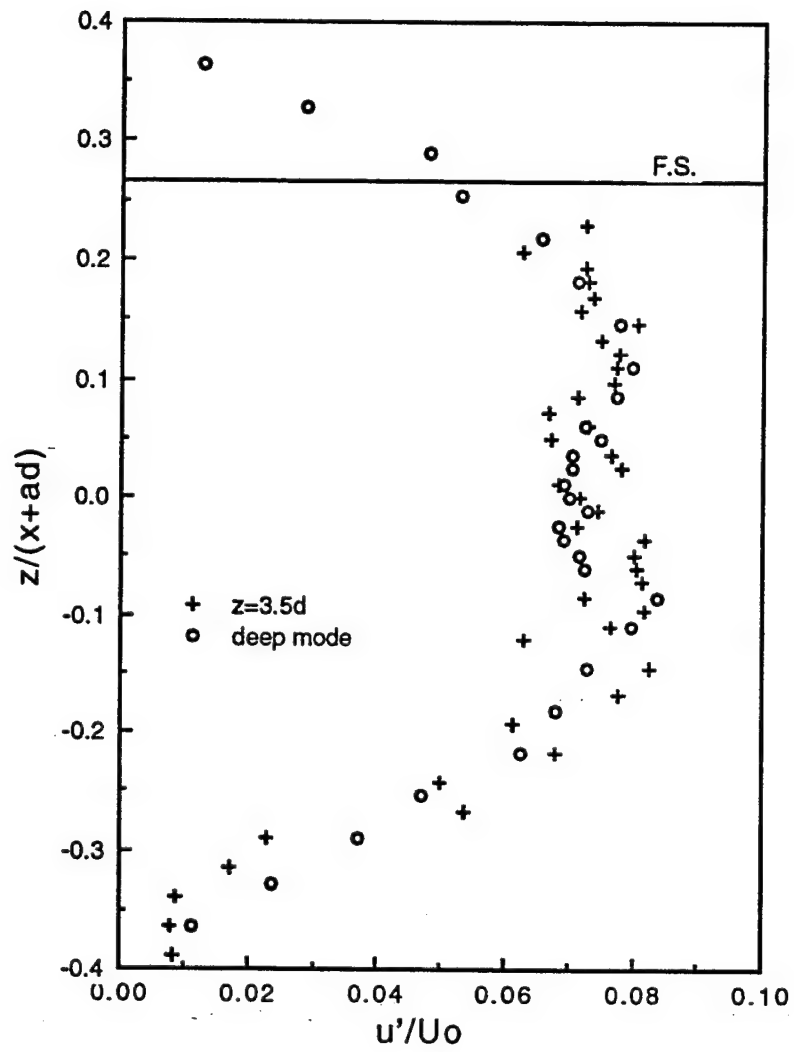   for S = 0.5 at x/d = 10

Figure 56.   u'/Uo versus z* in the deep and shallow modes
            for S = 0.5 at x/d = 10

113
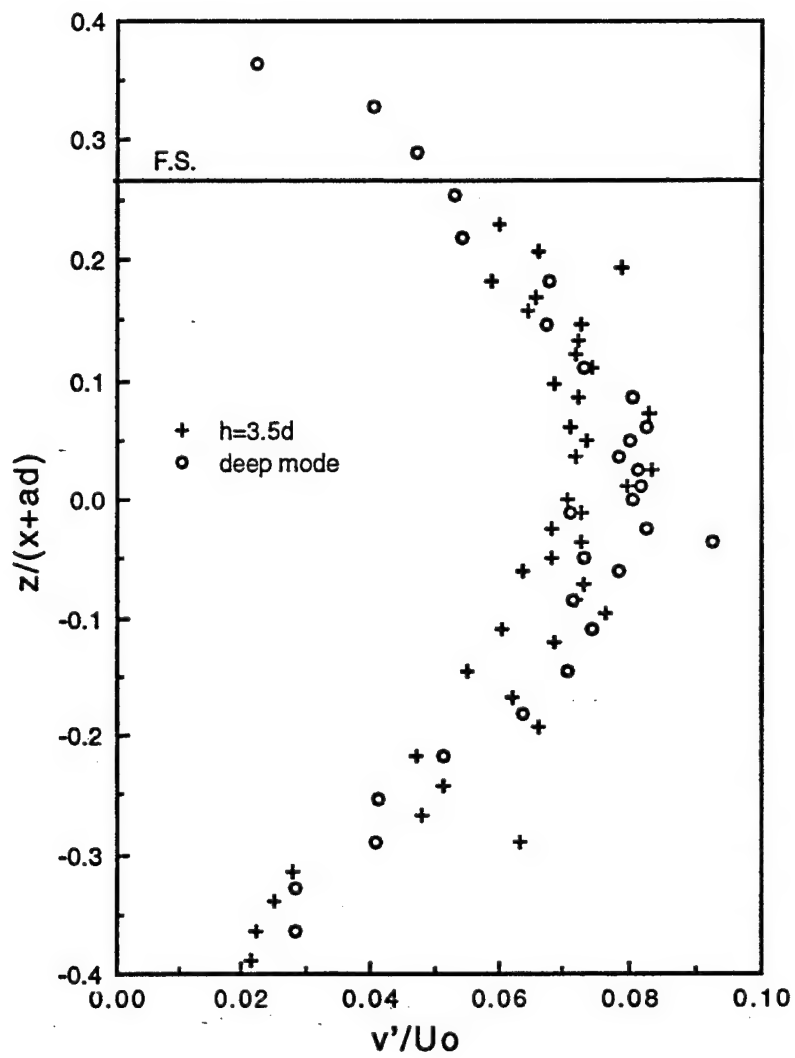
Figure 57.   v'/Uo versus z* in the deep and shallow modes
for S = 0.5 at x/d = 10

114

Figure 58.   w'/Uo versus z* in the deep and shallow modes
             for S = 0.5 at x/d = 10

115

Figure 59. $u'v'/U_0^2$ versus z^* in the deep and shallow modes
              for $S = 0.5$ at $x/d = 10$

Figure 60. $u'w'/U_0^2$ versus z^* in the deep and shallow modes
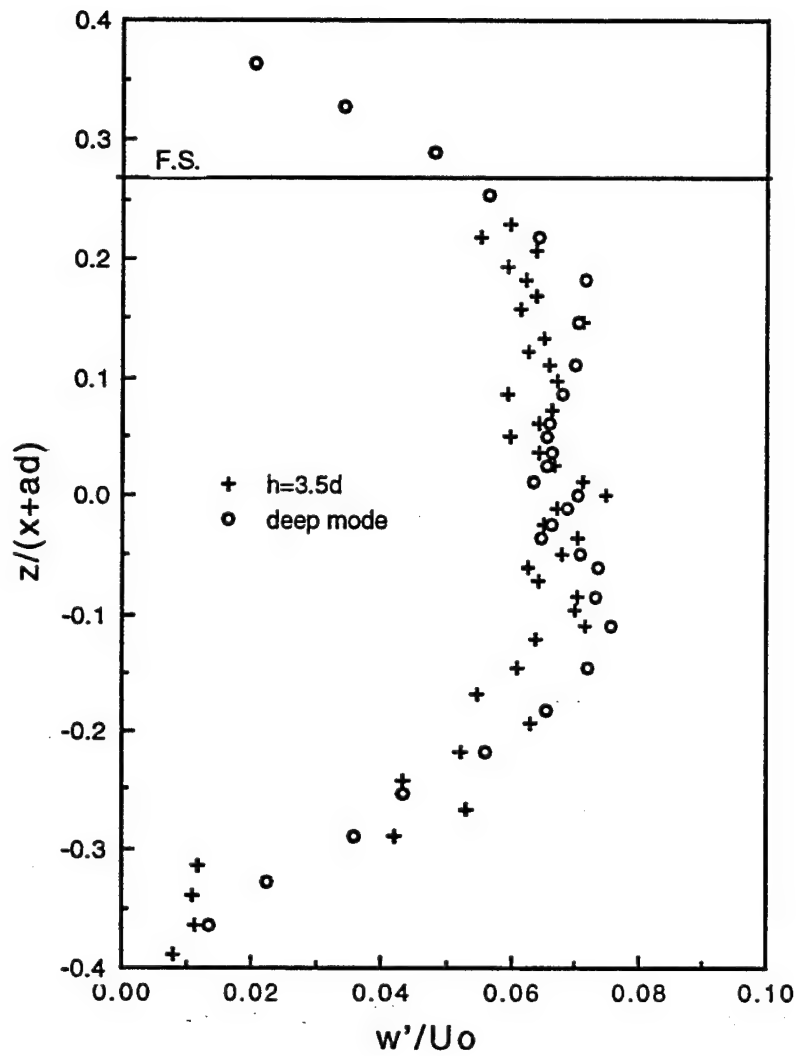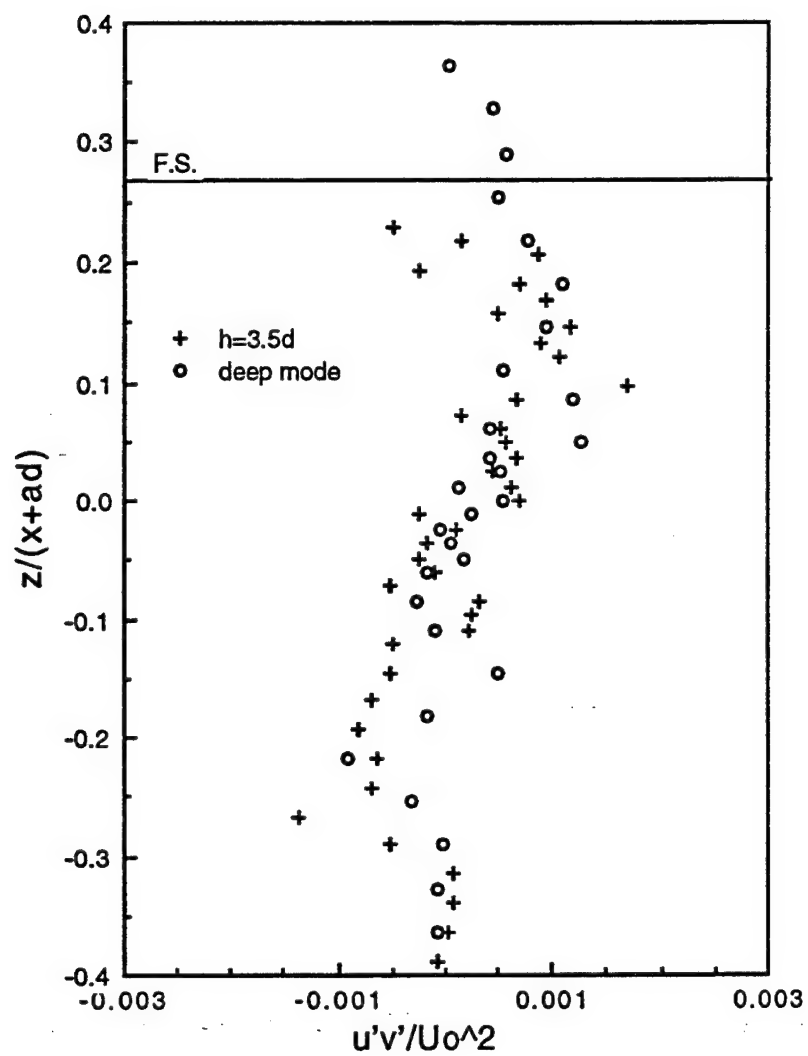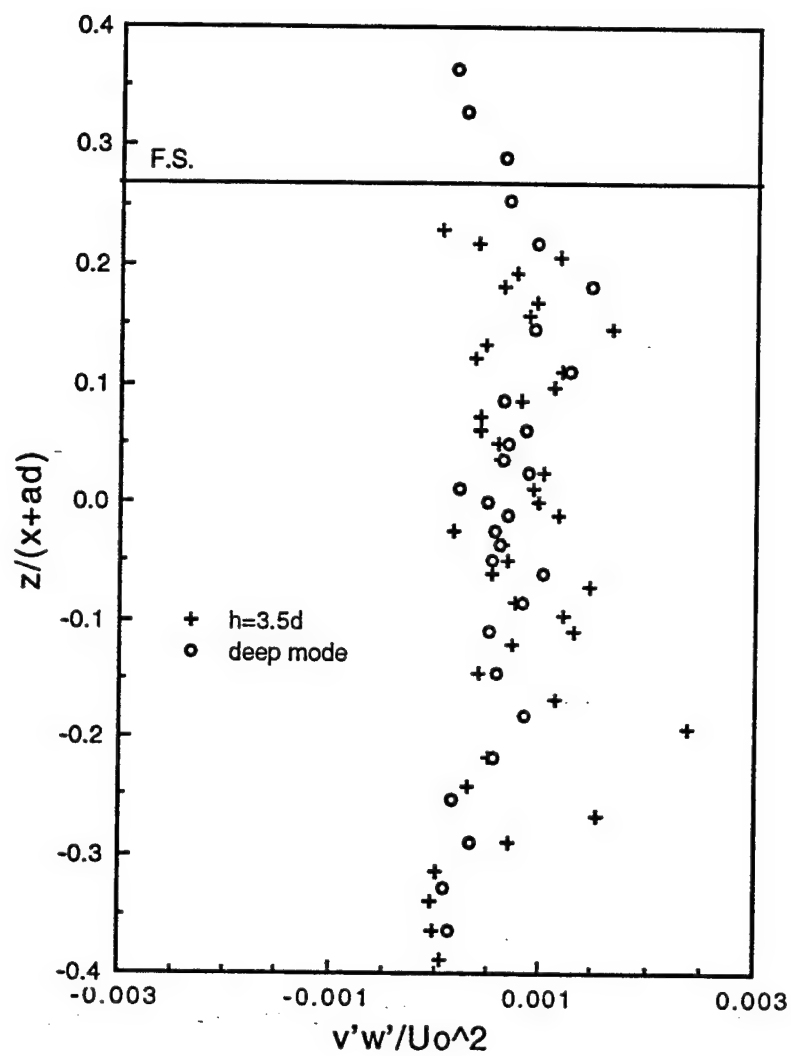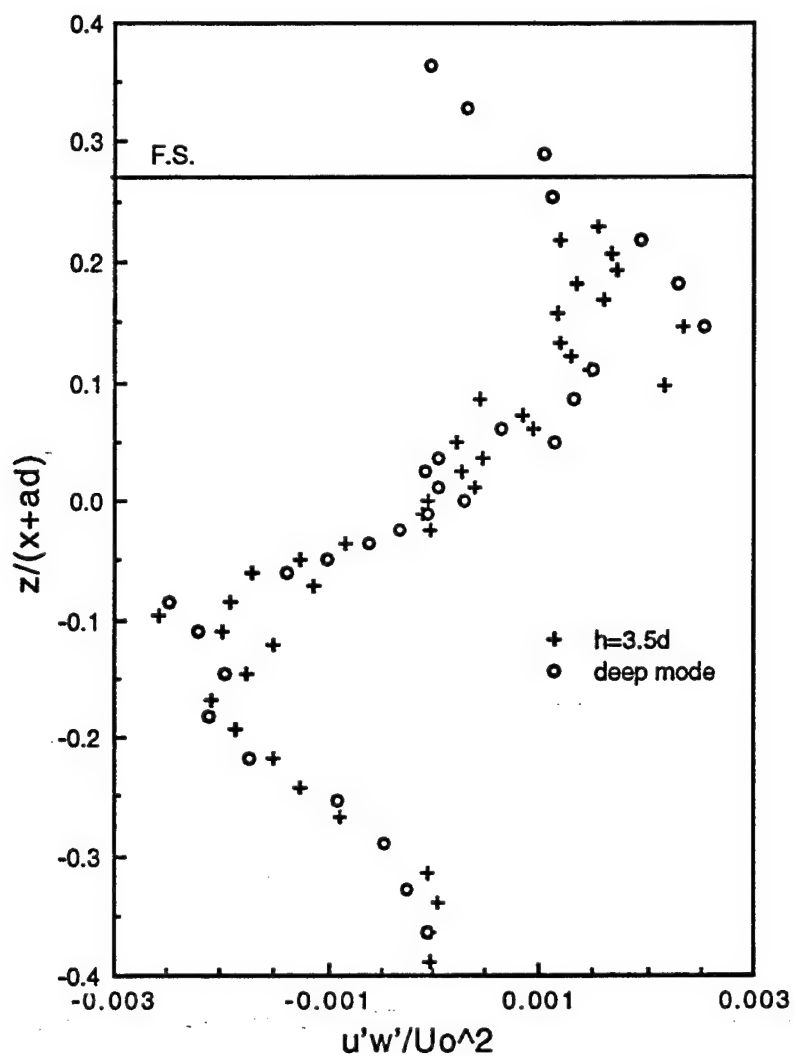   for $S = 0.5$ at $x/d = 10$

117

Figure 61. $v'w' / U_0^2$ versus z^* in the deep and shallow modes for $S = 0.5$ at $x/d = 10$
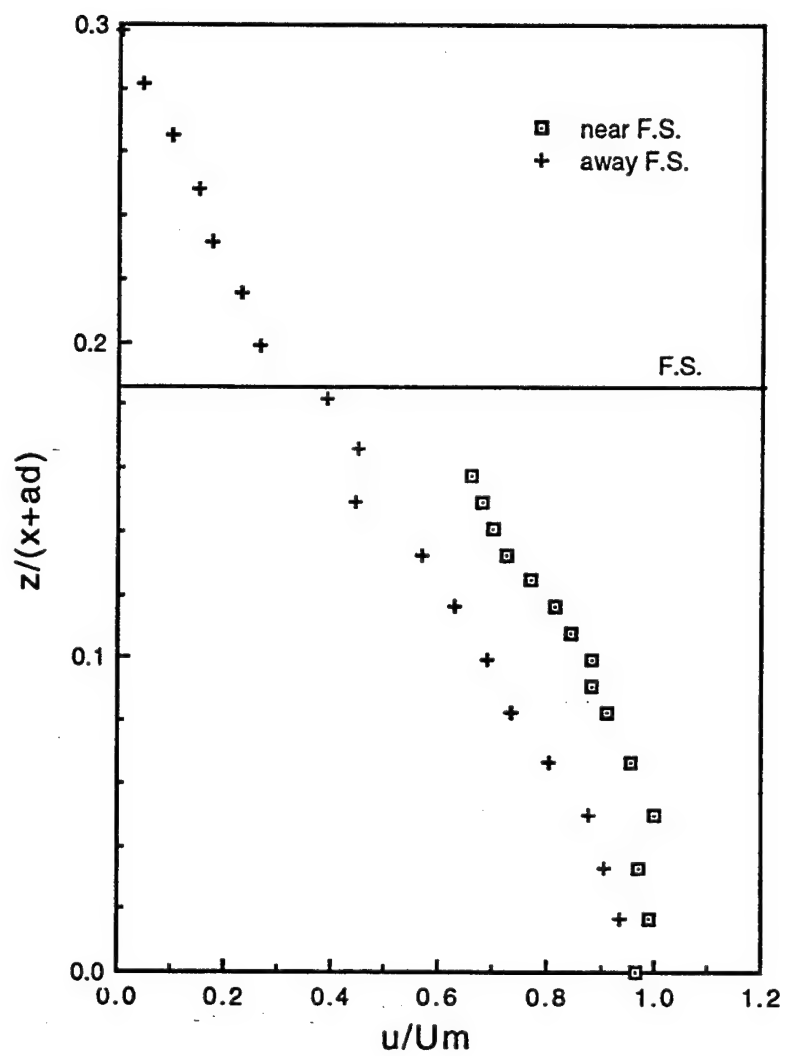
Figure 62.   u/Um versus z* in the shallow mode for S = 0.5
              at x/d = 16

Figure 63.   u/Um and v/Um versus z* in the shallow mode
               for S = 0.5 at x/d = 16

Figure 64.   v/Um and w/Um versus z* in the shallow mode
              for S = 0.5 at x/d =16

121

Figure 65.   u'/Uo versus z* in the shallow mode for S = 0.5
               at x/d = 16
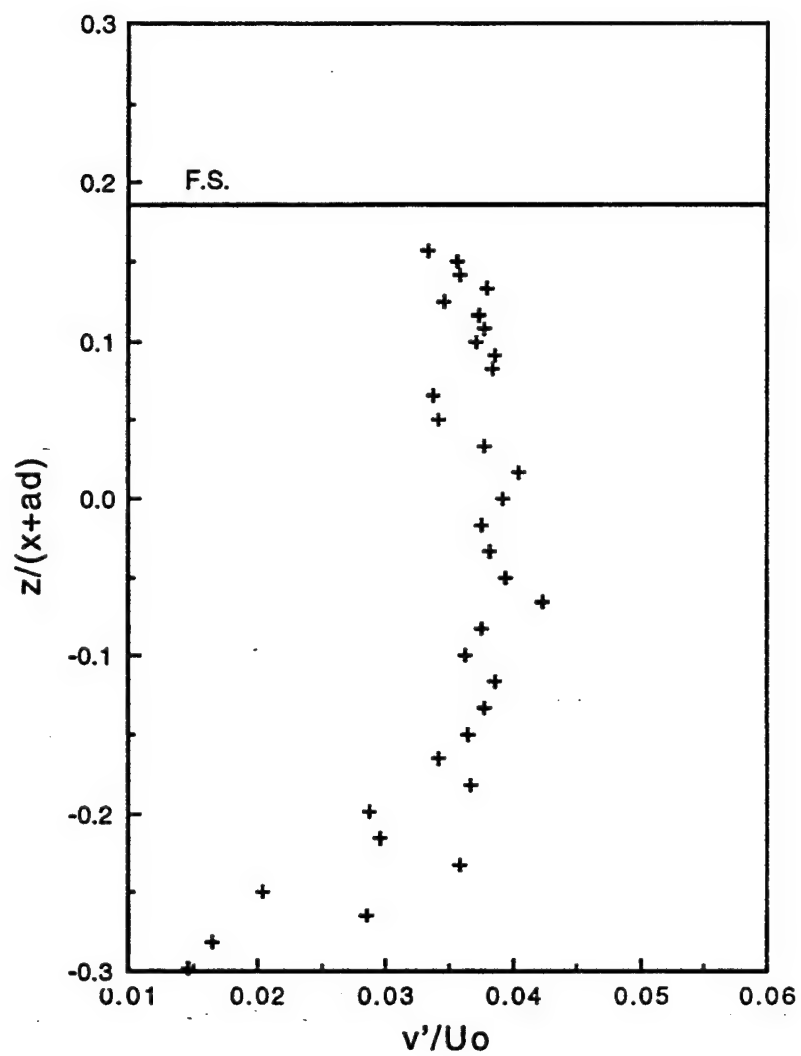
Figure 66.   v'/Uo versus z* in the shallow mode for S = 0.5
at x/d = 16

123
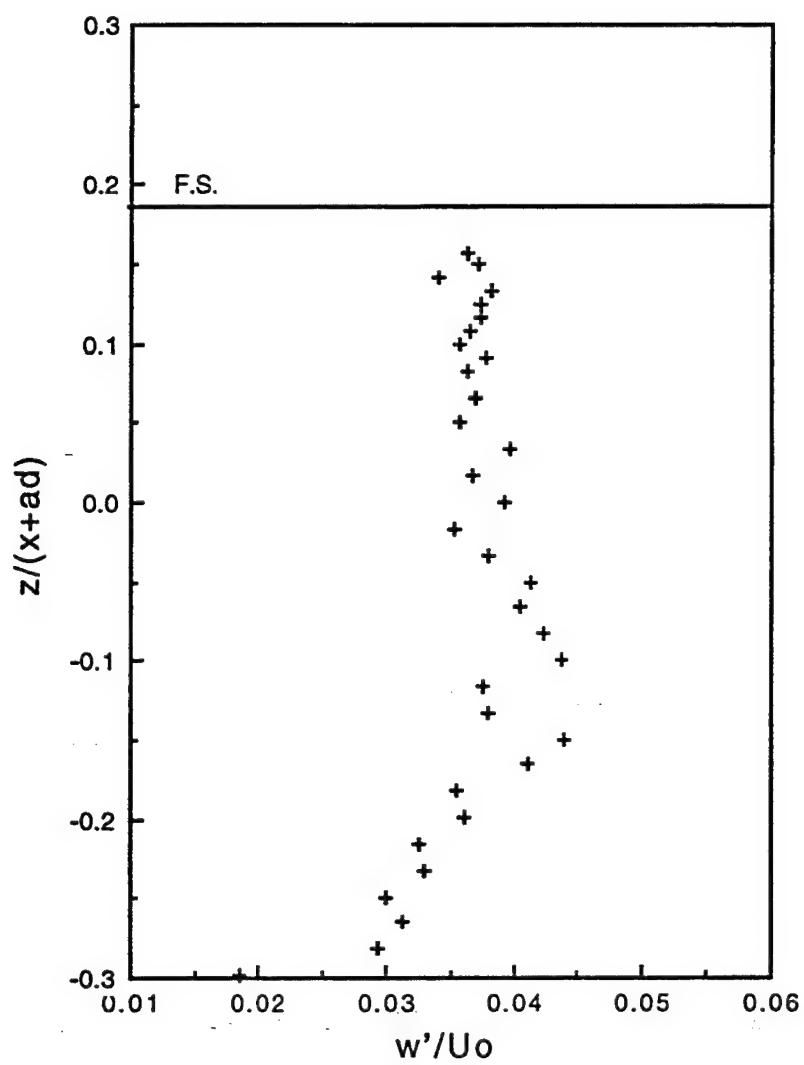
Figure 67.   w'/Uo versus z* in the shallow mode for S = 0.5
              at x/d = 16

124
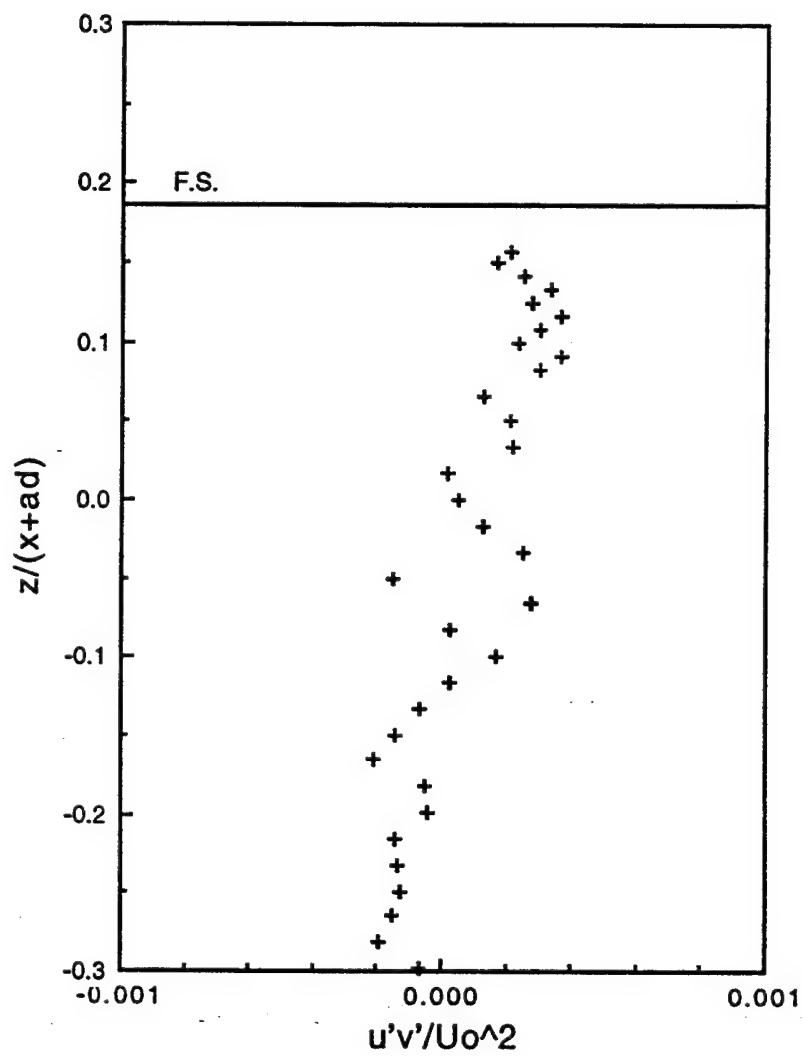
Figure 68. $u'v'/U_o^2$ versus z^* in the shallow mode for S = 0.5 at x/d = 16
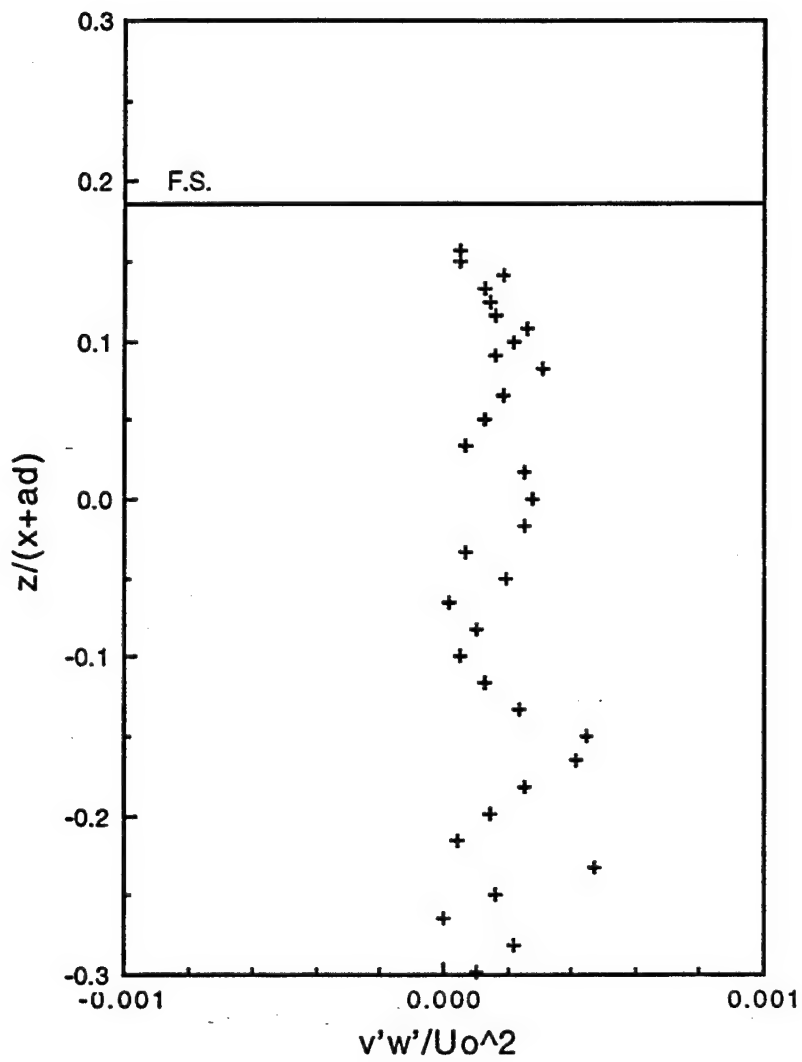
Figure 69.   v'w'/U_o^2 versus z* in the shallow mode for S = 0.5
at x/d = 16
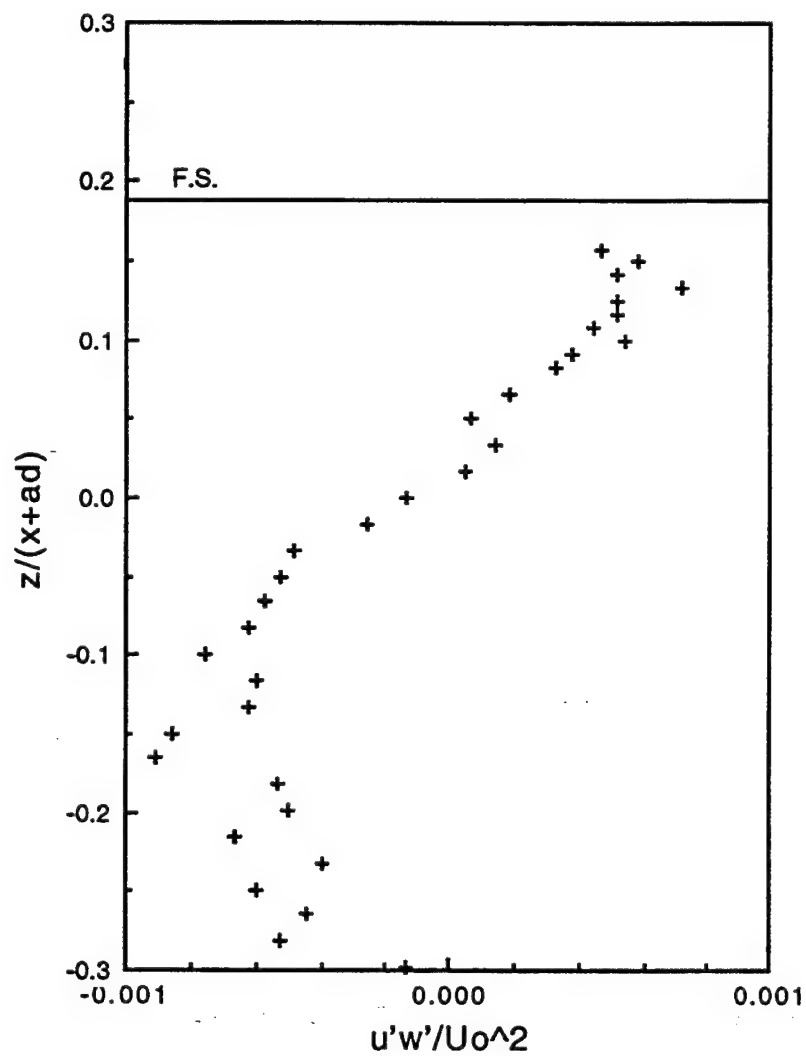
Figure 70.   u'w'/U_o^2 versus z* in the shallow mode for S = 0.5
at x/d = 16
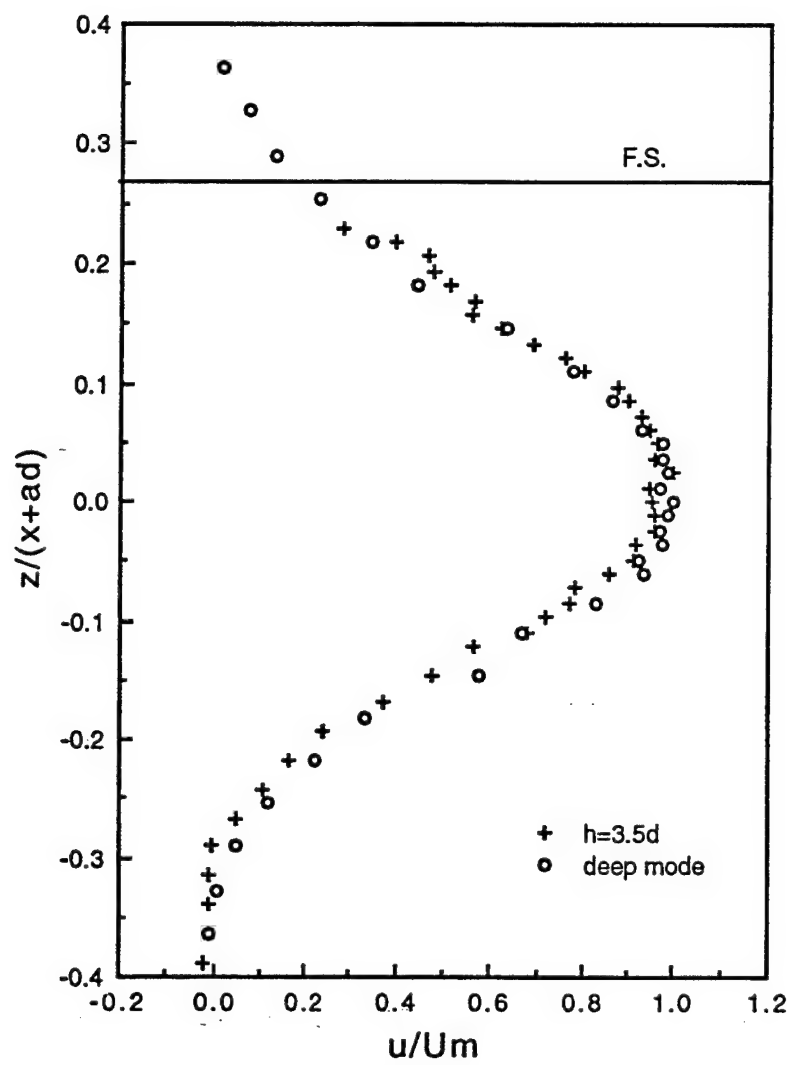
Figure 71.   u/Um versus z* in the deep and shallow modes for
              S = 0.522 at x/d = 10

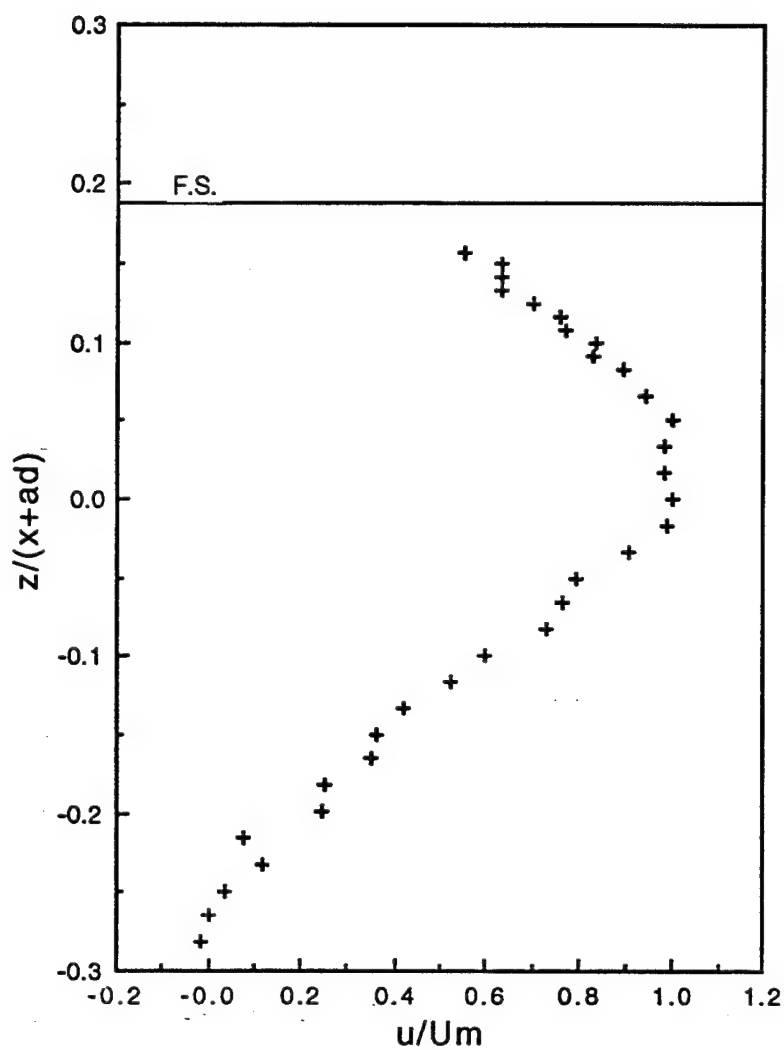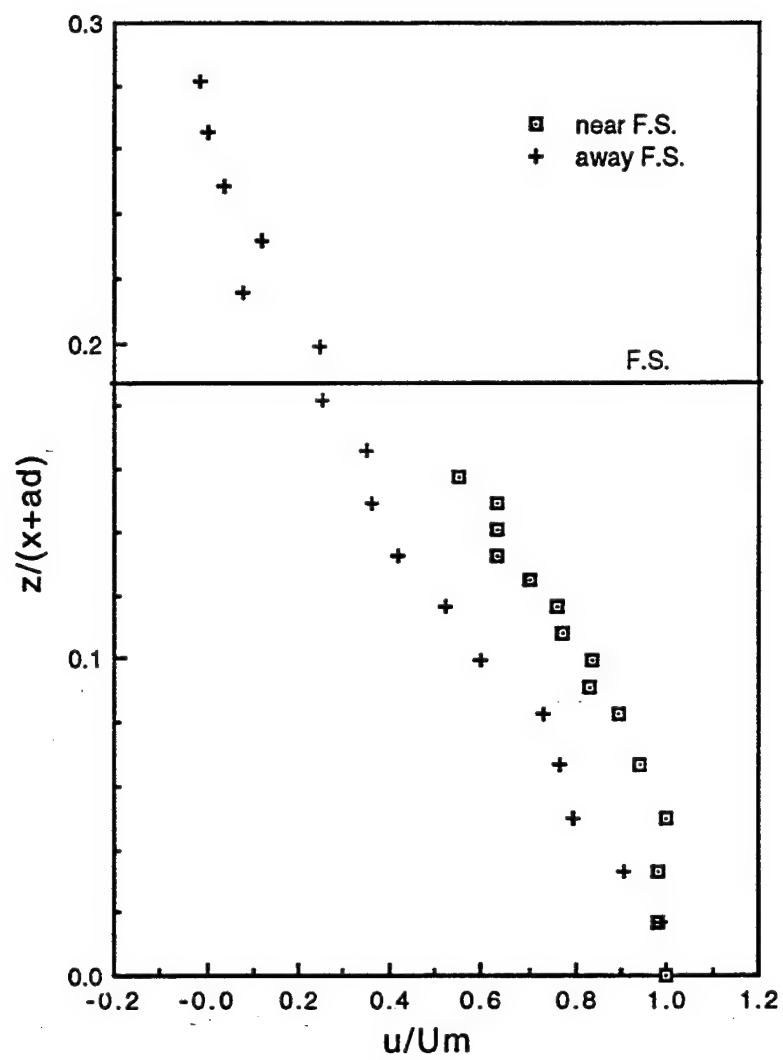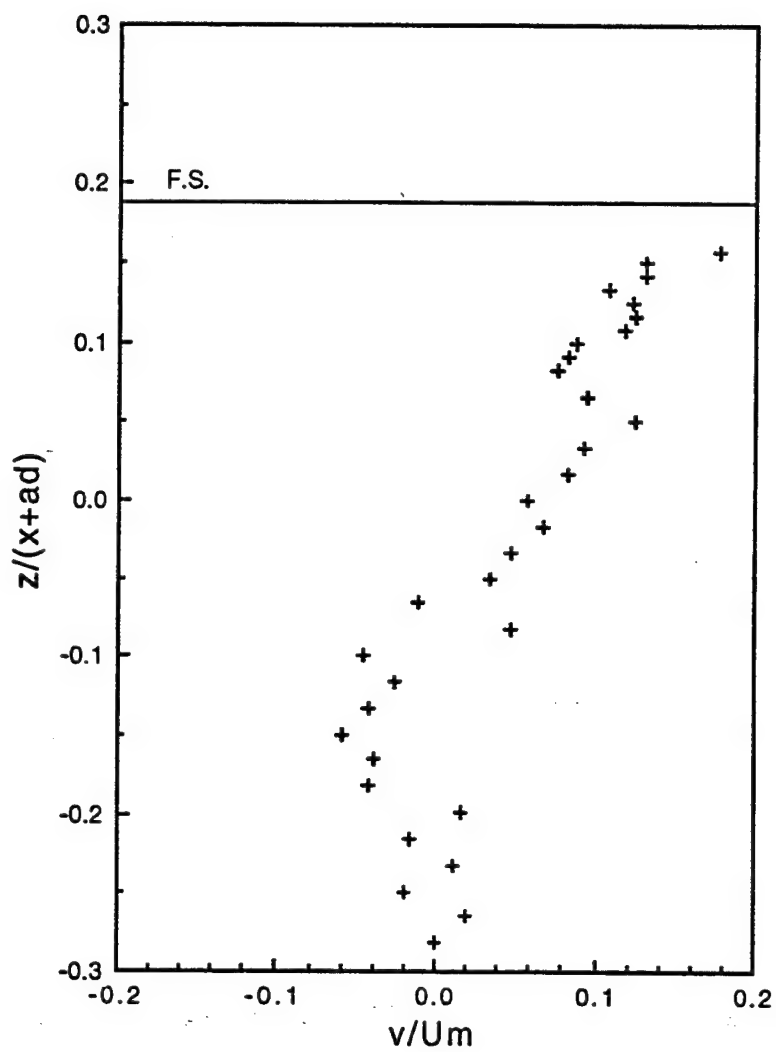Figure 72.   v/Um versus z* in the deep and shallow modes for
S = 0.522 at x/d = 10

129

Figure 73.   w/Um versus z* in the deep and shallow modes for
              S = 0.522 at x/d = 10

Figure 74.   u'/Uo versus z* in the deep and shallow modes for
              S = 0.522 at x/d = 10

Figure 75.   v'/Uo versus z* in the deep and shallow modes for
S = 0.522 at x/d = 10

Figure 76.   w'/Uo versus z* in the deep and shallow modes for
              S = 0.522 at x/d = 10

133

Figure 77. $u'v'/U_0^2$ versus z^* in the deep and shallow modes
for $S = 0.522$ at $x/d = 10$

Figure 78. $v'w'/U_0^2$ versus z^* in the deep and shallow modes for $S = 0.522$ at $x/d = 10$

135

Figure 79. $u'w'/U_0^2$ versus z^* in the deep and shallow modes for S = 0.522 at x/d = 10

Figure 80. u/Um versus z* in the shallow mode for S = 0.522
at x/d = 16

137

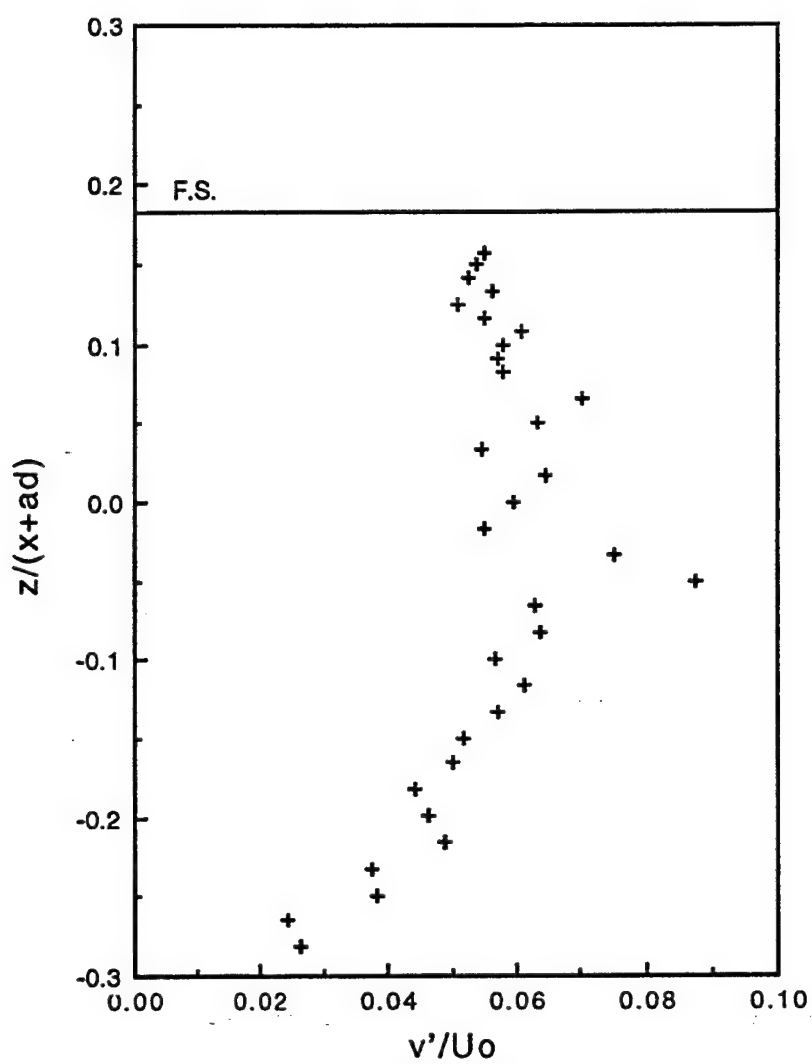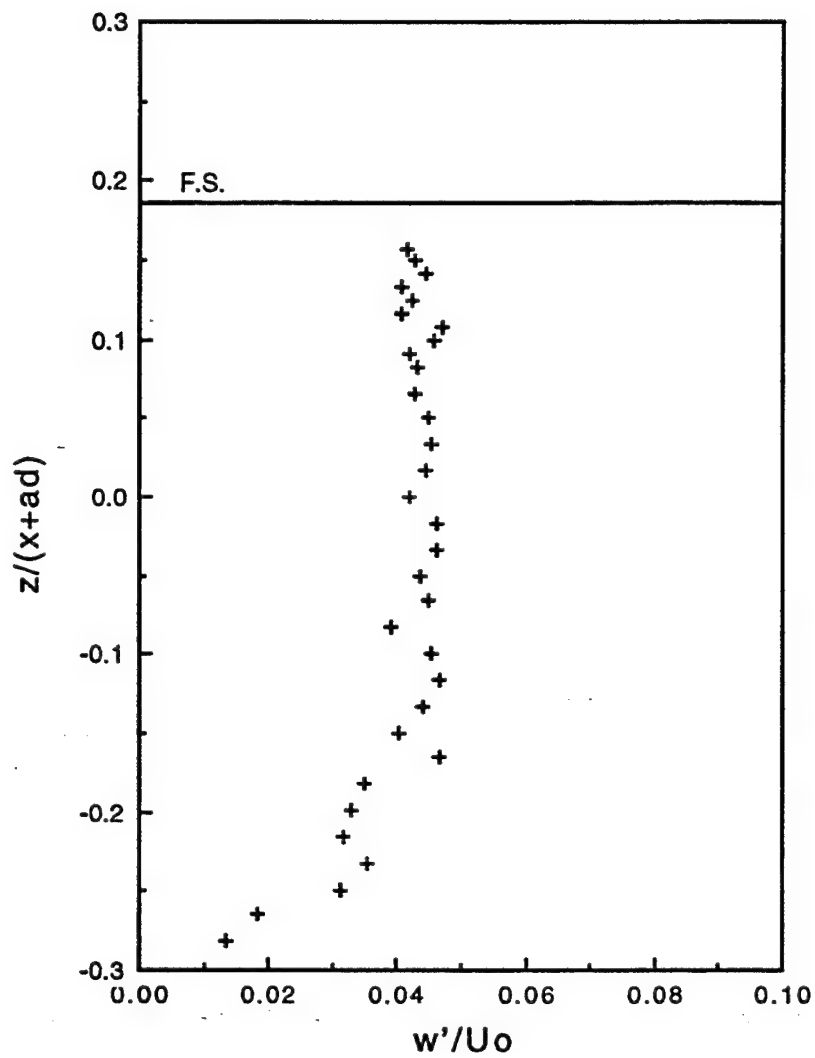Figure 81.   u/Um versus z* in the shallow mode for S = 0.522
              at x/d = 16

Figure 82.   v/Um versus z* in the shallow mode for S = 0.522
at x/d = 16
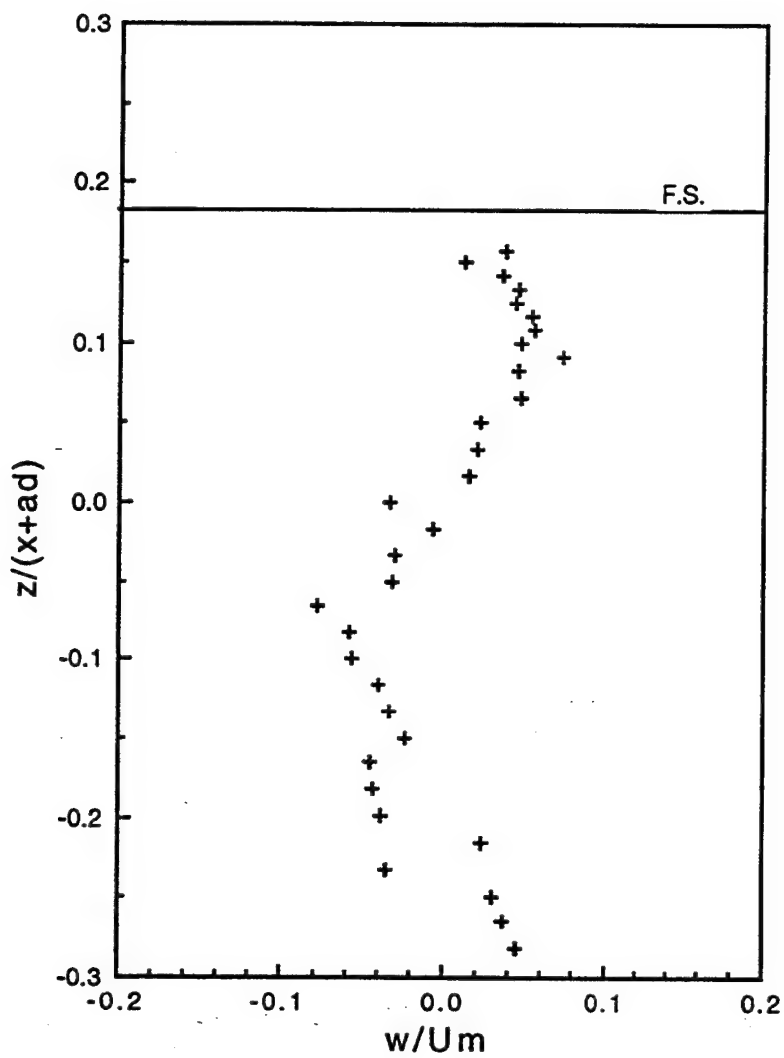
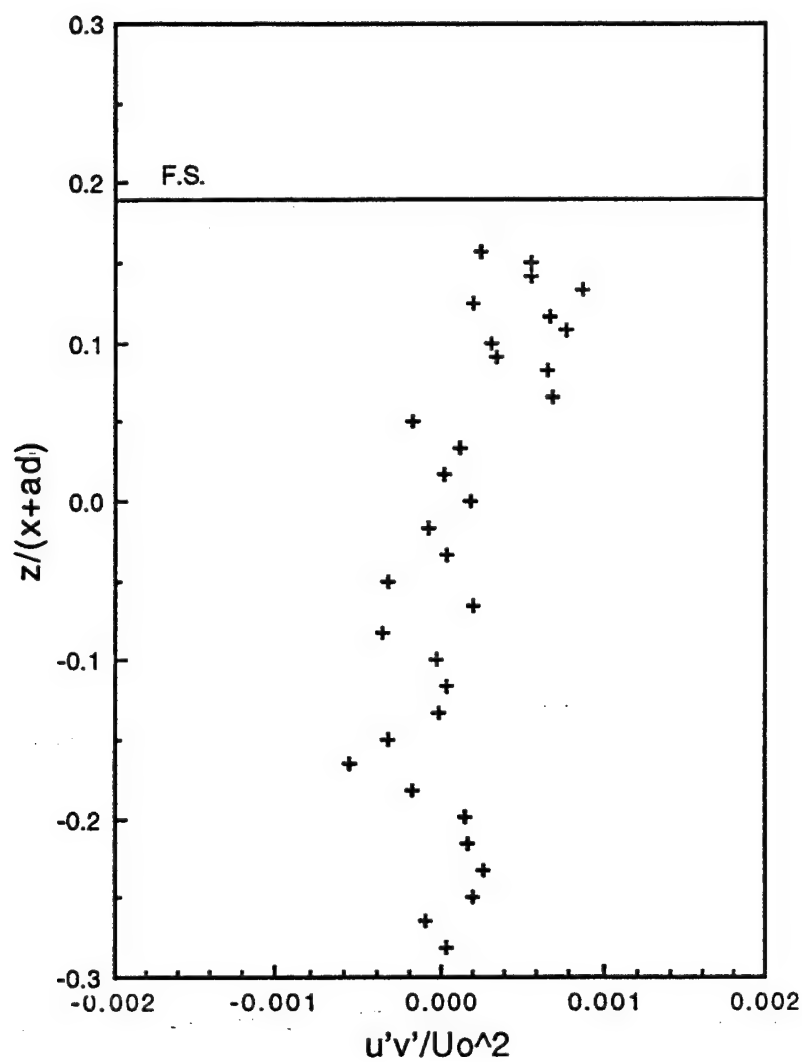Figure 83.   w/Um versus z* in the shallow mode for S = 0.522
               at x/d = 16
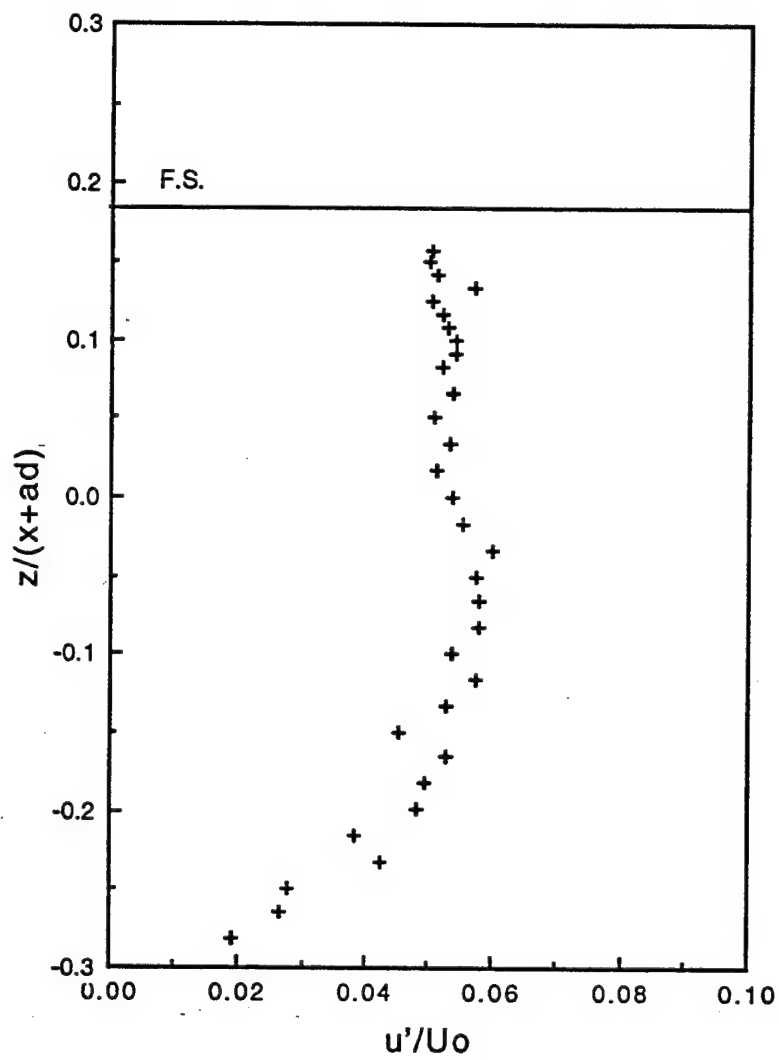
140

Figure 84.   u'/Uo versus z* in the shallow mode for S = 0.522
at x/d = 16

141

Figure 85. v'/Uo versus z* in the shallow mode for S = 0 .522
at x/d = 16

Figure 86.   w'/Uo versus z* in the shallow mode for S = 0.522
              at x/d = 16

Figure 87. $u'v'/U_o^2$ versus z^* in the shallow mode for $S = 0.522$
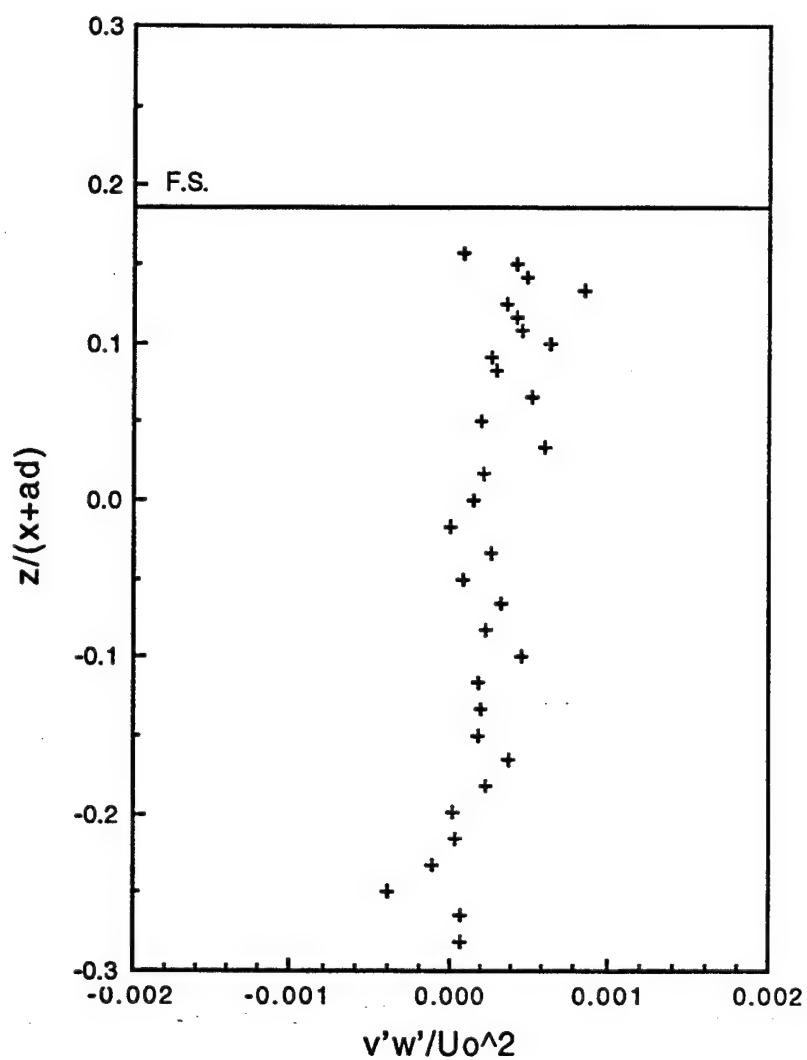   at $x/d = 16$

144

Figure 88. $v'w'/U_o^2$ versus z^* in the shallow mode for S = 0.522 at x/d = 16

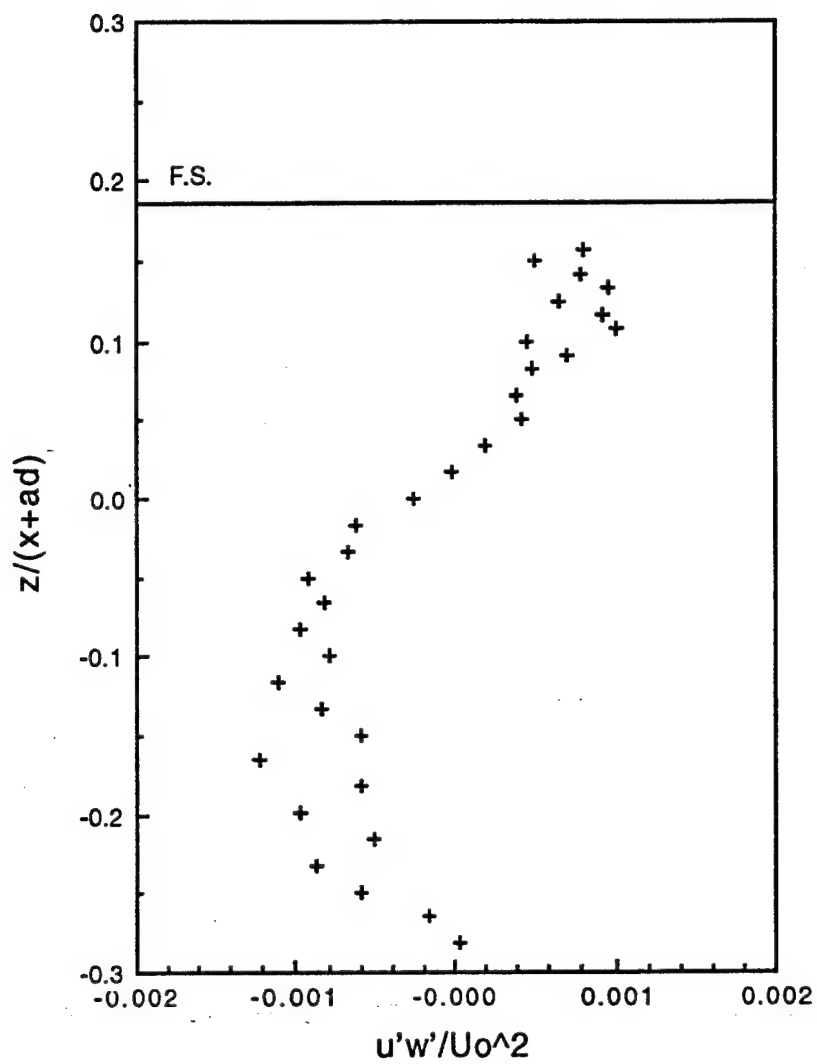Figure 89. $u'w'/U_0^2$ versus z^* in the shallow mode for S = 0.522 at x/d = 16
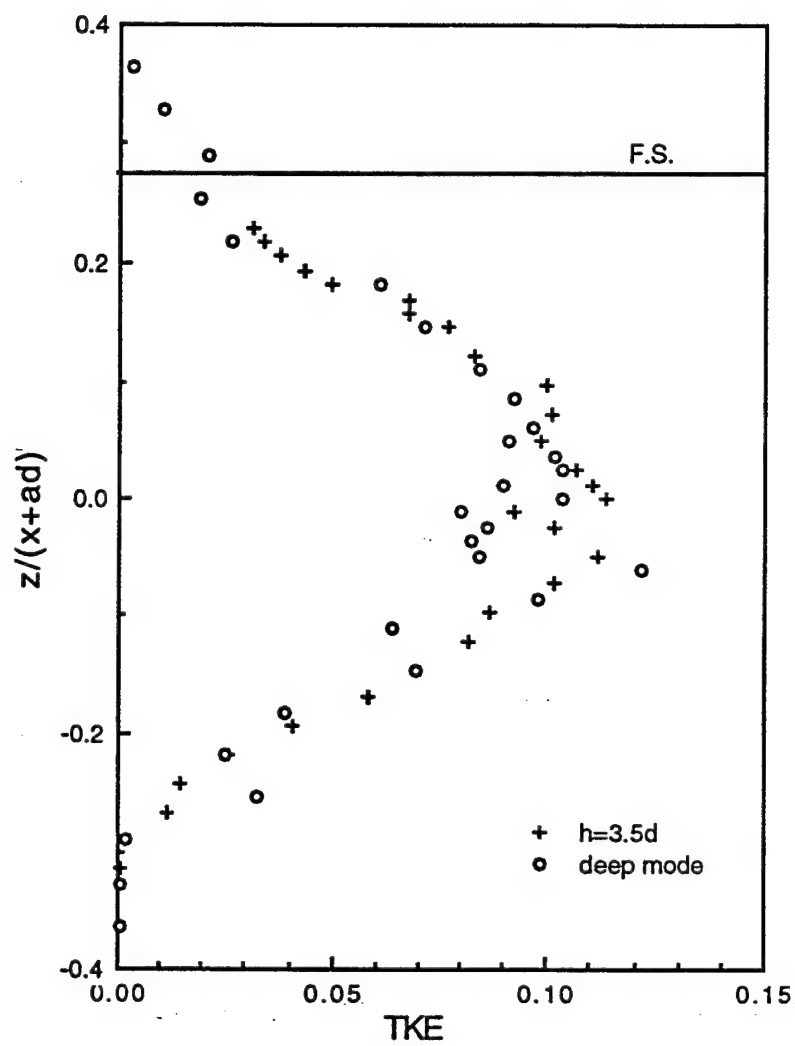
Figure 90.   TKE versus z* in the deep and shallow modes for
              S = 0.265 at x/d = 10
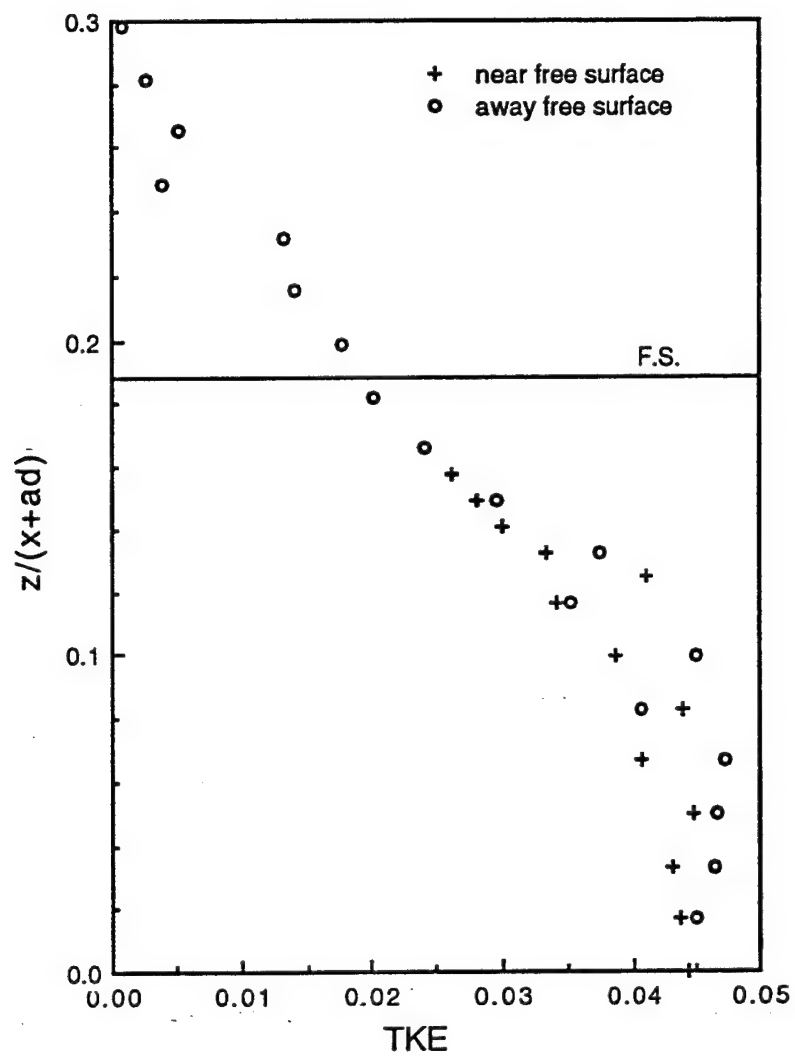
Figure 91.   TKE versus z* in the shallow mode for S = 0.265
              at x/d = 16

Figure 92.   TKE versus z* in the deep and shallow modes for
              S = 0.5 at x/d = 10

149

Figure 93.   TKE versus z* in the shallow mode for S = 0.5
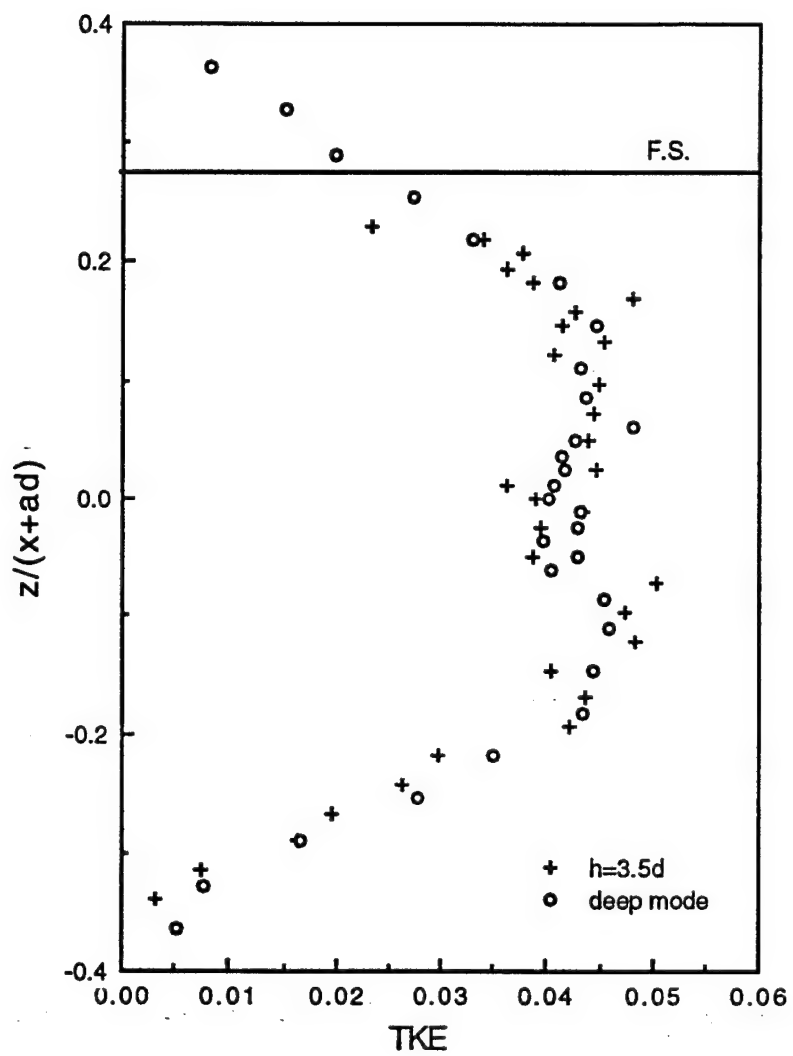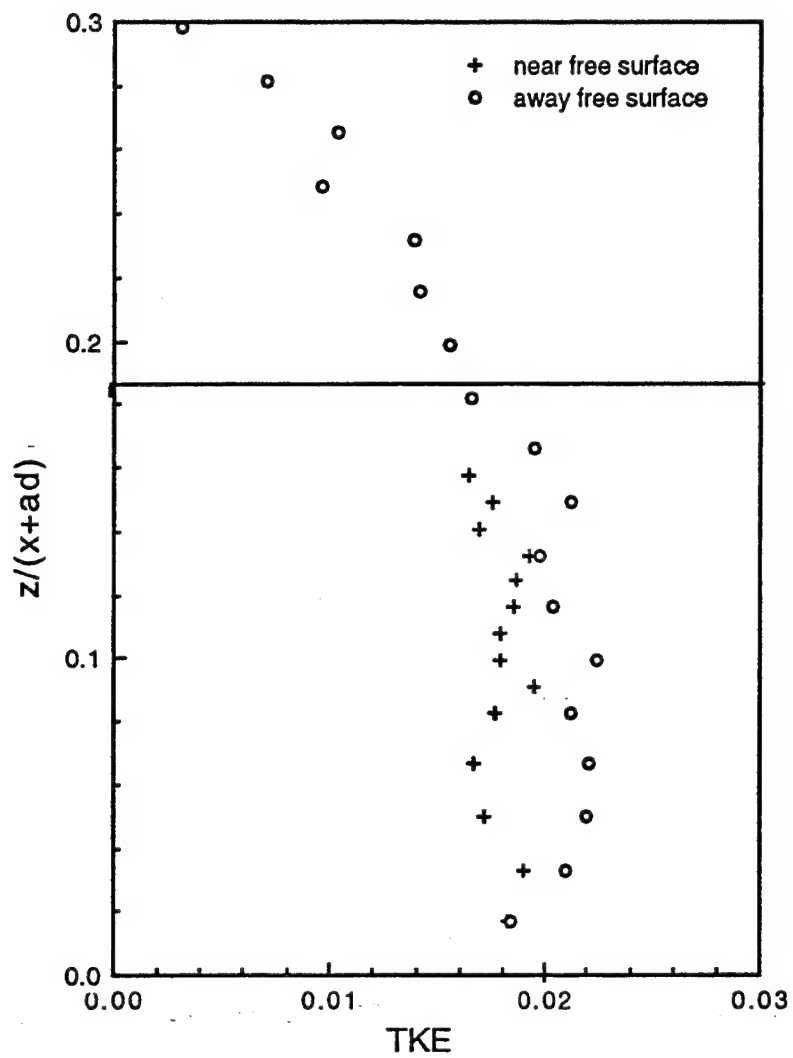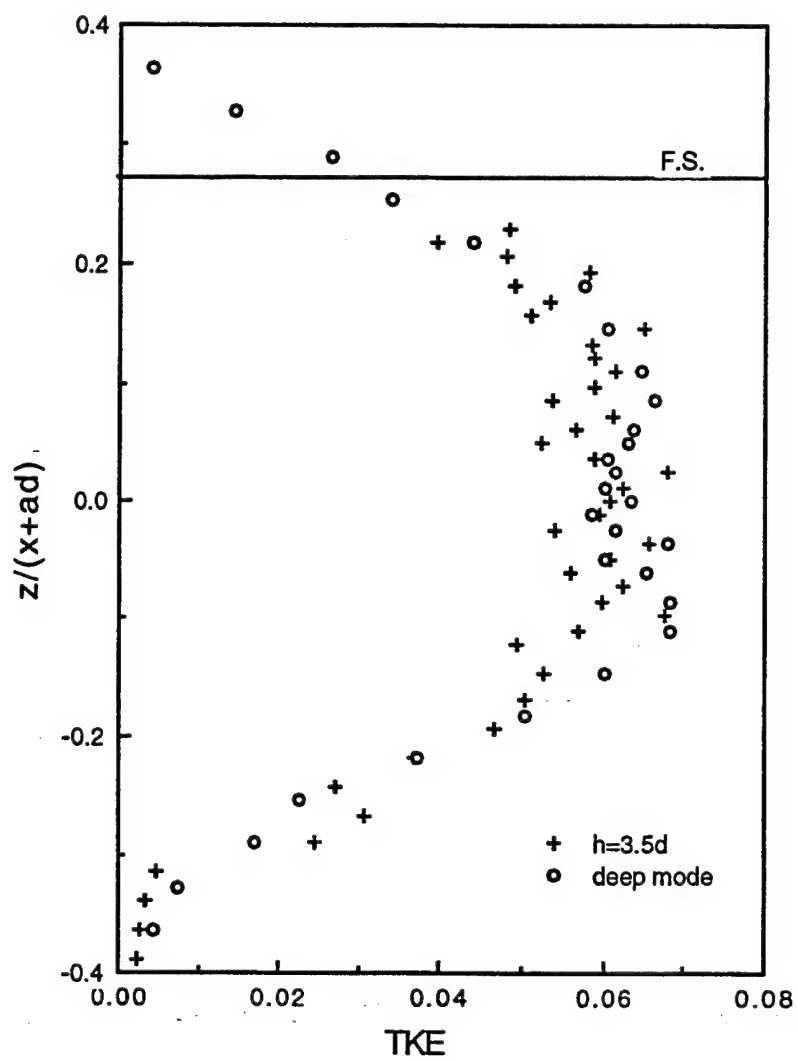at x/d = 16

Figure 94.   TKE versus z* in the deep and shallow modes for
S = 0.522 at x/d = 10

151
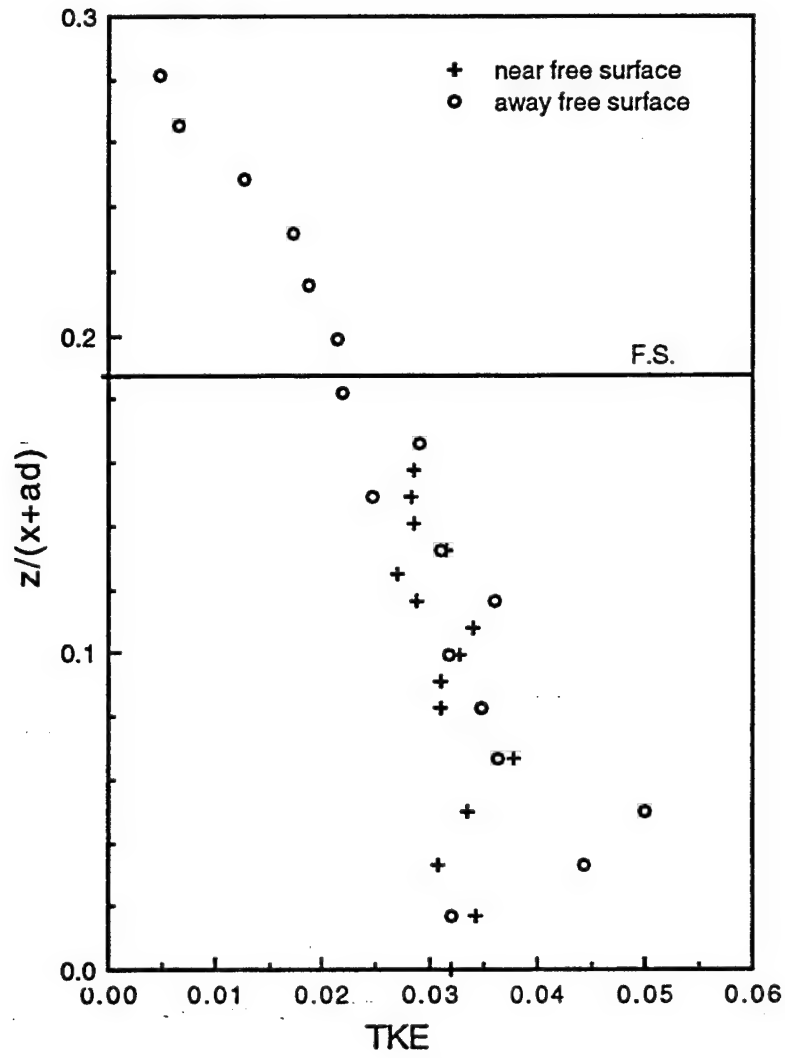
Figure 95.   TKE versus z* in the shallow mode for S = 0.522
              at x/d = 16

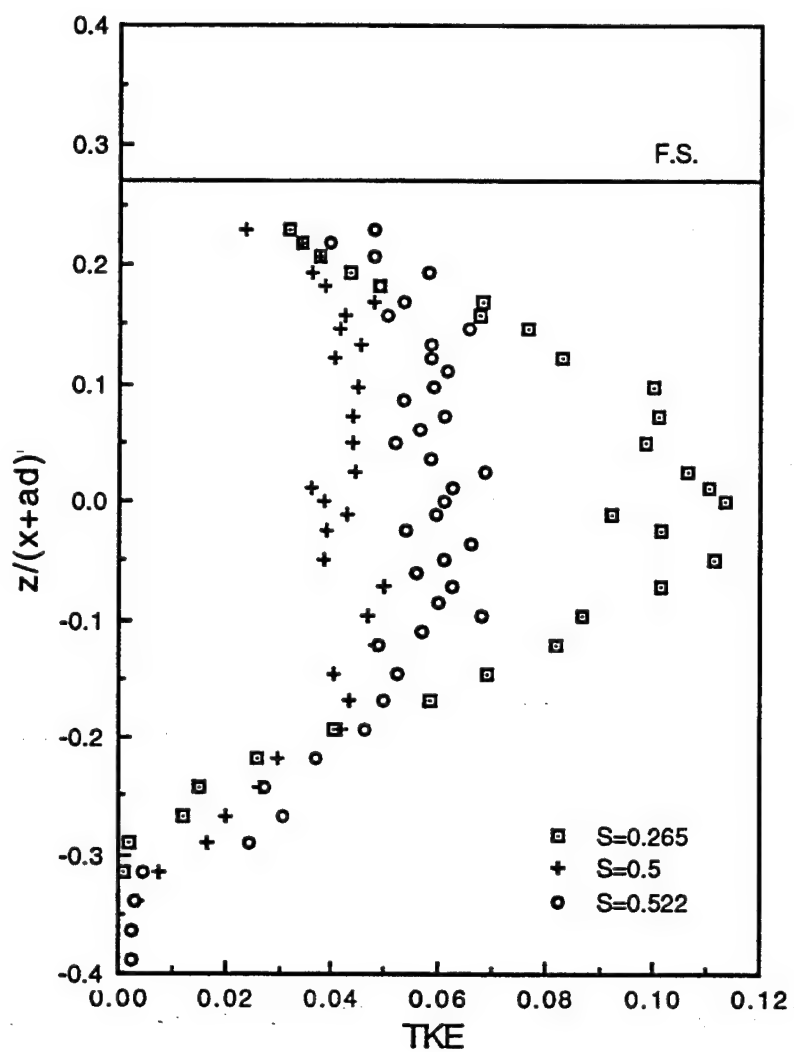Figure 96.   TKE versus z* in the shallow mode for various swirl
numbers at x/d = 10
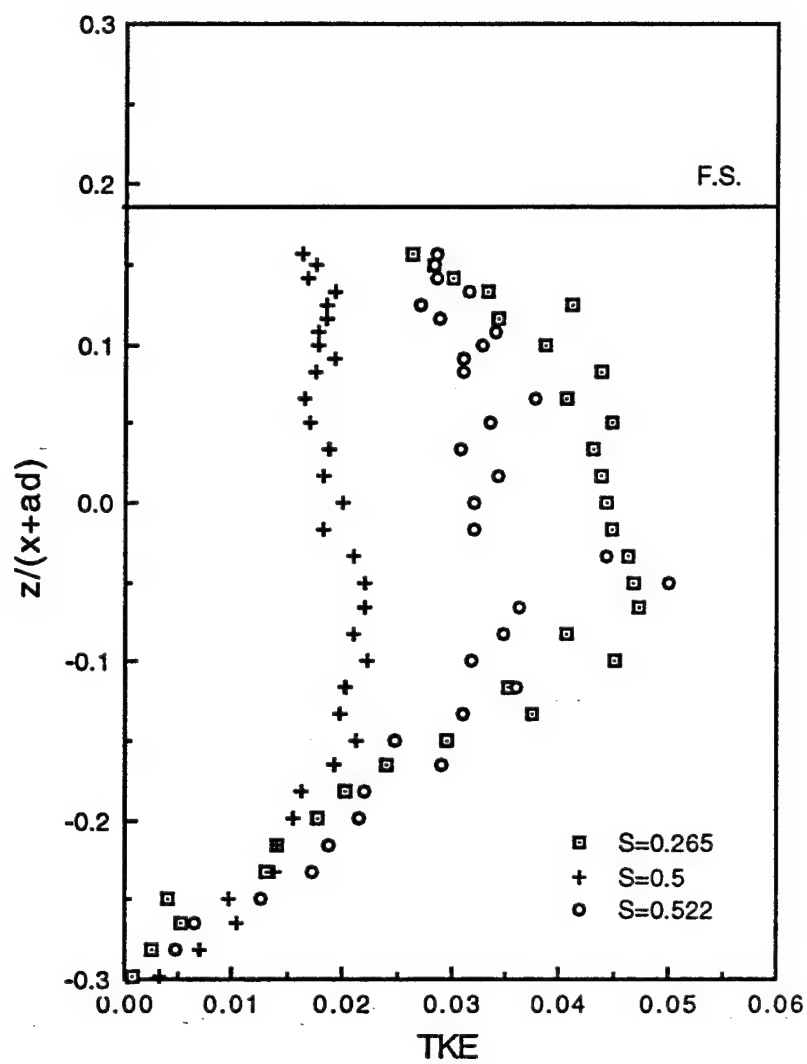
Figure 97.   TKE versus z* in the shallow mode for various swirl
               numbers at x/d = 16

154

(a)

(b)
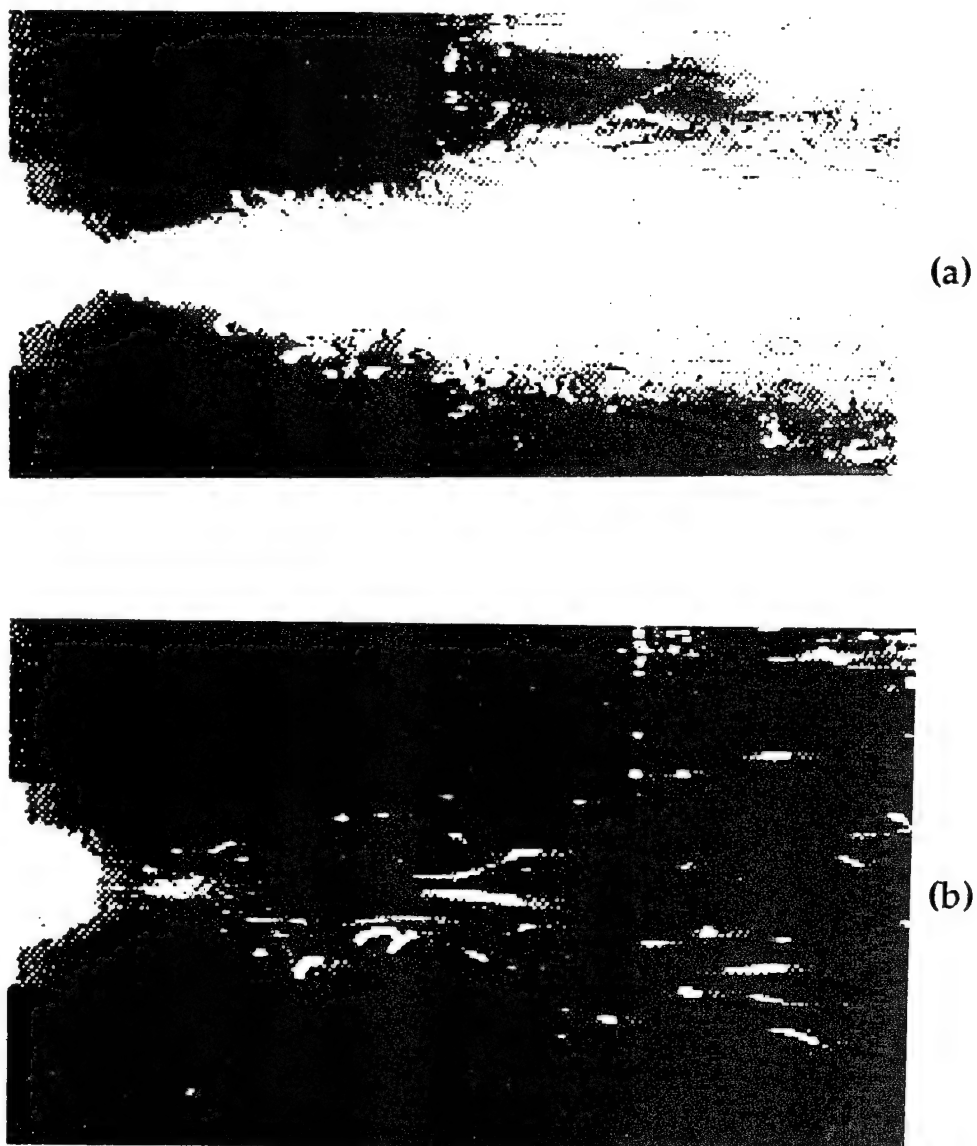
Figure 98.   Photograph of a swirling jet at S = 0.522, depicting the shape of flow near the nozzle exit: (a) with large number of particles, (b) with a relatively few particles to show the vortex breakdown

Figure 99.   Surface structures resulting from the impulsive start
of a swirling flow for h/d = 3.5, Re = 18,000, and F = 6

156

Figure 100.   Surface signatures at an arbitrary instant in time for the
conditions of Figure 99

157
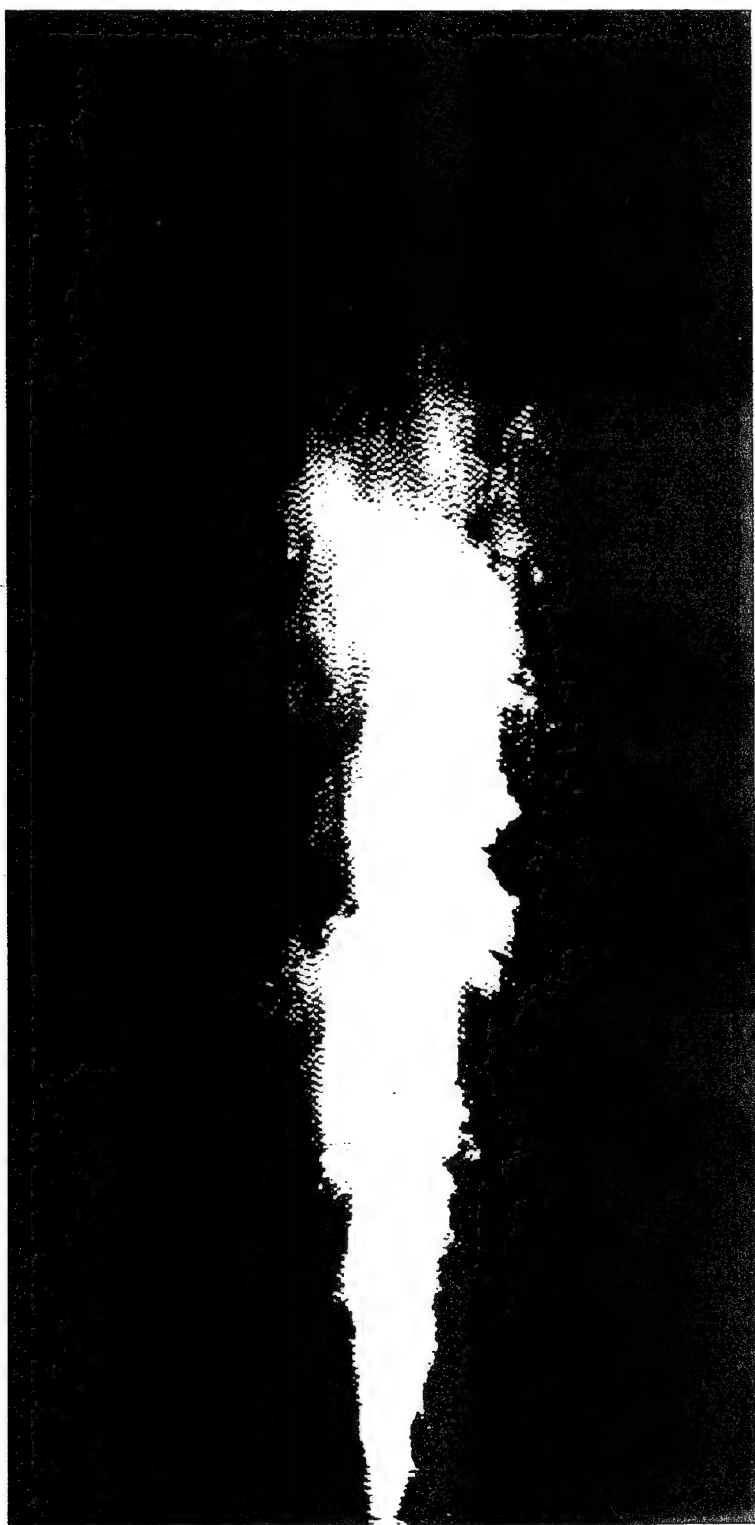
Figure 101.   Free swirling jet in deep-submergence mode

Figure 102.   Free swirling jet for h/d = 3.5 for the conditions of
Figure 101
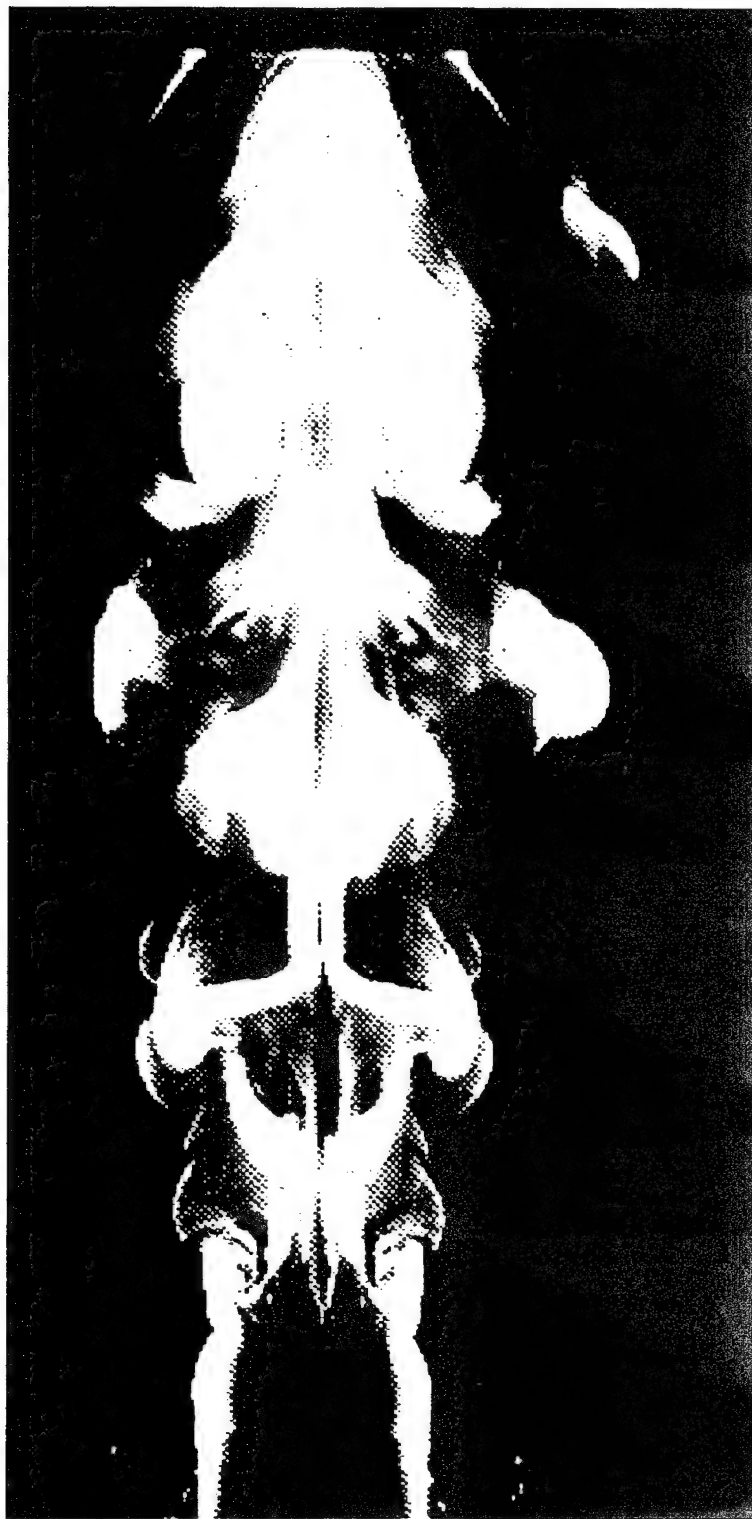
Figure 103.   Flow patterns resulting from a swirling jet decelerating in the vicinity of a free surface
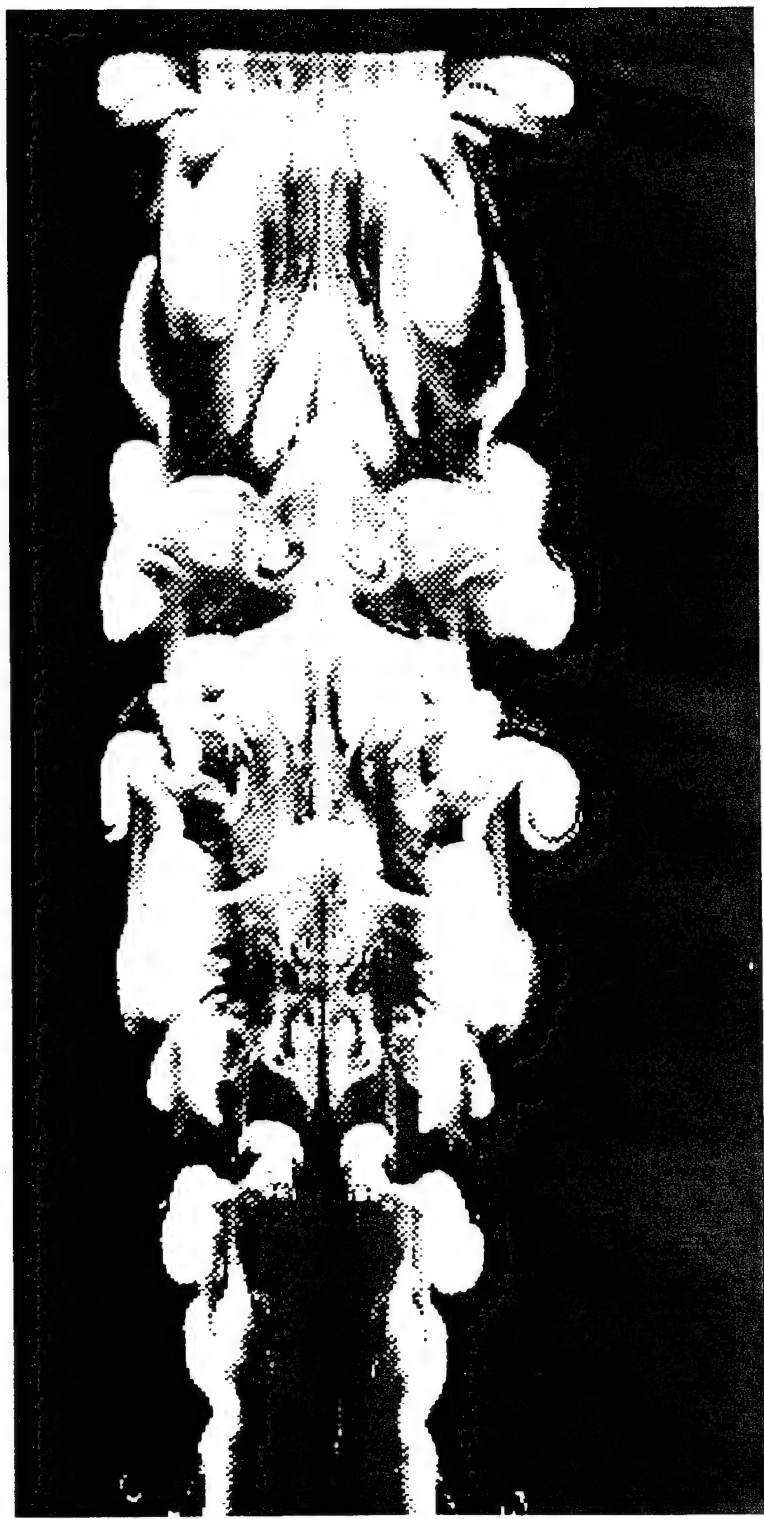
Figure 104.   Flow patterns resulting from a swirling jet decelerating in the vicinity of a free surface

Figure 105.   Comparison of the experimental and calculated values
               of u/Um in the deep mode at x/d = 4

Figure 106. Comparison of the experimental and calculated values of v/Vm in the deep mode at x/d = 4

Figure 107. Comparison of the experimental and calculated values of u'^2 / U_m^2 in the deep mode at $x/d = 4$

Figure 108.   Comparison of the experimental and calculated values
of v'^2/U_m^2 in the deep mode at $x/d = 4$

Figure 109.   Comparison of the experimental and calculated values
of w'^2/U_m^2 in the deep mode at $x/d = 4$

Figure 110.   Comparison of the experimental and calculated values
of $u'v'/U_m^2$ in the deep mode at $x/d = 4$

Figure 111. Comparison of the experimental and calculated values of $v'w'/U_m^2$ in the deep mode at $x/d = 4$

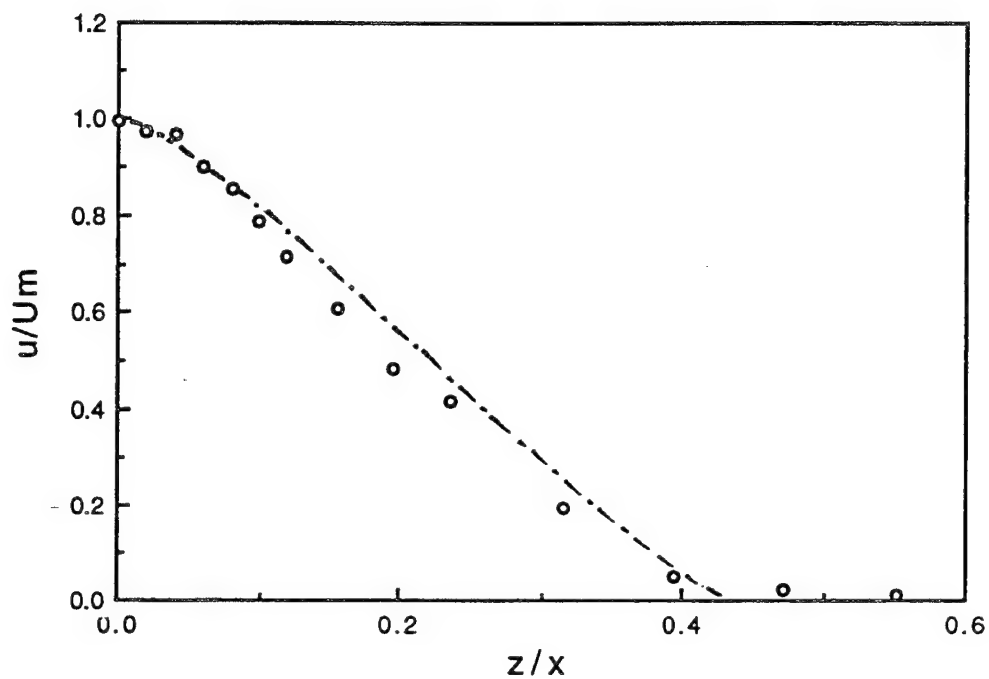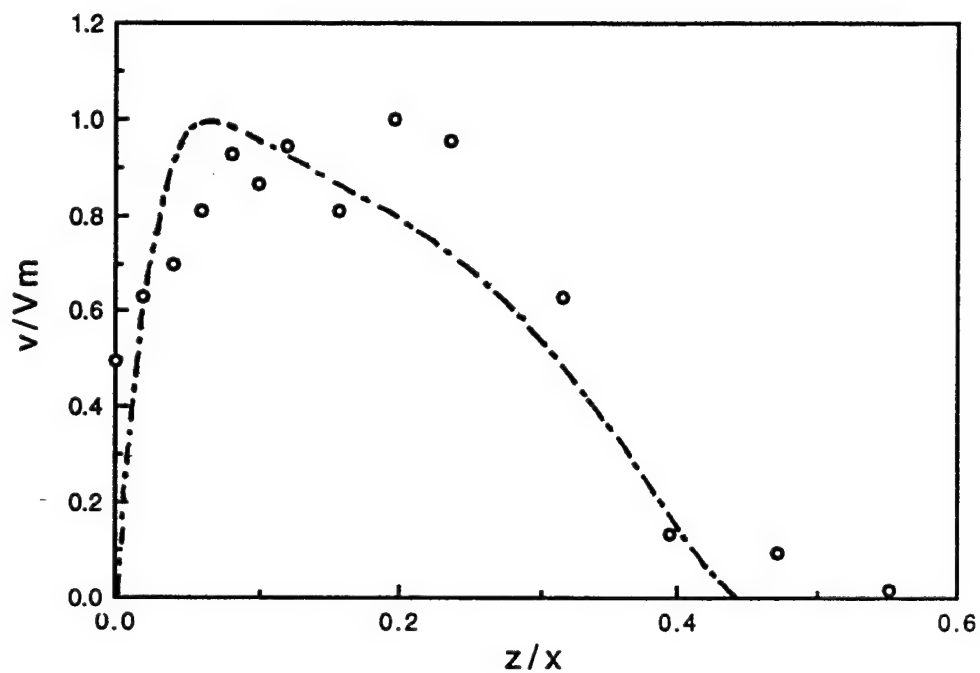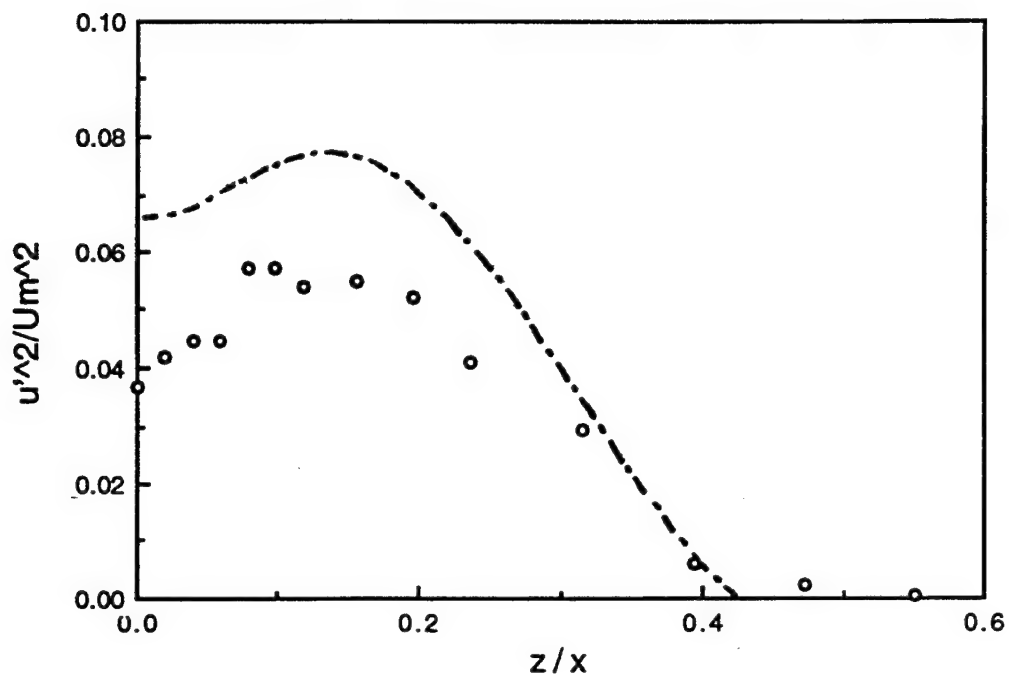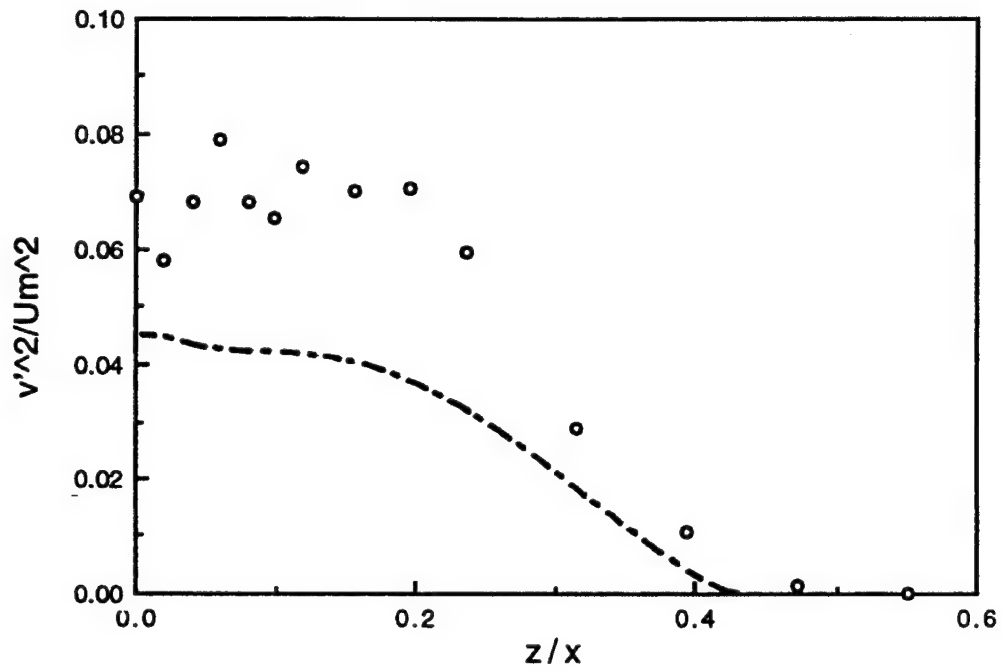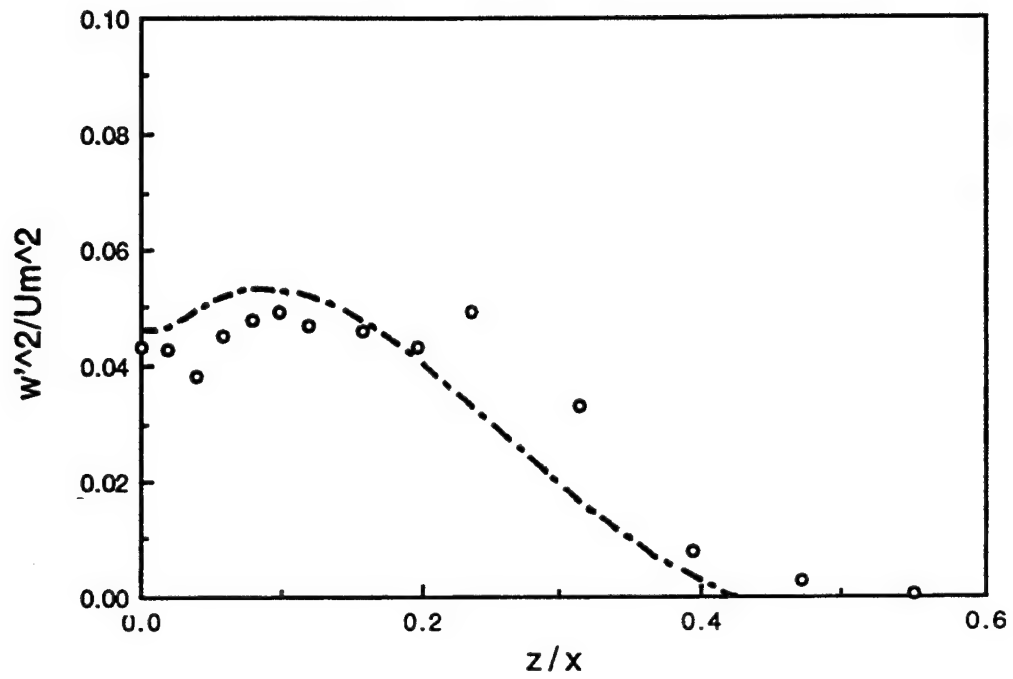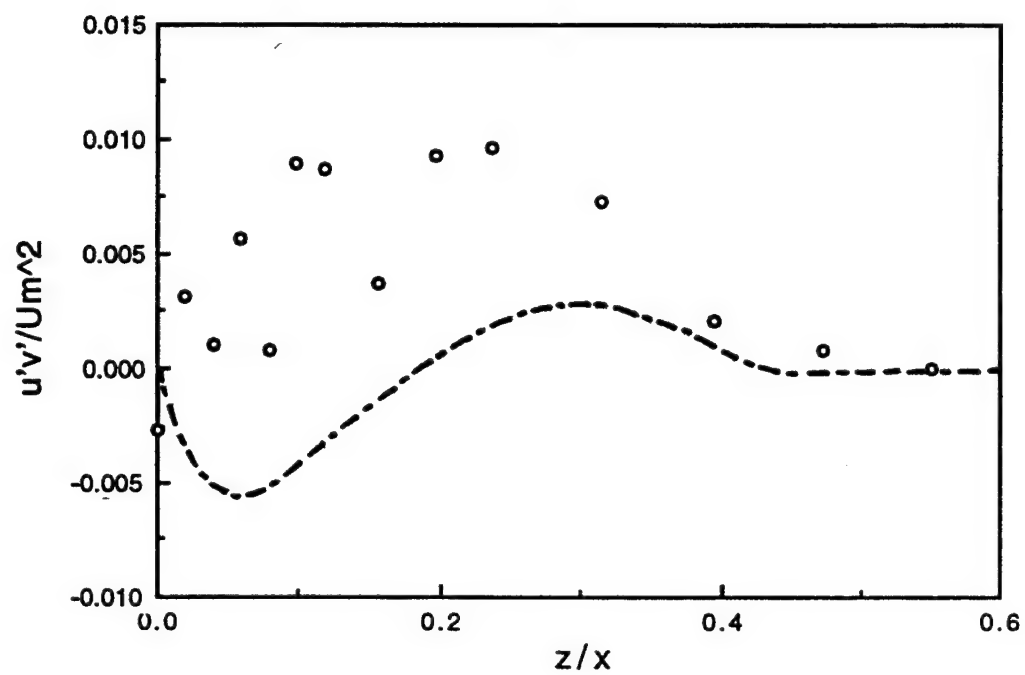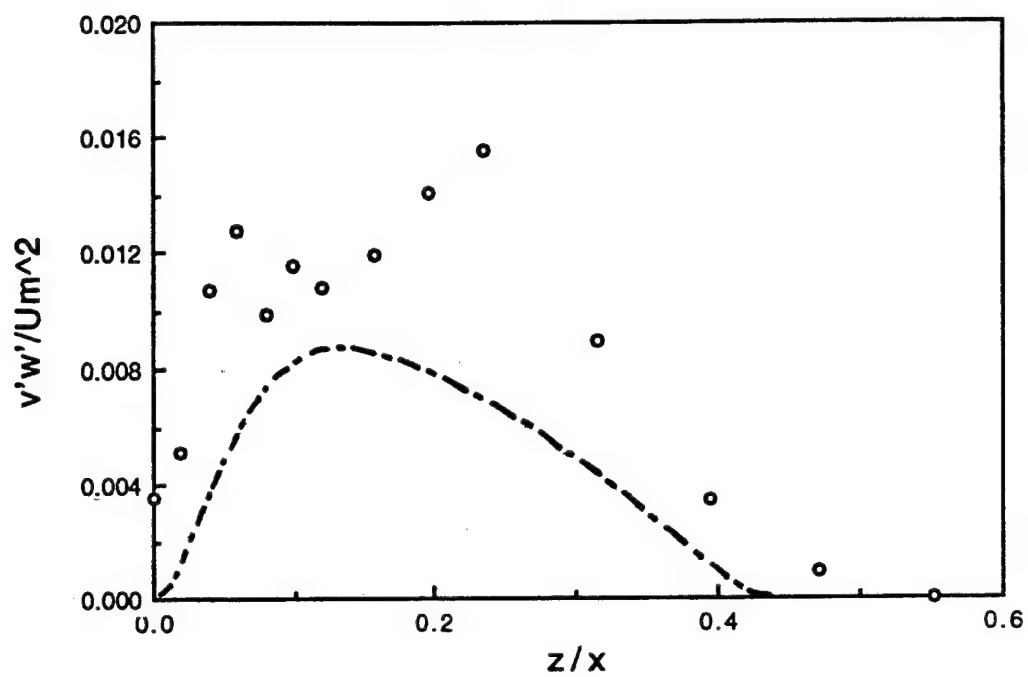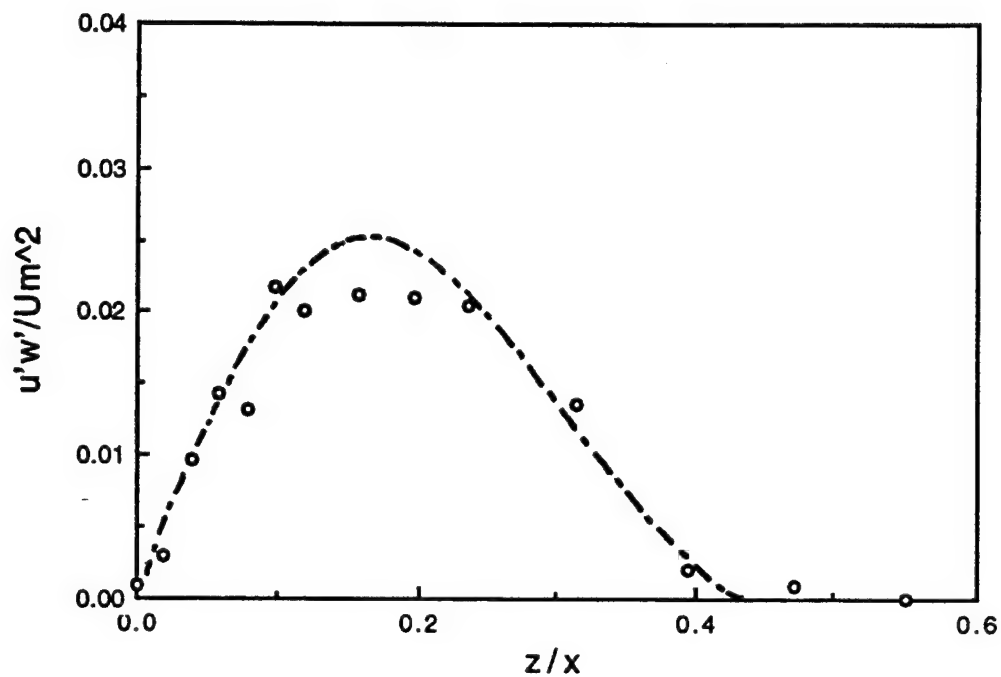Figure 112.   Comparison of the experimental and calculated values
of $u'w'/U_m^2$ in the deep mode at $x/d = 4$

REFERENCES

Batchelor, G. K. (1964). Axial Flow in Trailing Line Vortices. *J. Fluid Mech.*, Vol. 20, pp. 645-658.

Batchelor, G. K. (1967). *An Introduction to Fluid Dynamics.* Cambridge University Press, Cambridge.

Binnie, A. M. (1949). The Passage of a Perfect Fluid through a Critical Cross-Section or 'Throat'. *Proc. Roy. Soc.* A, Vol. 197, pp. 545-555.

Binnie, A. M. and Hookings, G. A. (1948). Laboratory Experiments on Whirlpools. *Proc. Roy. Soc.* A, Vol. 194, pp. 398-415.

Binnie, A. M., and Davidson, J. F. (1949). The Flow under Gravity of a Swirling Liquid through an Orifice-Plate. *Proc. Roy. Soc.* A, Vol. 199, pp. 443-457.

Browand, F. K., and Laufer, J. (1975). The Role of a Large Scale Structures in the Initial Development of Circular Jets. In *Proc. 4th Symp. on Turbulence in Liquids, University of Missouri-Rolla* (eds. J. L. Zakin and G. K. Patterson).

Brumley, B. and Jirka, H. (1987). Near-Surface Turbulence in a Grid Stirred Tank. *J. Fluid Mech.*, Vol. 183, pp. 235-263.

Burgers, J. M. (1940). Application of a Model System to Illustrate Some Points of Statistical Theory of Free Turbulence. In *Proc. Acad. Sci.*, Vol. 43, No. 1, Amsterdam.

Chigier, N. A., and Chervinsky, A. (1967). Experimental Investigation of Swirling Vortex Motion in Jets. *J. Appl. Mech.* Trans. ASME, pp. 443-451.

Dimotakis, P. E., Maike-Lye, R. C., and Papantoniou, D. A. (1983). Structure and Dynamics of Round Turbulent Jets. *Phys. Fluids*, Vol. 26, pp. 3185-3192.

Farokhi, S., Taghvi, R., and Rice, E. J. (1989). Effect of Initial Swirl Distribution on the Evolution of a Turbulent Jet. *AIAA J.*, Vol. 27, No. 6, pp. 700-706.

Gibson, M. M., and Younis, B. A., (1986). Calculation of Swirling Jets with a Reynolds Stress Closure. *Phys. Fluids*, Vol. 29, pp. 38-48.

Green, S. I. (1995). *Fluid Vortices.* Kluwer Academic Pub., Boston.

Gupta, A. K, Lilley, D. G., and Syred, N., (1984). *Swirl Flows*. Abacus Press, Tunbridge Wells, England.

Hallett, W. L. H., and Toews, D. J. (1987). The Effects of Inlet Conditions and Expansion Ratio on the Onset of Flow Reversal in Swirling Flow in a Sudden Expansion. *Experiments in Fluids*, Vol. 5, pp. 129-133.

Harvey, J. K., and Perry, F. J. (1971). Flow Field Produced by Trailing Vortices in the Vicinity of the Ground. *AIAA J.*, Vol. 9, pp. 1659-1660.

Khorrami, M. R. (1991). On the Viscous Modes of Instability of a Trailing Vortex. *J. Fluid Mech.*, Vol. 225, pp. 197-225.

Kihm, K. D., Chigier, N., and Sun, F. (1990). Laser Doppler Velocimetry Investigation of Swirler Flowfields. *J. Propulsion*, Vol. 6, pp. 364-373.

Komori, S., Ueda, H., Ogino, F., and Mizushina, T. (1982). Turbulence Structure and Transport Mechanism at the Free Surface in an Open Channel Flow. *Inter. J. Heat and Mass Trans.*, Vol. 25, pp. 513-521.

Kotsovinos, N. E. (1976). A Note on the Spreading Rate and Virtual Origin of a Plane Turbulent Jet. *J. Fluid Mech.*, Vol. 77, pp. 305-311.

Kotsovinos, N. E. (1978). A Note on the Conservation of the Axial Momentum of a Turbulent Jet. *J. Fluid Mech.*, Vol. 87, pp. 55-63.

Launder, B. E., and Morse, A. P., (1979). Numerical Prediction of Axisymmetric Free Shear Flows with a Reynolds Stress Closure. *Turbulent Shear Flows I*, (eds. F. Dusrt, F. W. Schmidt, and J. H. Whitelaw), Springer-Verlag, Berlin, Vol. 1, pp. 279-294.

Madnia, K., and Bernal, L. P. (1994). Interaction of a Turbulent Round Jet with the Free Surface. *J. Fluid Mech.*, Vol. 261, pp. 305-332.

Panda, J., and McLaughlin, D. K. (1994). Experiments on the Instability of a Swirling Jet. *Phys. Fluids*, Vol. 6, pp. 263-276.

Pratte, B. D., and Keffer, J. F. (1972). The Swirling Turbulent Jet. *J. Basic Eng.* pp. 739-748.

Rajaratnam, N., and Humphries, J. A. (1984). Turbulent Non-Buoyant Surface Jets. *J. hydraul. Res.*, Vol. 22, pp. 103-115.

Ramberg, S. E., Swean, T. F. and Plesnia, M. W. (1989). Turbulence Near a Free Surface in a Plane Jet. Naval Research Lab. Mem. Rep., p. 6367.

Rose, W. G. (1962) A Swirling Round Turbulent Jet. *J. Appl. Mech.* Trans. ASME, Vol. 84, Series E, pp. 616-625.

Rott, N. (1958). On the Viscous Core of a Line Vortex. *J. Appl. Math. and Phys.*, Vol. 9, pp. 545-553.

Sarpkaya, T. (1971). On Stationary and Traveling Vortex Breakdowns. *J. Fluid Mech.*, Vol. 45, pp. 545-559.

Sarpkaya, T. (1985). Surface Signatures of Trailing Vortices and Large Scale Instabilities. *Proc. of the Colloquium on Vortex Breakdown*, pp. 145-187, (ed. R. W. Staufenbiel), Aachen, Germany.

Sarpkaya, T. (1986). Trailing-Vortex Wakes on the Free Surface. *Proc. 16th Symp. on Nav. Hydrodyn.*, pp. 38–50. Washington, D. C, National Acad.

Sarpkaya, T. (1992a). Three-Dimensional Interactions of Vortices with a Free Surface. *AIAA Pap.* 92-0059.

Sarpkaya, T. (1992b). Interaction of a Turbulent Vortex with a Free Surface. Proc. *19th Sym. on Nav. Hydrodyn.*, pp. 479-90. Washington, D. C., National Acad.

Sarpkaya, T. (1995). Turbulent Vortex Breakdown. *Phys. Fluids*, Vol. 7, No. 10, pp. 2301-2303.

Sarpkaya, T. (1996). Vorticity Free Surface and Surfactants. *Ann. Rev. Fluid Mech.*, Vol. 28, pp. 83-128.

Sarpkaya, T., and Henderson, D. O. Jr. (1984). Surface Disturbances due to Trailing Vortices. *Tech. Rep. No.* NPS-69-84-004, Naval Postgraduate School, Monterey, California.

Sarpkaya, T., and Henderson, D. O. Jr. (1985). Free Surface Scars and Striations Due to Trailing Vortices Generated by a Submerged Lifting Surface, *AIAA Pap.* 85-0445.
Sarpkaya, T., and Neubert, D. (1994). Interaction of a Streamwise Vortex with a Free Surface. *AIAA J.*, Vol. 32, No. 3, pp. 594-600.

Sarpkaya, T., Magee, M., and Merrill, C. (1994). Vortices, Free-Surface and Turbulence. In *Free Surface Turbulence*, FED- ASME, Vol. 181, pp. 1-14. (eds. E. P. Rood, and J. Katz).

Schneider, P. E. M. (1980). Umbildung und Reflexion eines Ringwirbels an einer Platte, die schräg zu seiner Translationsrichtung orientiert ist. *Max-Planck-Institut für Strömungsforschung*, Göttingen, Bericht 12.

Schneider, W. (1985). Decay of Momentum Flux in Submerged Jets. *J. Fluid Mech.*, Vol. 154, pp. 91-110.

Scott, J. C. (1982). Flow Beneath a Stagnant Film on Water – The Reynolds Ridge. *J. Fluid Mech.*, Vol. 116, pp. 283–296.

Shabaka, I. M. M., Mehta, R. D., and Bradshaw, P. (1985). Longitudinal Vortices Imbedded in Turbulent Boundary Layers. Part 1. Single Vortex. *J. Fluid Mech.*, Vol. 155, pp. 37-57.

Shepherd, C. B., and Lapple, C. E. (1939). Flow Pattern and Pressure Drop in Cyclone Dust Collectors. *Ind. Eng. Chem.*, Vol. 31, pp. 972-984.

Sreedhar, M. K., and Ragab, S. A. (1994). Large Eddy Simulation of Longitudinal Stationary Vortices. *Phys. Fluids*, 6, pp. 2501-2514.

Swean, T. F., Jr., and Peltzer, R. D. (1984). Free Surface Effects on the Wake of a Flat Plate. NRL Memorandum Report 5426, Naval Research Laboratory.

Taylor, G. I. (1948). The Mechanics of Swirl Atomizers. In *Proc. 7th Int. Congr. Appl. Mech.*, Vol. 2, pp. 280-285.

Wygnanski, I., and Fiedler, H. E. (1969). Some Measurements in the Self-Preserving Jet. *J. Fluid Mech.*, Vol. 8, pp. 577-612.

Younis, B. A., Gatski, T. B., and Speziale, C. G., (1996). Assessment of the SCG Pressure-Strain Model in Free Turbulent Jets with and without Swirl. *J. Fluids Engng.*, ASME (pending publication).

Yule, A. J. (1978). Large-Scale Structure in the Mixing Layer of a Round Jet. *J. Fluid Mech.*, Vol. 89, pp. 413-432.

INITIAL DISTRIBUTION LIST

No. Copies

1. Defense Technical Information Center 2
   8725 John J. Kingman Rd., STE 0944
   Ft. Belvoir, VA 22060-6218

2. Dudley Knox Library 2
   Naval Postgraduate School
   411 Dyer Rd.
   Monterey, CA 93943-5101

3. Department Chairman, Code ME 2
   Department of Mechanical Engineering
   Naval Postgraduate School
   Monterey, CA 93943-5000

4. Professor T. Sarpkaya, Code ME-SL 5
   Department of Mechanical Engineering
   Naval Postgraduate School
   Monterey, CA 93943-5000

5. Curricular Officer, Code 34 1
   Department of Mechanical Engineering
   Naval Postgraduate School
   Monterey, CA 93943-5000

6. LT Michael S. Feyedelem 2
   2 Minard Place
   Norwalk, OH 44857

7. Prof. Ashok Gopinath, Code: ME-Gk 1
   Department of Mechanical Engineering
   Naval Postgraduate School
   Monterey, CA 93943-5000